Wireless Transport for Centralised Mobile Network Architectures

Dave Townend,

A thesis submitted for the degree of
Doctor of Philosophy

School of Computer Science and Electronic Engineering
University of Essex

May, 2024

Declaration

I declare that the work presented in this thesis is original and my own work. All figures and drawings, unless stated otherwise and referenced, are my own work. The material has not been submitted, either in whole or in part, for a degree at this, or any other university. This thesis does not exceed the maximum permitted word limit including appendices and footnotes, but excluding references and bibliography.

Dave Townend

Wireless Transport for Centralised Mobile Network Architectures

Dave Townend
School of Computer Science and Electronic Engineering, University of Essex

A thesis submitted for the degree of *Doctor of Philosophy*. May, 2024

Abstract

The objectives of this work aim to understand the role of wireless transport systems in future mobile network architectures. Mobile network deployments to date have been heavily dependent on point-to-point microwave radio links to connect geographically distributed cell sites into the network. New network architectures promise improved efficiency and cost reduction through centralisation of base station baseband functionality away from the traditional cell site. The extent to which wireless transport can fulfil the higher performance requirements of the resulting fronthaul connectivity is explored in this work.

A high resolution 3D environmental model is developed to facilitate the analysis of high frequency, line-of-sight wireless links across UK towns and cities. The model is used to determine the statistical properties of cell site infrastructure both in terms of physical environment and the probability of achieving line-of-sight radio conditions. These statistical results allow for a more detailed deployment analysis of smaller area to be reliably scaled to equivalent environments.

The possibility of routing high capacity wireless links between newly built street level cell sites and existing fibre locations using the discovered line-of-sight propagation paths is subsequently analysed. The performance requirements of emerging fronthaul transport interfaces and the capabilities of new mmWave and sub-THz spectrum bands (71 GHz - 174.8 GHz) are used as routing criteria in the geo-spatial deployment model in order to identify which combination of fronthaul interface and spectrum band could maximise the potential of wireless transport.

Incremental results in this work have demonstrated that the concept of wireless fronthaul networks are not only theoretically achievable but experimentally proven and practically realisable. The conclusions of this work have determined the optimum combinations of fronthaul interface and wireless spectrum which should be pursued in order to maximise the opportunity of wireless transport to support future centralised deployment architectures.

Acknowledgements

Thank you to all my collaborators and contributors, Professor Walker and the BT team. Also thank you to my children Jacob and Esther for their valuable input on the colour of my maps.

Contents

List of Figures

List of Tables

Chapter 1

Introduction

1.1 Motivation

Transport networks underpin the ability of mobile network operators (MNOs) to deploy the wide area, high capacity base station infrastructure necessary to meet the needs of modern society. Historically, the investment implications (financial as well as time and resource) of building 'ideal' fixed line transport solutions to connect mobile base station sites has given rise to more favourable wireless transport solutions. Worldwide, the majority of mobile base stations are connected to the core network using microwave point-to-point transmission links. While these solutions have proven sufficient for mobile technology generations to date, it is often the associated transport network capability that prevents significant re-architecting of the mobile network particularly towards promising new centralised deployment models.

With the advent of 5G, new transport interfaces are now defined. These new interface definitions provide new possibilities for operating base station functions, traditionally co-located at the cell site, at differing positions within the network using well established Ethernet transport protocols. In adopting new transport interfaces the cost and complexity of the cell site can be reduced whilst also benefiting from co-location, consolidation and coordination of more complex baseband processing functions at central locations in the network. While such developments have clear theoretical advantages in terms of efficiency and performance, these all come at cost to the underlying transport network. In such a scenario, the traditional backhaul interface evolves into a fronthaul interface which carries much more of the base station protocol stack to and from the cell site. The implications of such centralised deployments is that the transport requirements (in terms of bandwidth, latency and jitter etc.) become significantly more demanding relative to the existing backhaul orientated architectures.

In parallel to cellular standards, the wireless transport industry, recognising the demands for higher capacity radio access networks and the increasingly

overcrowded spectrum utilisation in traditional microwave bands seek to address new requirements and use cases through exploitation of higher millimetre-wave (mmWave) and sub-Terahertz (sub-THz) spectrum bands. In such bands, higher bandwidths and a step change in achievable performance is theoretically possible, promising wireless transport solutions more comparable with fibre optic solutions whilst still maintaining the benefits of the aforementioned cost implications.

As such, if the optimal transport interface and transport technology can be determined there exists an opportunity for wireless transport technology to help accelerate the adoption of centralised architectures. As these two paradigms mature it is important to consider their application in a realistic deployment scenario. This work aims to understand the role of wireless transport in future dense cell and centralised deployment architectures. In summary: *What will be the requirements imposed on wireless transport solutions in centralised mobile network architectures and what solutions should be pursued in order to meet such requirements in real-world deployments?*

1.2 Organisation of Thesis

An overview of each chapter in this work is summarised below. The organisation of this thesis aims to progressively build findings in each chapter in order to address the research objectives proposed.

Chapter 2 - Background. This chapter provides context to the over-riding research questions previously discussed. An overview of the state of the art technology concepts and background topics which have a direct influence on the role of wireless transport in mobile network deployments are explored. This chapter highlights the technical direction of research for the subsequent chapters.

Chapter 3 - An Environmental Framework. In this chapter the basis for more detailed analysis is set. The analysis in this chapter aims to provide statistical deployment characteristics of real mobile base station sites and their associated geographic environments throughout the UK. A detailed 3D model is constructed for large areas of the UK which serves as a deployment environment super-set for later modelling exercises. In providing a high level, large scale view of base station deployments and their environmental properties it is hoped that any findings which arise from this research can be reliably and accurately applied to equivalent geographies.

Chapter 4 - Macro Cell Line-of-Sight. The line-of-sight properties of existing macro cell infrastructure sites are studied in this chapter.The 3D model previously built is utilised to conduct a high resolution ray-tracing study of real-world macro cell sites in the UK. The rationale is to quantify the feasibility of using wireless transport links (assumed to exist on macro cell towers and roof tops) to

connect to surrounding lamp post sites as potential new small cell radio sites. As such, the line-of-sight propagation path between existing macro cell sites and lamp posts represent a potential high frequency wireless transport connectivity option that could support new dense cell deployments.

Chapter 5 - Micro Cell Line-of-Sight. This chapter aims to complement the previous chapter by analysing the feasibility of high frequency wireless transport links at street level and within street canyons. Here, the line-of-sight properties that exist in various environments between neighbouring lamp post sites are studied. These micro cell line-of-sight paths represent wireless transport links that could extend the transport network between lamp post sites representative of a multi-hop propagation path.

Chapter 6 - Wireless Multi-hop Deployment Characterisation. This chapter presents mobile network deployment analysis aimed at understanding the use of high frequency wireless transport to realise dense cell network architectures. Using a representative urban area of the 3D model, all the line-of-sight paths discovered from the macro and micro cell analysis are brought together to form a complete topology map of possible high frequency links between potential infrastructure sites. Findings aim to outline the fundamental deployment requirements that a multi-hop wireless transport solution must meet in order to maximise its potential as an alternative to fibred transport. This chapter focuses on understanding the necessary characteristics of a generic wireless transport network environment from an ideal deployment perspective rather than specific technologies or radio link performance.

Chapter 7 - Next Generation Transport Interfaces. In this chapter the theoretical performance requirements of the new fronthaul transport interfaces necessary for centralised deployments are explored. The objective of this chapter is to define meaningful performance metrics that can be utilised in the deployment model from previous chapters. The theoretical performance metrics are first derived and then experimentally assessed over an Ethernet based E-band (71-86 GHz) mmWave point-to-point radio link representative of the state-of-the-art wireless solutions currently available. Findings are used to model the equivalent performance and link budgets for future and anticipated wireless transport candidate bands above 100 GHz.

Chapter 8 - Wireless Fronthaul Deployment Feasibility. The findings supporting the underlying research objectives outlined in previous chapters are brought together in this chapter. The deployment model, environmental line-of-sight topologies, fronthaul interface requirements and wireless transport technology capabilities are combined into a single feasibility exercise. Representative wireless transport performance and realistic cell configuration fronthaul requirements are used as multi-hop routing criteria in the 3D model. Findings are used to outline the most appropriate wireless transport configuration to maximise the use of wireless transport and underline the feasibility of wireless fronthaul to realise dense,

centralised, radio access network architectures.

Chapter 9 - Conclusions. The individual contributions of constituent chapters and the overarching conclusions of this work are summarised in the chapter. Findings and recommendations are discussed which aim to address the initial research questions posed and identify areas for future and associated research resulting from this work.

1.3 Contributions

The key contributions of this work are summarised below:

1. Development and publication of the statistical properties of real-world mobile network deployments for use in accurate geo-spatial modelling based on the findings discussed in Chapter 3. The characteristics of real mobile base station sites and the physical environment within their coverage area is disclosed at scale for the first time. Many properties highlight inaccuracies in the system level simulation parameters and modelling assumptions of mobile network deployments proposed by industry recognised standards bodies such as the ITU and 3GPP. These contributions are published in [1].

2. A new line-of-sight probability model for the macro cell channel is proposed in Chapter 4. A large scale line-of-sight propagation path study has allowed a new line-of-sight probability model to be proposed for the macro cell channel. Analysis has highlighted the unsuitability of existing published models to accurately describe the probability of achieving line-of-sight radio conditions from existing macro cell base stations in the UK. Subsequently, a new model is developed which not only significantly improves accuracy of prediction but also extends the model definition to account for height dependency of the end-point as well as parametrisation of alternative cell types (urban, suburban and rural cell types). These contributions are published in [2] and [3].

3. A new line-of-sight probability model for the micro cell channel. A complimentary line-of-sight probability model is proposed for propagation paths from street level micro cell site deployments based on the findings of Chapter 5. Analysis carried out in this work has highlighted inaccuracies of recognised published models when applied to a real-world environments. New parametrisation is proposed to existing model definitions which address the inaccuracies whilst also extending the model capabilities to cover the end-point height and cell type definitions (urban, suburban and rural) for the first time.These contributions are published in [4].

4. A wireless fronthaul proof-of-concept. In Chapter 7, a testbed is developed enabling the wireless fronthaul concept to be experimentally demonstrated using a millimetre-wave point-to-point radio link. The most challenging fronthaul interface is successfully established to support operation of a remote 4G base station and characterise the theoretical limits of operation. These contributions are published in [5].

5. Development of a deployment model to demonstrate the feasibility of wireless fronthaul using the analysis in Chapter 6 and 8. A deployment model is built using a holistic approach underpinned by real-world datasets where line-of-sight propagation paths between potential mobile network infrastructure sites can be traversed to highlight the feasibility of wireless fronthaul. The modelling results are able to highlight the optimum technology selection to maximise use of wireless fronthaul transport as a connectivity solution in centralised network scenarios. These contributions are published in [6] and [7].

1.4 Publications

Journal and conference papers resulting from this work:

- **D. Townend** and S. D. Walker, "A 3D Statistical Framework for the UK's Mobile Network," 2020 IEEE 31st Annual International Symposium on Personal, Indoor and Mobile Radio Communications, London, UK, 2020, pp. 1-5, doi: 10.1109/PIMRC48278.2020.9217304.

- **D. Townend**, S. D. Walker, A. Sharples and A. Sutton, "Urban Line-of-Sight Probability for mmWave Mobile Access and Fronthaul Transmission Hubs," 2021 15th European Conference on Antennas and Propagation (EuCAP), Dusseldorf, Germany, 2021, pp. 1-5, doi: 10.23919/EuCAP51087.2021.9411447.

- **D. Townend**, S. D. Walker, A. Sharples and A. Sutton, "A Unified Line-of-Sight Probability Model for Commercial 5G Mobile Network Deployments," in IEEE Transactions on Antennas and Propagation, vol. 70, no. 2, pp. 1291-1297, Feb. 2022, doi: 10.1109/TAP.2021.3119099.

- **D. Townend**, S. D. Walker, A. Sharples and A. Sutton, "Line-of-Sight Probability for Urban Microcell Network Deployments," 2022 16th European Conference on Antennas and Propagation (EuCAP), Madrid, Spain, 2022, pp. 1-5, doi: 10.23919/EuCAP53622.2022.9769560.

- **D. Townend**, S. D. Walker, A. Sharples and A. Sutton, "Urban Wireless Multi-hop x-Haul for Future Mobile Network Architectures," ICC 2022 -

IEEE International Conference on Communications, Seoul, Korea, Republic of, 2022, pp. 1883-1887, doi: 10.1109/ICC45855.2022.9838366.

- **D. Townend**, R. Husbands, S. D. Walker and A. Sharples, "Toward Wireless Fronthaul for Cloud RAN Architectures". In: 2023 IEEE Wireless Communications and Networking Conference (WCNC) (IEEE WCNC 2023). Glasgow, United Kingdom (Great Britain), Mar. 2023.

- **D. Townend**, R. Husbands, S. D. Walker and A. Sutton, "Challenges and Opportunities in Wireless Fronthaul," in IEEE Access, vol. 11, pp. 106607-106619, 2023, doi: 10.1109/ACCESS.2023.3319073.

Other publications:

- ETSI Group Report mWT 012 V1.1.1 - 5G Wireless Backhaul/X-Haul – November 2018 [Contributing Author]

- ETSI White Paper No. 37 - E-Band - Survey On Status Of Worldwide Regulation 1st edition – September 2020 ISBN No. 979-10-92620-32-2 [Contributing Author]

Chapter 2

Background

The following chapter outlines the background topics which have a direct influence on the role of wireless transport in the evolution of mobile networks. As the mobile access network advances, new requirements are placed on the transport network on which it is built. This chapter aims to frame the context for the direction of subsequent research by highlighting the technology trends around mobile network architecture and wireless transport networks.

2.1 Introduction

The demand for capacity growth in mobile communication networks is a perpetual challenge for network operators and is the principle driving force behind the evolutionary steps in mobile standards such as those governed by the 3rd Generation Partnership Project (3GPP). The growth in capacity however, is not a new problem nor is it specific to mobile networks. The fixed line broadband network is projected to hit a capacity requirement of over 60 Tbps beyond 2024 with the mobile network following the same trend approaching 2 Tbps beyond 2024 as shown in Fig. 2.1 and 2.2 [8]. While monthly mobile data consumption has risen steeply and monotonically over the 10 years since the roll-out of 4G Long Term Evolution (LTE) services, the price subscribers have been willing to pay for such services has remained relatively flat. As a result, network operators have found necessity to plan, build and operate their network for more scalable and efficient delivery of data driven services.

The observed growth in end user demand can be attributed to many factors including technological advancements as well as behavioural changes. Each of these is underpinned by the evolution of new on-line services and applications such as on-demand video stream, gaming and social media. While such services are not fundamentally new to mobile networks, it is the continual improvements in mobile customer experience that enables such services to cross the boundary from traditional fixed line broadband networks consumed within the home to the wide

area mobile networks. When considering the long term forecasting of capacity growth in mobile networks it is again the evolutionary steps in mobile network technology teamed with promising new applications that threaten to continue the exponential growth profile observed in recent years. The recent introduction of 5G New Radio (NR) radio access network (RAN) technologies has allowed traffic growth to continue through adoption of new radio system technologies and services. The future requirements of mobile networks however, become more challenging to reliability forecast as we observe applications fundamentally dependent on mobile services rather than establishing popularity on fixed networks and transitioning to mobile. In addition, traffic forecasts which historically have been driven by predictable user habits have the potential to be complicated by data consumption and generation by new artificial intelligence or machine to machine type applications. The anticipated growth in mobile specific applications such as gaming, augmented and virtual reality (AR / VR), internet of things (IoT), autonomous cars and drone delivery are expected to drive a fourfold increase in 5G data consumption between 2019 and 2026 [9].

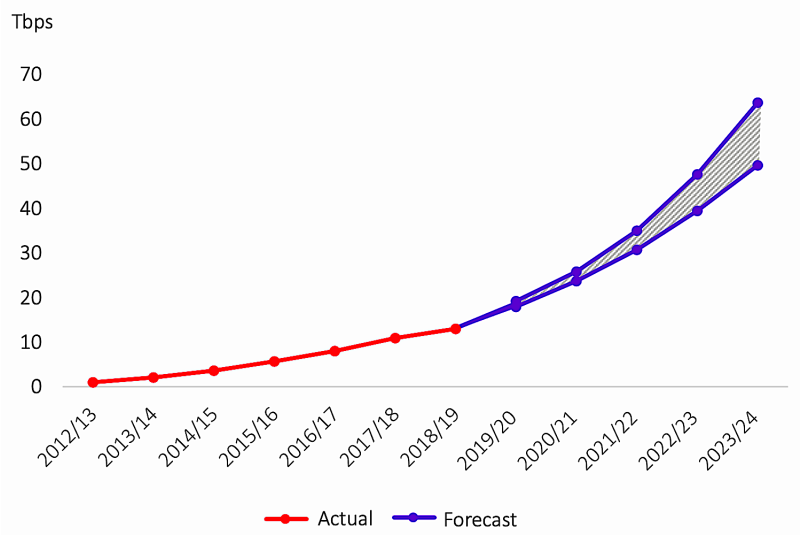

Figure 2.1: Capacity growth in a UK fixed network from [8].

There are many routes which network operators may pursue in order to grow capacity and efficiency in the network. This may come in the form of advanced antenna technology investments such and massive multiple-in multiple-out (mMIMO), beamforming and multi-user MIMO where spectral efficiency can be increased without the need for additional spectrum resource. Alternatively, capacity can be improved with the acquisition of new spectrum assets to aid higher bandwidth services or improved coverage. Finally, and perhaps the most forward looking of capacity growth advancements is the deployment or re-deployment of the network itself. This may come in the form of physical deployment scenarios such

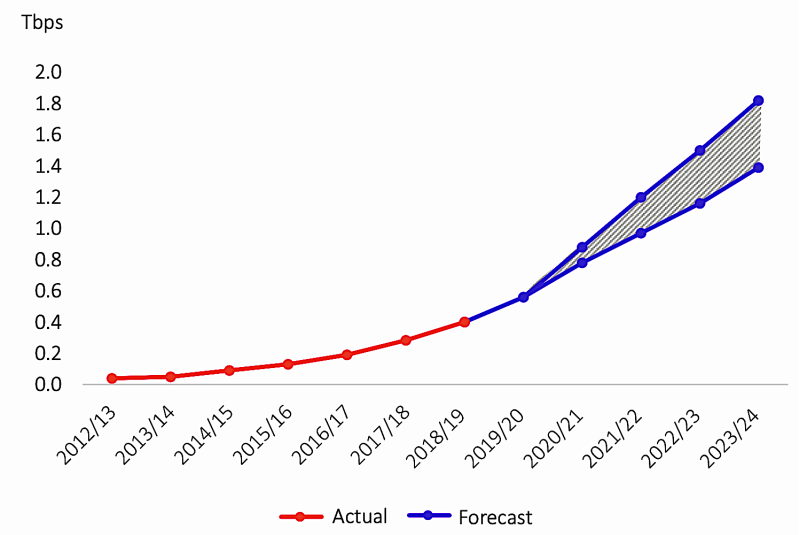

Figure 2.2: Capacity growth in a UK mobile network from [8].

as densification of cell sites or architectural re-design of the network topology to consolidate or coordinate network functions. Although none of these concepts are particularly new ideas, it is the enabling technologies such as those specified in 5G standards which allow new architectures to become more economically realisable.

2.2 Progression in Mobile Network Architectures

At the time of writing 5G is in it's infancy. The introduction of 5G in 3GPP release 15 in late 2019 enabled the first commercial 5G deployments in the UK by BT / EE in March 2019. While the immediate applications of the 5G non-stand-alone (NSA) specifications were primarily driven my marketing and enhanced mobile broadband (eMBB) use cases aimed at driving higher end user data rates, the underlying 3GPP specifications also set out the framework for new and alternative deployment architectures beyond this initial roll-out.

2.2.1 RAN Architectural Splits

To address the long term capacity driven deployment scenarios of future networks, 5G standards introduced new concepts based on RAN architectural splits. The ultimate aim of these new architectural split definitions is to allow further break up the logical functions of the traditional eNodeB (eNB) 4G base station to allow greater flexibility of deployment. From the outset, the 5G standardisation efforts aimed to better address the diverse requirements in how RAN networks are

architected where the transport network and geographic infrastructure availability often dictate the deployment model of the region or operator.

The 5G 3GPP release 15 RAN is built of gNodeB (gNB) base stations. Where the 4G eNB conventionally consists of a main baseband unit (BBU) and radio unit (RU), the gNB is built of three main functional network elements referred to as the centralised unit (CU), the distributed unit (DU) and the RU which allow the RAN to be deployed in a number of different ways to meet the operator needs as depicted in Fig. 2.3. Each of these functional components communicates to the next using the newly defined interfaces as described in 3GPP TS 38.401.

- The CU is the network element which is primarily concerned with centralised processing of higher layer elements of the gNB protocol stack such as the Radio Resource Control (RRC) and Packet Data Convergence Protocol (PDCP) layers. It has a one to many relationship with the DU. On the network side, the CU operates a direct interface to the 5G core or NGC (Next Generation Core) known as NG-C (control plane) and NG-U (user plane) interfaces but traditionally known as the 'backhaul' transport interface.

- The DU is responsible for the lower layer gNB protocol stack functions such as Radio Link Control (RLC) and Media Access Control (MAC). Due to reduced processing requirements relative to the CU, the DU offers a lower cost deployment option when deployed close to the RU site. The connectivity between the CU and DU is known as the F1-C (control plane) and F1-U (user plane) interface or 'midhaul' transport interface.

- The RU is deployed at the cell site and deals with the physical layer functions for radio layer transmission and reception converting analogue radio frequency (RF) signals into a digital signals for transmission over the transport network. The interface between the DU and RU operates between lower and upper parts of the physical layer and is known as the F2-C (control plane) and F2-U (user plane) interface referred to as 'fronthaul'.

2.2.2 Evolving Deployment Architectures

With the flexible deployment and infrastructure topology introduced by the functional break up of the RAN, a range of new deployment architectures becomes more realisable for mobile network operators. The conventional base station deployment model established through 2G, 3G and 4G cellular generations has focused on a 'cell centric' or distributed RAN (D-RAN) approach. In this model, the coverage environment is constructed of a large number of neighbouring and partially overlapping cell sites. There are relatively few building blocks with the BBU and RU co-located at the cell site and any traffic generated in the cell carried

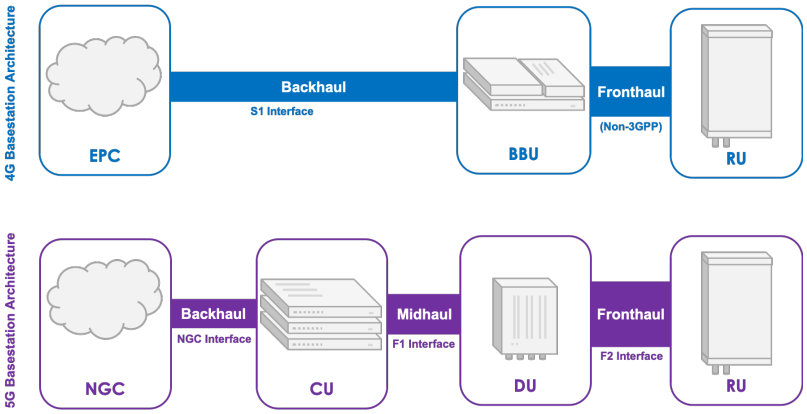

Figure 2.3: Architectural split evolution.

over a backhaul based transport interface to the core network. In this scenario the backhaul interface traffic closely mirrors the real-time user traffic demand on the cell with only a small amount of control plane and security overhead. The main disadvantage of the cell centric approach is that it is fundamentally an interference limited system defined by cell boundaries. This makes re-deployment or capacity uplift a challenging and time consuming radio planning process.

Advances aimed at minimising co-channel and inter-site interference whilst also improving aggregate RAN performance have evolved through 4G standards towards a more 'network centric' architecture. Early cell site coordination features such inter-cell interference coordination (ICIC) were first defined for 4G cells in 3GPP release 8. Such features allowed for non-real-time signalling exchange of frequency-domain information between neighbouring cells using the inter-eNB X2 logical interface. Techniques aimed at enhanced and more dynamic coordination came with advancements in 3GPP release 10 and 11 and the introduction of coordinated multipoint (CoMP) transmission and reception. CoMP was first introduced in 3GPP release 11 as an inter-cell and inter-user interference mitigation technique that allowed coordinated eNBs, to simultaneously transmit / receive with respect to end user equipment (UE). The steps toward a more network driven architecture underpinned by CoMP allowed for two categories of cell cooperation; multi-point coordination and multi-point transmission. In multi-point coordination, eNBs are able to exchange information about transmission decisions to dynamically adjust scheduling decisions and ultimately control interference, adjust UE link rates or improve performance. In multi-point transmission, cooperation between eNBs allows for coordinated transmissions to UEs from multiple locations either simultaneously or by switching dynamically to optimise performance.

While there are many benefits to inter-cell coordination including reduced interference, enhanced performance and energy saving, CoMP requires cells

to be synchronised and connected via low latency backhaul links to ensure signalling information remains accurate. Such transport network requirements in a conventional cell centric deployment architecture are typically unrealisable without significant redesign. As such, cell coordination techniques such as CoMP have failed to gain traction in commercial mobile deployments to date. Despite this, the evolution of CoMP in 5G, referred to as multi transmission and reception points (M-TRPs) is now supported by the new architectural splits. These fundamental concepts remain the key enabling technologies for more centralised and coordinated network centric deployment architectures such as cloud or centralised RAN (C-RAN).

The extrapolation of the evolving RAN coordination techniques finds a logical conclusion in centralised architectures where coordinated / cooperative processing functions of multiple cell sites can be efficiently rationalised deeper in the network - a 'network centric' architecture as highlighted in Fig. 2.4. As such, the centralised RAN architecture has gained significant interest in recent years with the aim of pooling baseband functions or capability into geographically common locations. In re-architecting the network to a centralised topology not only do the advance coordination techniques become easier to implement but they also present opportunities to reduce operational costs by removing complexity away from cell sites. To coincide with this strategic direction, a parallel, industry wide initiative is also under-way aimed at embracing virtualisation of telecom infrastructure for similar cost and efficiency reasons. In the mobile industry, this had become known as virtualised RAN (V-RAN) where all non-hardware dependent functions - i.e. excluding the antennas or RU, become software driven components deployed on commodity computing hardware rather than dedicated custom appliances. In merging these centralised and virtualised RAN concepts the opportunities for the flexible deployment goals of the 5G architectural splits become more achievable whilst also promising performance benefits and cost reduction.

The term cloud RAN (C-RAN) effectively encompasses the centralised and virtualised ideologies where RAN functions can exist anywhere in the network topology or hierarchy. In the context of long terms capacity growth and cost reduction, the decision points for mobile operators becomes one of how much of the baseband capability is brought away from the cell site itself. As more baseband functionality is centralised the requirements on the transport network inherently increase as more of the RAN protocol stack is required to traverse the transport network between the radio unit and the baseband processing function. In this approach the conventional backhaul driven transport network evolves to a fronthaul driven solution.

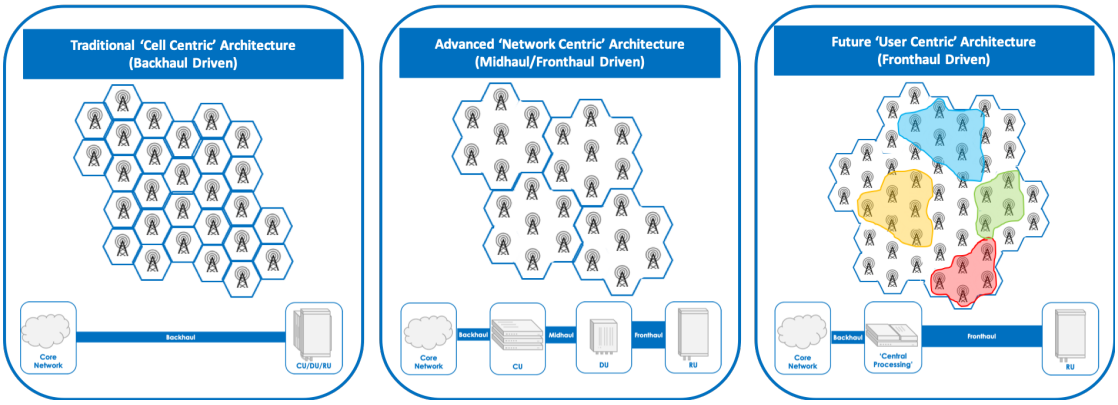

Figure 2.4: Evolution of deployment architectures.

The most novel research concepts looking beyond the established network centric models and toward a 'user centric' architecture is the research topics commonly referred to as 'cell-free' mMIMO (CF-mMIMO). Cell-free mMIMO aims to address the scalability issues evident in network centric deployments which although facilitate the coordination of geographically distributed cells are limited by small fixed boundary regions or predefined clusters of cells which share common baseband functions. In a cell-free model, the base station antennas can be distributed throughout the coverage area rather than being constrained to large arrays at a single site. In doing so, users are served by coherent joint-transmissions from multiple 'access points' or TRPs within range as they move throughout the environment. As the user moves the cluster of serving cells dynamically move with them - Fig. 2.4. Such an architecture is based on a fully centralised system where all TRPs are homed at one or more common centralised processing units (CPUs) for their baseband capability. This concept effectively eliminates the cell boundaries resulting in no inter-cell interference or inefficient inter-cell handover procedures. A fully centralised or disaggregated RAN model becomes particularly attractive as the access points become simple, low cost radio heads where any signal processing is carried out for a large number of access points deeper in the network.As with the network centric models, these user centric architectures are also fully dependent on high capacity, low latency fronthaul transport interfaces but rather than the logical peer-to-peer connectivity between CoMP cells, the CF-mMIMO access point lends itself towards a star topology with the centralised CPU locations.

2.2.3 RAN Functional Splits

The theoretical gains of new deployment models built on centralised and cloud RAN architectures promise much in the advancement of scalable capacity and aggregate network performance but are fundamentally built on stringent require-

ments of the fronthaul transport interface. As such, the architectural splits as outlined in Fig. 2.3 go hand in hand with 5G standardisation efforts looking to specify interface signalling within the RAN protocol stack known as RAN functional splits. The functional splits as outlined in [10] define eight possible split options in the RAN protocol stack which exist between the traditional BBU and RU. The objective here is to permit new flexibility on how the RAN components are built and deployed and allow for a greater choice of transport interface that may underpin the now somewhat flexible definitions of backhaul, midhaul and fronthaul. 3GPP specifications define and specify the function split point in the protocol stack but crucially (at the time of writing) do not standardise these interfaces for the purposes of interoperability for any split other than Option 2. As such, significant research and standardisation effort from a variety or industry forums in recent years have focused on the definition and interoperability of functional splits interfaces. Particular effort has be made in the those splits referred to a 'lower layer splits' which collectively form the fronthaul interface. This standardisation effort has been driven in part by my the desire to realise centralised architectures whilst also diversifying the RAN equipment supply chain as components become virtualised and software defined.

The many specification bodies and industry forum involved with such standardisation effort has inevitability led to alternative definitions and fragmentation within the over-riding 3GPP scope. The high level definitions are outlined against the RAN protocol stack in Fig. 2.5 with the most promising definitions gaining industry traction highlighted. For the purposes controlling the of scope of this work only those definitions which are directly aligned with 3GPP specifications or gaining early adoption are considered in detail. Whilst there are many initiatives seeking standardisation of new lower layer functional split interfaces the most significant advances have been with the Common Public Radio Interface (CPRI) consortium, Open-RAN (O-RAN) Alliance and Small Cell Forum (SCF) amongst others. These in turn have been supported by transport specific standards such as those developed by the Institute of Electronic and Electrical Engineers (IEEE).

In 2017 the CPRI consortium released the enhanced specification (eCPRI) [11] which builds on the CPRI protocols [12] widely adopted by the contributing major RAN vendors and utilised in 4G deployments worldwide. The evolution of the CPRI specification to eCPRI was aimed at decreasing the data rate requirements between the between the eCPRI Radio Equipment Control (eREC) interface at the DU and the eCPRI Radio Equipment (eRE) interface at the RU whilst enabling use of packet based transport networks. Historically, the CPRI interface was dependent on dedicated fibre for delivery of the equivalent 3GPP option 8 PHY / RF split (typically at very short distances between a cabinet based BBU and mast head RU within the same cell site location). The eCPRI specifications however, focus on fronthaul interfaces and primarily on new split definitions below the MAC layer. The eCPRI option D and E are aligned with 3GPP definition for option 6

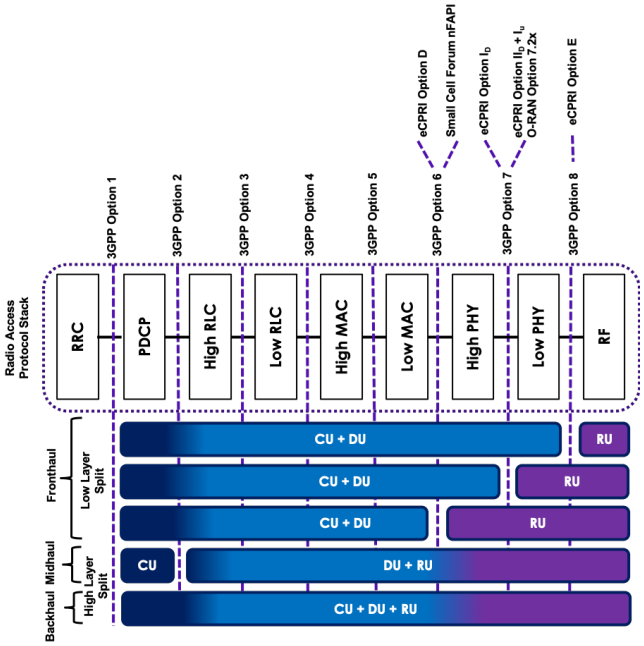

Figure 2.5: 3GPP functional split definitions.

and 8 respectively. Within the 3GPP option 7 split, eCPRI defines three different reference splits between the high PHY and Low PHY functions in the protocol stack - options I_D (bit orientated) and II_D for downlink and I_u for uplink (both I/Q orientated). With this approach the eCPRI specification allows for flexibility not only of the functional split which in turn dictates the transport interface requirements from a date rate, latency, jitter and packet loss perspective but also allow flexibility on the transport media itself through use of generic widely deployed Ethernet transport networks.

The O-RAN Alliance was formed in 2018 by mobile network operators with the objective of developing open and interoperable standards as an alternative to the traditionally closed, hardware-based RAN architecture such as those used in CPRI / eCPRI. The O-RAN fronthaul specifications focus on the definition of a 7.2x split which sits between a high and low PHY function broadly aligned with eCPRI split II_D. The 7.2x split transmits and receives I/Q sampling sequences of the Orthogonal Frequency Division Multiplexing (OFDM) waveform signal in the frequency domain [13]. The O-RAN open standard framework not only defines control, user, synchronisation and management plane functions in line with eCPRI specifications but extends to the detailed signal formats necessary for multi-vendor interoperability.

As part of efforts to a align development in the 4G / 5G small cell sector, the Small Cell Forum has defined a MAC / PHY split aligned with 3GPP option

6 [14]. The primary driver for this standardisation effort was to avoid industry fragmentation as the technology and vendor ecosystem grew around small cell based V-RAN and C-RAN concepts. The option 6 split was developed as an open and interoperable interface called nFAPI (network Functional API) and enables virtualisation of MAC functions at the DU whilst retaining the physical (non-virtualised) network function of the RU.

What all such standardisation efforts have in common is the desire to deliver these fronthaul interfaces over a cost efficient packet based transport network such as Ethernet with a realistic performance criteria. Ethernet based transport for mobile fronthaul allows for scalable, low cost deployments by leveraging existing infrastructure and mature standards. The demanding requirements of new fronthaul interfaces can be realised in Ethernet transport with the inherent standards based design capabilities including quality of service (QoS), resiliency, synchronisation and security. In support of the wide range of new fronthaul interface types under development, the IEEE developed standardisation specifically for the underlying Ethernet transport protocol for encapsulation of such interfaces. The 1904.3 Radio over Ethernet (RoE) working group supported by 1904.1 (Standard for Packet-based Fronthaul Transport Networks) group defined standards for encapsulation and mapping of lower layer split interfaces such as CPRI for delivery over generic Ethernet transport networks [15], [16]. In addition, complimentary standards such as IEEE 802.1CM [17] were developed to address expectations in increased performance requirements for fronthaul interfaces, in particular latency and synchronisation requirements. Together the IEEE standards allow the transport network of time sensitive fronthaul interfaces over more complex bridged or multi-hop Ethernet networks.

2.3 Progression in Wireless Transport Networks

The evolving architectures anticipated in the 5G era may promise scalable capacity and improved efficiency in RAN deployments but they are underpinned by the ability to connect a multitude of dense new cell sites to centralised baseband capabilities deeper in the network. Conventionally, fibre optic connectivity is the preferred medium to carry transport network traffic owing to its high bandwidth, low latency performance characteristics. In some deployment scenarios however, the use of fibre is simply too costly or time consuming to deploy. Whilst the operational cost of fibre once installed is very low, it is often the capital expenditure (CAPEX) of the initial installation that is the limiting factor. Often, rural and suburban cell sites do not have immediate access to local fibre and where urban sites may have fibre ducts near by, challenges with road closures and street works, particularly in busy areas can be just as demanding. As a result, wireless transport solutions have historically found favour in traditional 2G / 3G / 4G cell site

backhaul.

2.3.1 Microwave Backhaul

The role of wireless transport technologies in the UK's mobile network in vital. As of 2020 approximately two thirds of the mobile radio access network is serviced through microwave fixed service transport links (conventionally considered to be between 6 GHz and 42 GHz) [18]. This has primarily arisen through the historically high cost of fibre or leased line circuit installation in the diverse geographies where base stations are needed in order to achieve national coverage objectives. Until the introduction of 5G, the fundamental characteristics of traditional microwave transmission radios have been well matched, or at least kept pace with, the radio access network in terms of the associated link budgets (link lengths to next hop or aggregation points) and the available capacity that can ultimately be delivered.

A study of the active licensed links in the UK has been conducted from Ofcom publicly available Wireless Telegraphy Register (WTR) in January 2020 which outlines how traditional microwave bands are deployed in the UK by major mobile operators and infrastructure providers. The analysis forms a representative view of the inherent suitability of each bands for the transport link lengths required. This high-level view of microwave backhaul links in mobile networks also highlights a second order measure of the underlying UK mobile network deployment topology which is discussed next in Chapter 3. The majority of links used for mobile backhaul fall within the 26 GHz and 38 GHz bands. This has arisen primarily due to the overcrowding in the lower frequency 18 GHz and 23 GHz allocations. The channel arrangements in these bands follow Electronic Communications Committee (ECC) recommendations with a channel raster of 3.5 MHz and an exclusively frequency division duplex (FDD) configuration. Key microwave transport bands not included in the analysis of registered links are those of the fully licensed bands (block allocated) in the UK such as 28 GHz and 32 GHz. These bands are not included as these are self-managed unpublished data held the license holders. It can however be inferred where the cumulative distribution functions (CDFs) of these bands would lie based on adjacent bands in Fig. 2.6 and 2.7.

The approach used in dimensioning of mobile site backhaul site capacity can often vary between operator and depend on a range business factors. This may be influenced by cost, marketing requirements or technical constraints. Generally speaking, the cost per MHz of access spectrum used in mobile networks considerably out weights the cost of the backhaul / transport spectrum and so design emphasis is usually placed on ensuring transport connectivity does not become the bottleneck in performance. As such, operators often utilise a dimensioning formula for a three sector macro cell site based the expected peak and average load generated by the cell such as (2.1).

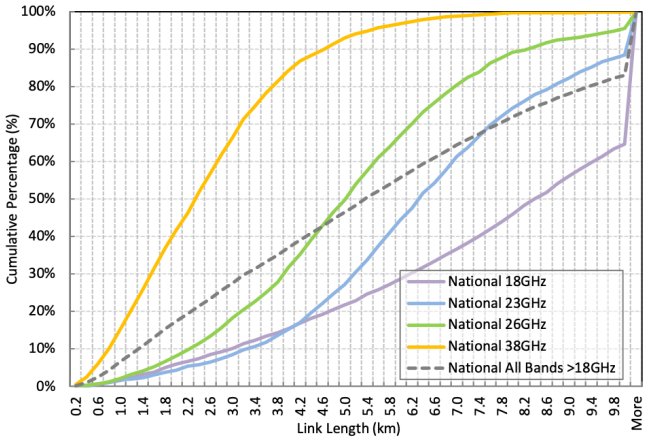

Figure 2.6: UK national microwave link length usage.

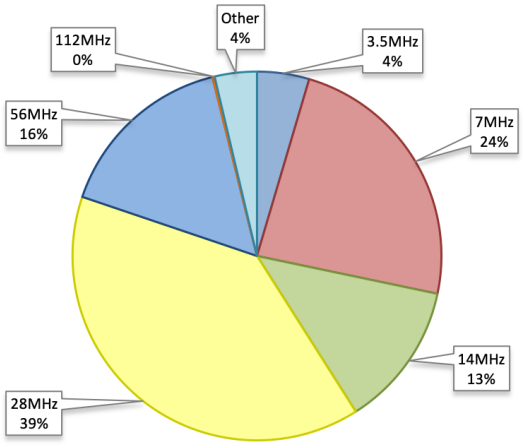

Figure 2.7: UK national microwave channel bandwidth usage.

$$BackhaulProvisioningforNCells = max(N \times busytimemean, Peak) \quad (2.1)$$

Based on such dimensioning rules, a typical 4G 20 MHz cell might expect a backhaul requirement in the order of 150 Mbps [19] . Even for a multi carrier site the dimensioning data rates are comparable with those that could be offered by microwave bands with common 28 MHz or 56 MHz channel bandwidths and polarization multiplexing techniques such as cross polar interference cancellation (XPIC) which could potentially offer up to 500 Mbps [20]. Nevertheless, microwave transport still presents the potential as the bottleneck on the access network especially as more access spectrum is added to cell sites and incremental upgrades to the access radio technology further increase the dimensioning require-

ments particularly with the introduction of 5G.

2.3.2 mmWave Backhaul

To address the inevitable challenges placed on the transport network as RAN capacity increases, exploration of higher frequency bands and their suitability for fixed service wireless transport solutions were undertaken as 4G matured. Prior to 2002, the maximum channel spacing possible was use of 220 MHz channels in the 18 GHz-band [21] as highlighted in Fig. 2.8. In reality, the overcrowding of traditional microwave bands used by mobile network operators in similar geographies meant channel sizes of 56 MHz or 28 MHz were the largest assignment generally used (Fig. 2.7), as such, exploitation of high frequency bands capable of providing substantially higher bandwidths became necessary. The terminology 'millimetre wave' spectrum (mmWave) was adopted for new bands above the established microwave bands despite some of the higher microwave bands already having wavelengths sub-centimetre. The exploitation of new transmission bands presented opportunities for a step change in backhaul performance now capable of multi-gigabit capacity and a significant reduction in packet delay relative to microwave. The initial focus of the wireless transport industry targeted spectrum around 60 GHz known as V-band and spectrum around 80 GHz known as E-band.

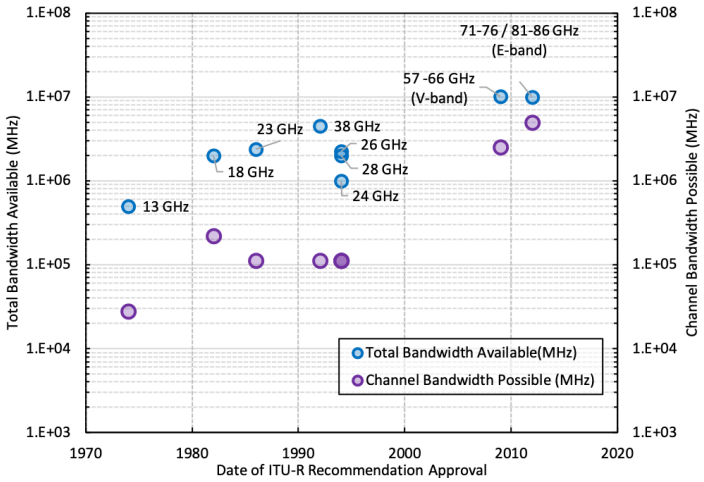

Figure 2.8: Fixed service spectrum and permissible channel bandwidths

The regulation of V-band has evolved over time from fragmented regional definitions initially outlined in 2000 between 55.78 – 59 GHz [22]. Over time, a harmonised wideband continuous definition was outlined by the ITU (ITU-R F1497-2) in 2014 [23] covering 55.78 – 66 GHz where sub-bands 55.78 – 57 GHz, 57 – 64 GHz and 64 – 66 GHz are covered by different annexes. One major reason for the fragmented history and variety of recommendations / regulations (at

least in Europe) in V-band is the significant propagation impact from atmospheric attenuation and in particular variation in oxygen absorption across different parts of the band. At its peak, and assuming an atmospheric pressure of 101.3 kPa and a temperature of 15 °C and a water vapour density of 7.5 g/m^3, V-band has an specific atmospheric attenuation of 15.05 dB/km as shown in Fig. 2.9. Such propagation effects limit link range but also lend themselves to high frequency re-use in dense deployments. This, together with the the large amount of spectrum available (up to 9 GHz), initially made V-band a promising band for dense urban and street level backhaul solutions. Despite this, a combination of low take up in 4G small cells and a growing requirement to co-exist with an expanding ecosystem of consumer products build around 60 GHz Wi-Fi protocols such as 802.11ad meant that large scale carrier grade adoption failed take off. Ultimately, the V-band ecosystem converged on consumer Wi-Fi products and higher volume, lower cost transport and fixed wireless access solutions build on Wi-Fi chipsets and protocols more suited to the enterprise market.

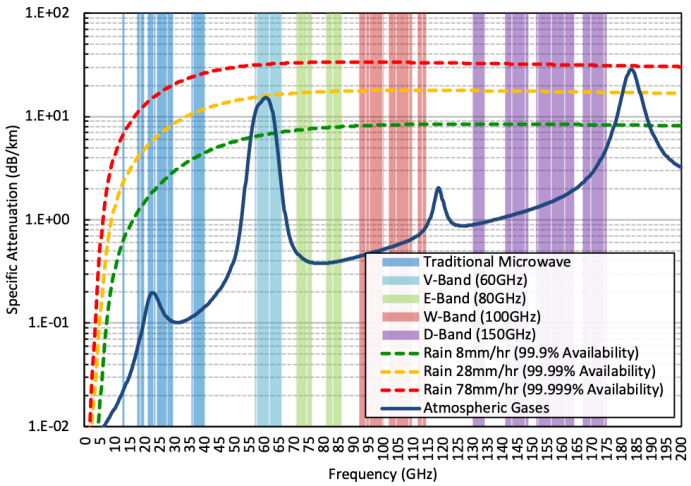

Figure 2.9: Fixed service band attenuation resulting from atmospheric gases

In 2012 the ITU published recommendations for the use of frequency block arrangements in the 71 - 76 GHz and 81 - 86 GHz bands also known as E-band (ITU-R F.2006) [24]. The E-band allocation made channel allocation upto 5 GHz possible for the first time. In the UK, E-band spectrum for fixed service applications was initially available in 2007 by the national regulator Ofcom but reviewed and restructured in 2013 following consultation. As a result, the previously light licensed regime based on a public database, was subdivided into a coordinated and self-coordinated block licensing regime separated by a 250 MHz guard band. The lower part (71.125 - 73.125 GHz / 81.125 - 83.125 GHz) is regulated as fully coordinated (link-by-link) license and the upper part (73.375 - 75.875 GHz / 83.375 - 85.875 GHz) as self-coordinated (light licensing)

approach. Analysis of the Ofcom Wireless Telegraphy Register (WTR) as of 2020 highlights the deployment characteristics and volume of link registrations in the early adoption phases of E-band within the UK in Fig. 2.10 and 2.11.

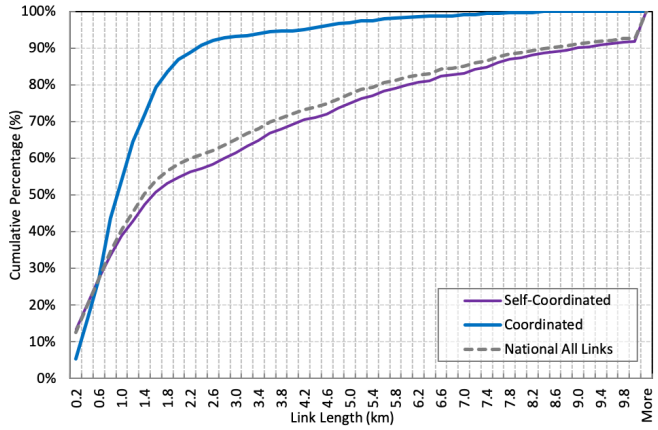

Figure 2.10: UK E-band link length usage

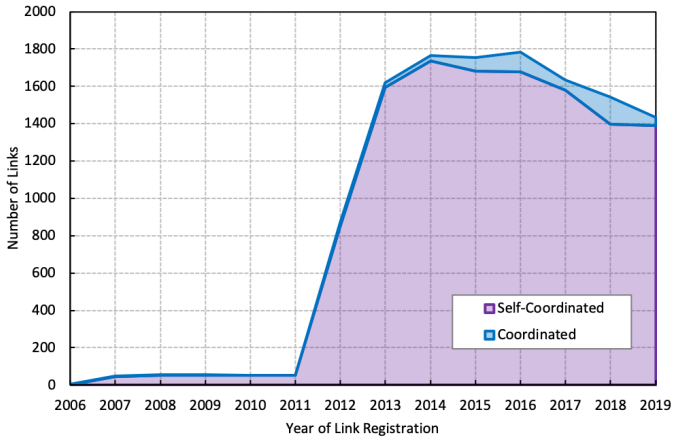

Figure 2.11: UK E-band number of registered links

Typically, the self-coordinated part of the spectrum is utilised by small / medium enterprise applications where the interference coordination is the responsibility of the license holder and channel definitions are not defined or regulated. The self-coordinated allocation therefore allows for low total cost of ownership and rapid deployment of high capacity fixed link services using unregulated channel and bandwidth allocation as shown in Fig. 2.12. The coordinated portion of the band offers a centrally coordinated and interference managed scheme allowing for high availability (99.99% - 99.999%) applications

such as mobile backhaul by mobile network operators. Initial channel bandwidth restrictions in the coordinated band (up to 1 GHz channelisation aligned to ECC/REC(05)07) as in Fig. 2.13 were increased in 2019 making the full 2 x 2 GHz of spectrum available for single link assignment and permitting data rates >10 Gbps.

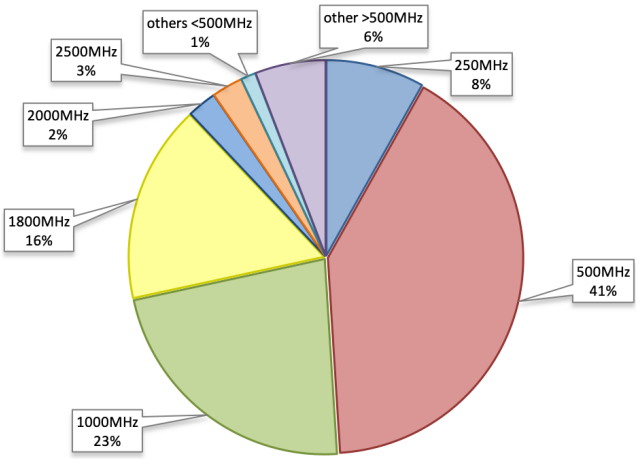

Figure 2.12: UK E-band channel bandwidth use in the self-coordinated band.

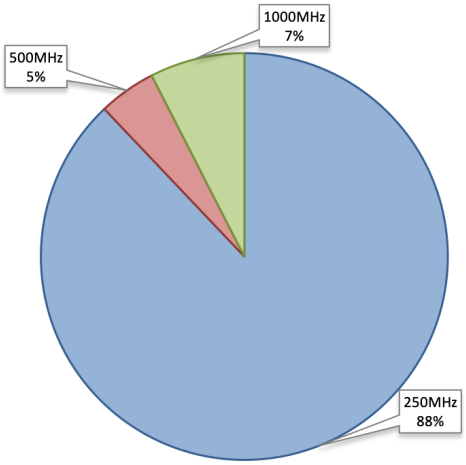

Figure 2.13: UK E-band channel bandwidth use in the coordinated band.

2.3.3 Bands Above 100 GHz

In the search to address the step change in performance requirements anticipated for the next generation mobile transport, significant effort has been placed in recent years on the exploitation of new spectrum assets above E-band. Between 92 GHz and 200 GHz nine different portions of spectrum have already been allocated

for fixed service applications, this accounts for 46% of the whole band. These allocations have collectively become known as W-band (92 - 114.25 GHz) and D-band (130 - 174.8 GHz) following CEPT (European Conference of Postal and Telecommunications Administrations) recommendations published in 2018 [25] [26]. These fixed service bands promise ultra low latency, ultra high-capacity performance resulting from the very large channel bandwidths that are technically possible. Such bands are prime candidates to support fronthauling of lower layer functional split interfaces as well as the higher layer functional splits of mid-haul and backhaul interfaces [20].

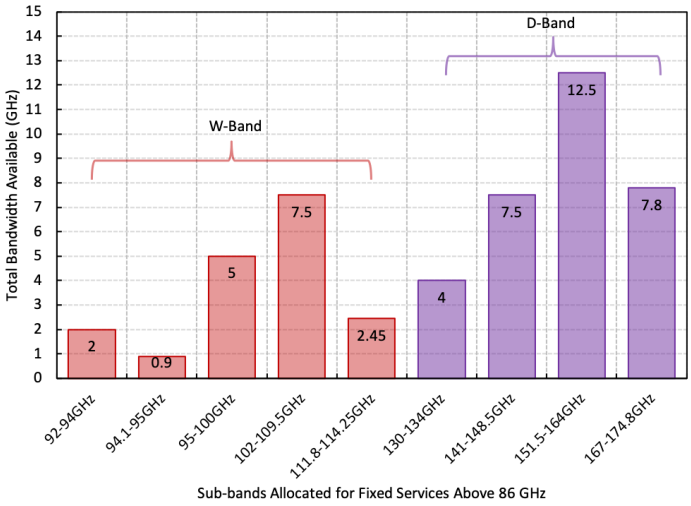

Figure 2.14: Fixed service spectrum bandwidth between 92 GHz and 200 GHz

The W-band allocation consists of sub-bands 92 - 94 GHz; 94.1 - 95 GHz; 95 - 100 GHz; 102 - 109.5 GHz and 111.8 - 114.25 GHz. W-band offers some commonality with existing E-band solutions where propagation characteristics (Fig. 2.9) as well as potential semiconductor technology are well aligned [27]. As such, it is expected that system integrators and operators will utilise W-band as an extension / expansion band for existing E-band deployments growing data rate capabilities beyond 10 Gbps. Early research of W-band systems include European collaborative projects such as Horizon 2020 TWEETHER (Travelling wave tube for W-band wireless networks with high data rate distribution, spectrum and energy efficiency) where the use of travelling wave tube amplifiers is studied to address the high cost and low power output of existing solid-state amplifiers which are seen to be preventing large scale exploitation of this band [28].

A more concerted research effort in recent years has been placed on the band allocations 130 - 134 GHz; 141 - 148.5 GHz; 151.5 - 164 GHz and 167 - 174.8 GHz which collectively make up D-band. This band is of significant interest due to the large contiguous bandwidths that are possible - as much as 12.5 GHz as shown in Fig. 2.14. The propagation effects and semiconductor output power

in this band are however even more challenging than those of W-band meaning D-band has largely been foreseen as short range (hundreds of meters) street level point-to-point and point-to-multipoint transport solution.Initial research into future transport network applications in D-band have reported on early prototype hardware feasibility and experimental propagation results. Long term propagation studies over short distance terrestrial paths have been published with research systems starting in 2018 [29]. Such studies aim to validate theoretical propagation models such as the precipitation and atmospheric adsorption models published by the ITU [30] [31]. Here, findings highlight improved modelling accuracy of rain attenuation in D-band through application of disdrometer data to not only account for rain rate but also the size and distribution of raindrops. Initial hardware prototypes based on GaAs MMIC fabrication have demonstrated a number of beneficial properties in the physical design of such high band systems. At such high frequencies, physically small solutions are possible resulting from the associated operating wavelengths. This allows for reductions in antenna (array) size and associated RF packaging but also physical separation of transmit (Tx) and receive (Rx) antennas within an FDD operating mode. The physical separation of antenna elements has been shown to provide sufficient isolation between Tx and Rx elements removing the necessity of the RF front end duplex filter. This in turn allows for a 'flexible duplex' scheme to be proposed [32]. A number of related research projects have also studied the requirements and deployment challenges of D-band transport including the EU Horizon 2020 funded project DREAM (D-band Radio solution Enabling up to 100 Gbps reconfigurable Approach for Meshed beyond 5G networks) [33]. This research aims to develop a D-band radio solution based on a low cost BiCMOS transceivers supporting data rates up to 100 Gbps and covering link distances of up to 300 m [34], a key objective in this project is exploitation of the large channel bandwidths possible in D-band (multiple GHz) whilst incorporating beam steering functionality for mesh and auto alignment operation at street level.

2.4 Chapter Summary

The argument for cell site densification and centralised deployment architectures in mobile networks seem obvious in light of a capacity growth trend that shows no sign of slowing down. In densifying the network with smaller and smaller cells, the base station to user distance is reduced and signal quality theoretically improved. In a traditional cell centric architecture however, such densification of co-channel small cells come at a price of degrading system signal-to-noise ratio (SNR). Cloud-RAN and Cell-free architectures go some way to reducing such scalability challenges whilst maintaining improvements in spectral efficiency through centralised or coordinated processing of resource allocation to minimise

interference. Although the theoretical benefits of centralised architectures are yet to be fully qualified in real-world deployments, they highlight a trend which profoundly impact the underlying transport network. As such, the mobile networks of the future become completely dependent on a vast connectivity requirement of very high capacity very low latency fronthaul based radio nodes. The present day reality for operators is that the requirements of such a fronthaul based wide area transport network are undoubtedly cost prohibitive. While significant research effort is being placed on both the architectural advancements in mobile networks as well as the direction of wireless transport technologies, there is little research which aligns these fields in order to better understand the role wireless transport has in future network deployments. As such this will be the focus of subsequent chapters.

Chapter 3

An Environmental Framework

A key challenge in deploying new wireless cellular technologies or architectures is accurate modelling of their impact on the wider network. In this chapter, a new statistical framework and large scale deployment analysis is carried out in order to characterise a real mobile network as it looks today. Current industry guidelines relevant to the modelling of mobile networks and their deployments are often over simplified and based on generalisation of the propagation environment and network topology. The analysis in this chapter details statistical deployment characteristics of real mobile base station sites and their associated geographic environment using a highly detailed 3D environmental model of large areas of the UK. High resolution LIDAR (Light Detecting and Ranging) data and cell mast properties are utilised to generate statistical descriptions of urban, suburban and rural cell types as well as distributions for the clutter properties that can be found within each cell type's coverage area. With the ability to accurately describe the deployment characteristics of different cell types any subsequent findings that result from this work can be reliably applied to equivalent geographies. The aim of this stage of work is to provide a reference point which gives credibility to later research findings from smaller representative areas which cannot be practically analysed on a national basis.

3.1 Introduction

The need for improved deployment models for both system level and radio propagation simulations are of increasing relevance in the context of 5G. Emerging radio technologies such as the use of mmWave spectrum for access networks (24.25 GHz – 52.60 GHz) have been extensively studied [35] and subsequently standardised [36] in recent years. The fundamental propagation characteristics of mmWave systems lend themself to small cell street level use and mean commercial deployments are underpinned by effective modelling of the network and its associated environmental properties. The same challenges are true

for use of high frequency wireless transport solutions that may underpin the associated connectivity solution to such street level cell sites. Where previously, deployment generalisations and low resolution environmental approximations have proven adequate for radio planning and evaluation of low frequency (<6 GHz) legacy systems, the introduction of mmWave systems whether used for access or transport mean this is no longer the case. The shortening wave length and line-of-sight (LoS) propagation characteristics mean traditional simulation techniques are becoming increasingly less suitable. New 3D deployment model methodologies based on representative data sets are therefore required to ensure any system level evaluations are statistically relevant for commercial deployments.

Traditionally, the more favoured approach in system modelling of wireless network deployments is geometry-based stochastic methodologies such as those historically used by industry standards bodies including ITU and 3GPP [37], [38]. Significant research has also been carried out in recent years relating to mathematical deployment approximation of cell sites through application of Poisson point process (PPP) where base station locations (densities) are randomly and independently distributed over a 2D plane [39]. The PPP has also been shown to provide reasonable accuracy for real base station deployments when considering the non-random nature of real urban deployments [40], [41]. Studies to date however have been largely confined to relatively small urban datasets and inherently do not consider the 3D properties of the system.

Such simulation approaches are typically complemented with generalised radio propagation models outlining path loss decay exponents or average environmental clutter loss contributions for different cell types [42]. Alternative approaches through application of deterministic methodologies, namely ray tracing, are of increasing popularity resulting from the continually improving availability and accuracy of public domain geo-spatial data sets. Deterministic approaches have the benefit of high accuracy but are often computationally complex and require site specific and highly detailed environmental data not easily scaled to large deployments [43]. As such, to support the wider research of this work a novel deterministic methodology is subsequently developed allowing key attributes to be summarised with an accuracy previously unpublished at such scale.

3.2 System Model

In order to define system attributes of a representative mobile network deployment, a full system model of the network topology and geographical topography must first be built. A deterministic modelling approach has been developed to analyse the properties of a real mobile network deployment which is based on two levels of detail. The first is a base station topology layer of the whole of the UK (>20,000 sites of a single operator) where cell sites are modelled with their accurate physical

properties such as geographic location and height above ground. A second layer is highly detailed 3D environmental model constructed for notable large areas of the UK covering a number of representative large and mid-size towns and cities including central London, Sheffield, Salford, Manchester and Rotherham. The total area of the 3D environmental model is approximately 1875 sq km. The environmental model is constructed of multi-resolution LIDAR surveys publicly available from the Department for Environmental and Rural Affairs [44] with resolutions 0.25 m, 0.5 m and 1 m. These surveys are re-sampled into a single digital surface model (DSM) of raster resolution 0.25 m.

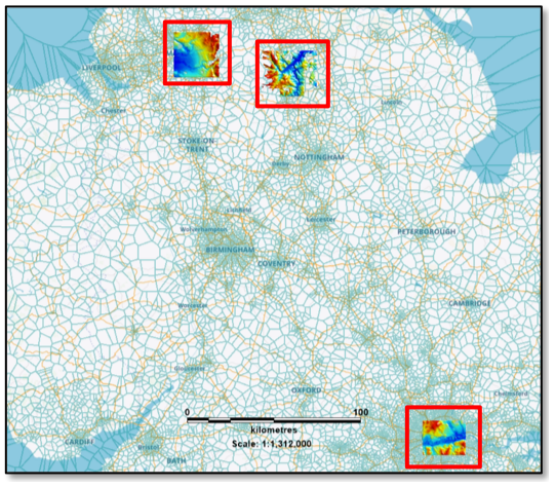

Figure 3.1: National cell site locations highlighting areas of high resolution DSM.

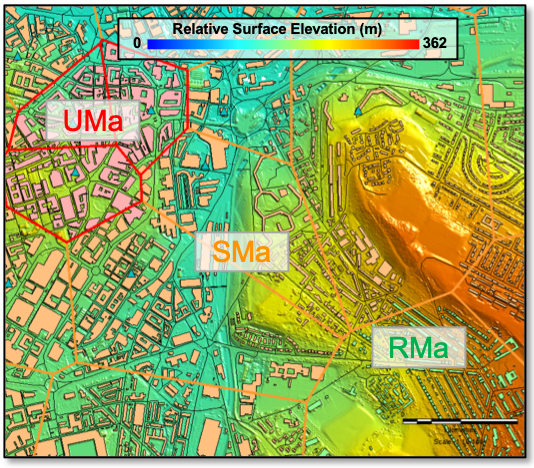

Figure 3.2: 2D DSM graphical representation with cell site classifications.

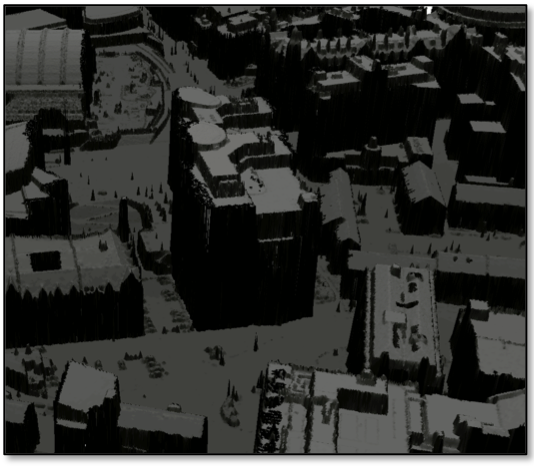

Figure 3.3: 3D graphical representation of DSM area.

The application of high resolution LIDAR data in this work is key in addressing the research questions formally set out. Not only does it provide a means of calculating the environmental properties of the existing network deployment orders of magnitude higher accuracy than the equivalent radio planning terrain data does today, it also allows for accurate propagation modelling of very high frequency wireless transport links under investigation in later chapters. Unlike conventional low resolution radio planning datasets with clutter class definitions or rudimental 3D building structures, the LIDAR data holds no information about the underlying terrain. As such notable 3D projections in the DSM are characterised through geo-spatial processing of augmented terrain, building, road and green space datasets from Ordnance Survey [45].The DSM areas of the model comprises of 2154 macro base station sites which account for a little over 10% of the total national network.

Using the outlined system model the fundamental characteristics of the mobile network can be derived. This compromises of two areas; cell site and cell environment characteristics. In the subsequent analysis, cell site characteristics are calculated over the entire geographic network (>20,000 sites) and the cell environment characteristics calculated over the representative areas (serviced by 2154 sites) of the high resolution DSM environment as in Fig. 3.1 - 3.3.

3.3 Cell Site Characteristics

Conventionally, large scale theoretical simulations of wireless networks are based on qualitative descriptions of urban, suburban and rural cell types. These cell types are typically defined by cell radius or inter-site distances (ISD) of a uniform hexagonal cell topology for example in Table 3.1. Before attributes for the real-world UK cell sites are calculated, each cell in the network is categorised into discrete urban, suburban and rural classifications. The cell size classification definitions are derived for alignment with conventional ITU and 3GPP definitions of urban, suburban and rural macro cells where cells with mean inter-site distance (ISD) $\leq$500 m are classified and analysed as urban macro sites (UMa), >500 m and $\leq$1299 m as suburban macro sites (SMa) and >1299 m and $\leq$1732 m as rural macro sites (RMa).

Table 3.1: ITU-R Recommendations for System Simulation [37].

Deployment Scenario	**Urban Macro**	**Suburban Macro**	**Rural Macro**
Layout	Hexagonal grid	Hexagonal grid	Hexagonal grid
Inter-site distance	500 m	1299 m	1732 m
Antenna Height	25 m, above rooftop	35 m, above rooftop	35 m, above rooftop
Channel Model	UMa	SMa	RMa

Using the real network topology, each cells nearest neighbour boundaries are

derived through construction of Voronoi polygons formally defined in (3.1). The 2D ISD between each geometric neighbour is calculated through construction of the associated Delaunay triangulation lines in Fig. 3.4 and subsequently used to classify the cell as UMa, SMa or RMa. The Voronoi coverage definition allows abstraction of the network topology independent of specific cell site configurations which may influence the coverage areas such as operating frequency, radio access technology, transmit power level or antenna gain and orientation. The resulting neighbour relation definitions do not necessarily describe the system level interactions (such as validity of handover candidates) but rather a physical description of the network topology.

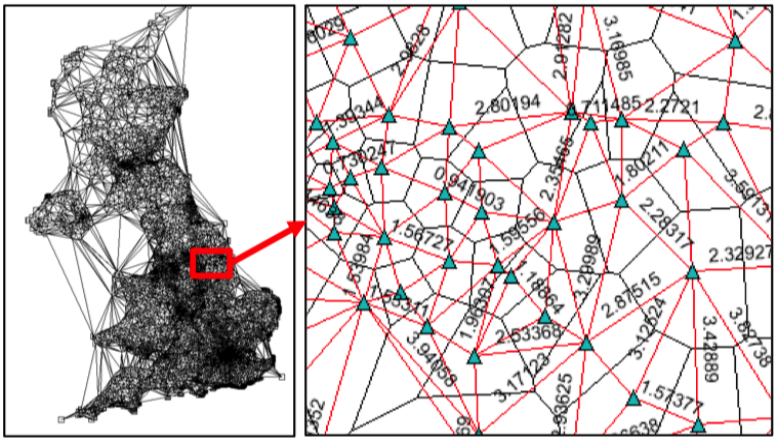

Figure 3.4: Voronoi polygons (black lines) and Delaunay triangulations (red lines) of all cell sites.

Geo-spatial analysis of the base station locations allows each cell type to be better characterised as shown in Fig. 3.5 and using the following attributes:

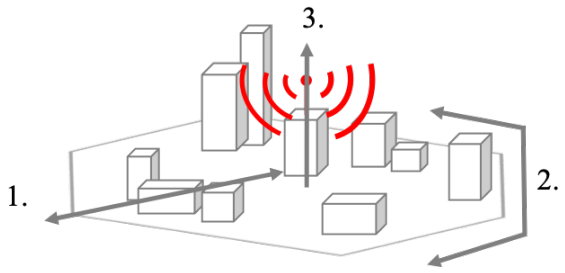

Figure 3.5: Cell site characteristics.

1. The mean inter-site distance calculated for each cell - model results outlined in Fig. 3.6.

2. The typical number of geometric neighbours of each cell - model results outlined in Fig. 3.7.

3. The base station antenna height relative to ground level of each cell - model results outlined in Fig. 3.8.

To align actual cell site classifications (urban, suburban, and rural) with ITU / 3GPP definitions, the mean ISD for each cell is calculated (cell neighbour relationships over large water bodies or intersecting coastlines are excluded). In Fig. 3.6 the peak or mode of the distribution highlights the most common ISD of around 1.2 km. As a result of typical cellular link budget limitations, cells with a mean ISD much greater than 5 km typically represent infill or remote sites with only partial logical (radio link layer) neighbours that could practically be used for mobile handover. It should also be noted that configurations such as radio operating frequencies, transmit power and sector orientations are considered site or operator specific and so are not further differentiated. A description for

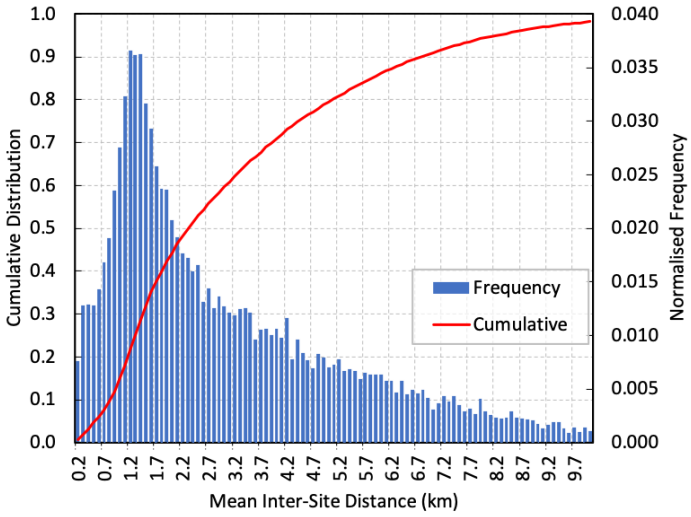

Figure 3.6: Mean inter-site distance distribution.

the typical number of cell neighbours is defined by the sum of boundary edges of each Voronoi polygon which in turn defines the coverage region of the cell. The complete Voronoi diagram is defined based on the distinct cell location points (sites) $P = \{p_1, ..., p_n\}$ over the 2D plane $\mathbb{R}^2$. Each cell site p_i, with coverage region given by $V(p_i)$, is defined as the set of points x whose nearest site is p_i, formally:

$$V(p_i) = \{x \in \mathbb{R}^2,\ |x - p_i| \leq |x - p_j|,\ \forall i \neq j\} \tag{3.1}$$

Analysis of boundary edge count for each cell classification is shown in Fig. 3.7 which outlines distribution characteristics similar to those expected from a generalised homogenous PPP [46]. Results do however indicate a clear trend towards fewer neighbours as the cell area decreases emphasising that underlying network topology should not simply be treated as a truly random spatial process when considering real deployments.

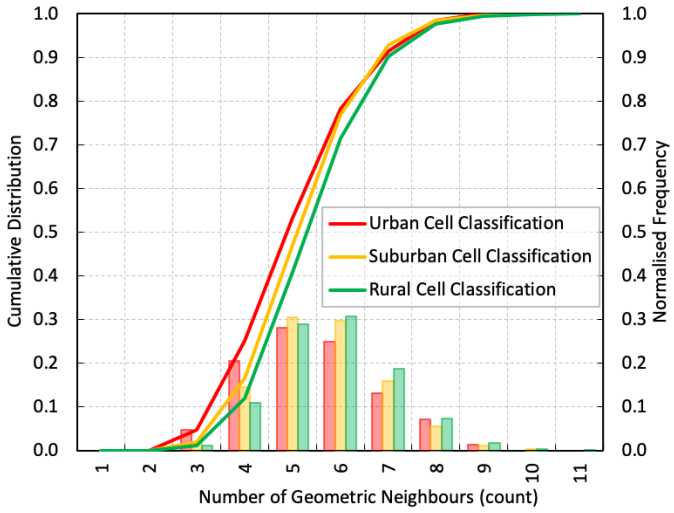

Figure 3.7: Voronoi neighbour count distribution.

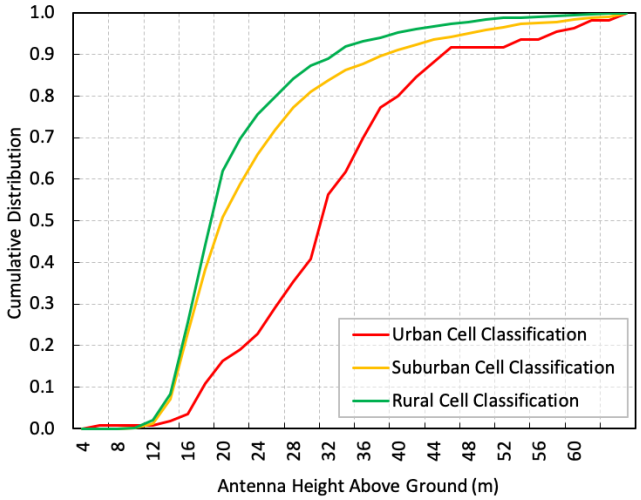

Figure 3.8: Base station antenna height distribution.

Base station antenna height is a fundamental factor affecting propagation paths

toward end user equipment. The base station antenna height is also representative of the height at which a wireless transport antenna could be mounted if the site were served by a wireless backhaul solution. The distribution of antenna height relative to ground level is shown in Fig. 3.8. These results disagree with established simulation guidelines such as those in Table 3.1 where antenna height is typically assumed to increase with cell area. Statistically, urban sites have been shown to exploit more high roof top spaces where suburban or rural sites utilise more dedicated masts. Furthermore, the suburban and rural cell distributions are closely aligned at heights below 15 m resulting from historical cell mast planning permission requirements in these environments within the UK.

3.4 Cell Environment Characteristics

Cell environmental properties are derived through geo-spatial analysis of 3D projections within the DSM cell coverage area (the Voronoi polygon). The statistical clutter or blockage data can be fundamentally described using the probability distributions of attributes as depicted in Fig. 3.9 and described below:

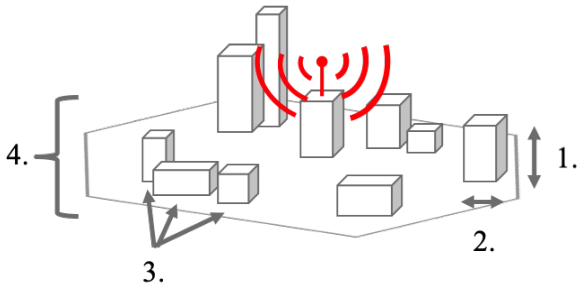

Figure 3.9: Cell environment characteristics.

1. The 3D height of all the potential blockers (individual buildings) within the cell - model results outlined in Fig. 3.10.

2. The size of individual blockers (the 2D footprint area of individual buildings) - model results outlined in Fig. 3.11.

3. The total number of distinct potential blockers within the cell - model results outlined in Fig. 3.12.

4. The proportion of the whole cell area that is occupied by potential blockers - model results outlined in Fig. 3.13.

Clutter properties derived from analysis of each of the cell classification coverage areas are presented using the cumulative distribution functions outlined

in Fig. 3.10 - 3.13. Such properties are characterised with a view to using as inputs to established statistical modelling techniques such as [47] or refining spatial point processes [48], [49], but using deterministic datasets extended to 3D descriptors. In order to remove any large scale influence of the underlying terrain profile across the DSM, 3D clutter properties are also presented relative to ground level. Further blockage attributes also worthy of analysis including building shape and orientation are also under consideration in further work.

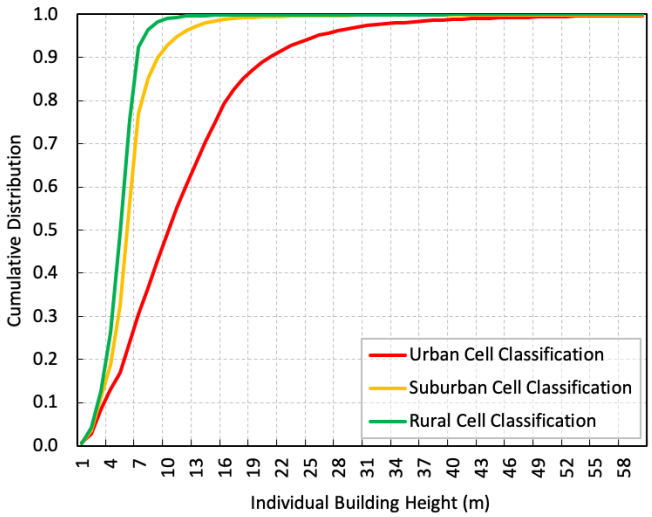

Figure 3.10: Individual building height distribution.

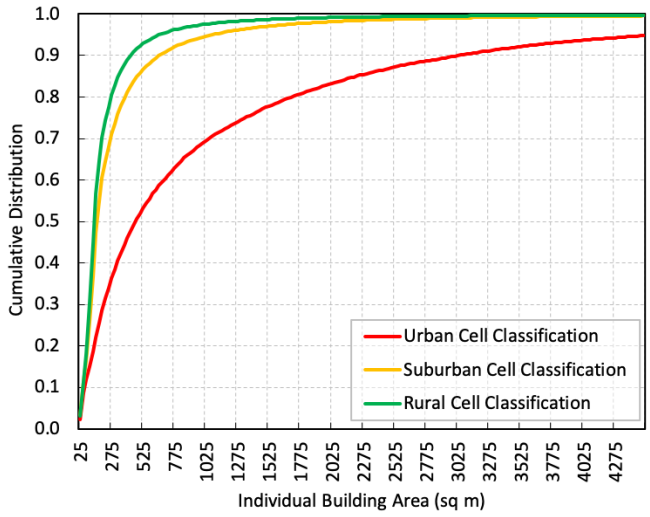

Figure 3.11: Individual building area distribution.

Results show that individual blocker properties (given by building height and

footprint areas in Fig. 3.10 and Fig. 3.11) are closely aligned for suburban and rural classes below building heights of 7 m and areas of <150 sq m, this is primarily attributed to the dominance of residential premises in these areas where characteristics agree well with national property statistics [50].

The major distinction between suburban and rural cell classifications in terms of clutter characteristics is highlighted through building density analysis (building count per unit area (sq km) in Fig. 3.12 and total proportion of the cell occupied with buildings in Fig. 3.13) where intuitively, densities are much lower within the equivalent coverage area for rural cell types.

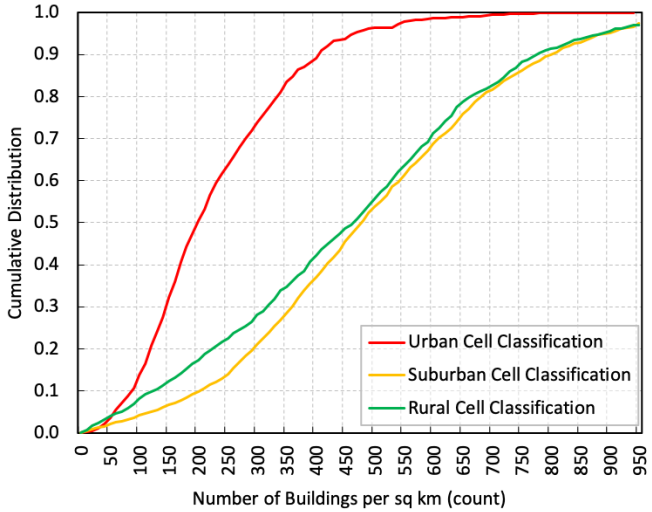

Figure 3.12: Individual building count within cell coverage area distribution.

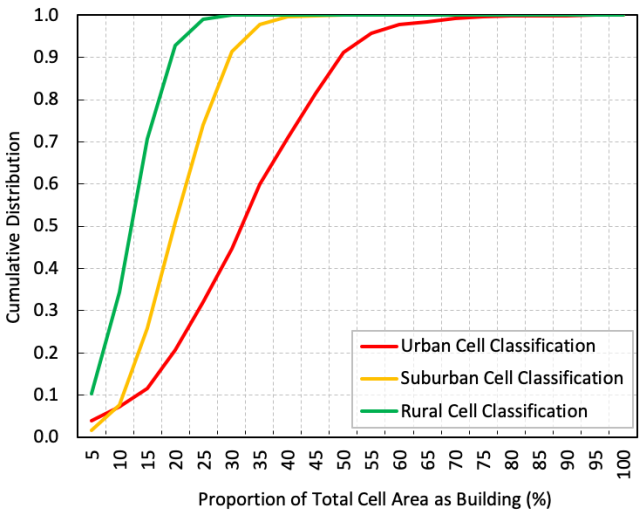

Figure 3.13: Proportion of total cell area occupied by building distribution.

3.5 Chapter Summary

This chapter presents analytical insight into real mobile network deployments where previous studies have been scarce or based on small scale analysis. Findings provide a means of accurately describing key statistical characteristics for use in system level simulations that employ stochastic geometry techniques such as spatial point processes. While further work is necessary to quantify the accuracy of point process methodologies relative to the distributions such as those outlined in this chapter, results highlight the importance of accurate cell type classification in these approaches.

Findings demonstrate that for conventional definitions of rural and suburban cell types many environmental attributes are closely aligned and distinguished primarily by the proportion of the cell area occupied by potential blockers. Urban cells have been shown to be a special case where no single attribute shares common characteristics with other cell types. While this analysis is confined to the UK, findings are based on a sufficiently large dataset to be meaningful and applicable to equivalent environments or geographies such as other major European towns and cities.

In publishing the geo-spatial statistics for the cell site and cell environment characteristics of a real mobile network it is envisaged that further such work could be conducted using only stochastic models underpinned by the probabilistic spatial distributions of the real network properties outlined - i.e. without need for the underlying physical model or datasets. In addition, any further contributions made throughout this work in the areas of network deployment modelling and line-of-sight probability modelling are strengthened through statistical evidence of scalability in commercial networks.

Chapter 4

Macro Cell Line-of-Sight

In this chapter the statistical likelihood of achieving line-of-sight (LoS) conditions from existing macro cell base station locations is explored. The approach considers the use of lamp post sites as potential new infrastructure sites where future small cell or TRP radio nodes could be sited in order to densify the mobile network and enhance aggregate capacity. As such, the LoS path between existing macro cell sites and lamp posts represent a potential high frequency wireless transport connectivity solution for fronthaul / midhaul / backhaul (collectively referred to as xhaul) of dense cell deployments. Analysis is built on the high resolution (0.25 - 1 m) 3D digital surface model from the previous chapter which is based on real network and environmental datasets. In addition, supporting field measurements are used to validate the accuracy of calculated LoS predictions.

4.1 Introduction

The capacity demand on cellular networks is the fundamental factor driving spectrum usage into ever higher bands. This is the case both for access bands operated on the RAN but also the wireless transport bands needed to connect the RAN sites as described in Chapter 2. This has been no more evident than in the adoption of mmWave spectrum for access technologies in 3GPP standards as of release 15 [51]. Whilst progression towards mmWave radio in both access and transport networks promise a step change in capacity resulting from larger channel bandwidth availability, it equally presents significant deployment challenges relative to lower frequency bands [52]. A high path loss exponent ($n \geq 2.55$ [53]), susceptibility to blockage and unfavourable diffraction properties as well as poor in-building penetration characteristics [54] present coverage constraints for conventional outdoor environments.

Accurate deployment modelling and reliable system level assessments in built up environments remain the same regardless of how mmWave spectrum is ultimately utilised. Although the non line-of-sight (NLoS) or near line-of-

sight (nLoS) propagation characteristics of high frequency radio systems have been experimentally proven in real environments [54] [55] [56], the accuracy of corresponding theoretical predictions is not well reported particularly at scale. It is often the resolution of the radio planning or simulation environment relative to the frequencies of interest ($\lambda = 0.012$ m for lowest 3GPP FR2 access band and $\lambda = 0.004$ m for lowest E-band transport band) that is the fundamental barrier to reliable exploitation of NLoS propagation paths in commercial deployments. Collection of environmental data sufficient to more accurately predict mmWave diffraction, scattering and reflection characteristics is generally considered cost prohibitive and as such the desired service availability targets underpinning new technology investments may only be achieved in the LoS case. In its fundamental form, the LoS evaluation can be considered frequency independent (near optical), however the underlying practical validity of any LoS assessment should be considered as a function of frequency owing to the necessary Fresnel zone clearance requirements.

In this chapter, the direct applications of mmWave spectrum on (or co-located with) macro cell base station sites is assessed. The LoS probability statistics are used as a metric to assess deployment viability of specific mmWave use cases. For the primary use case under consideration the relevance of the LoS statistics to the transport network (TN) is examined. To compliment this, the relevance to the radio access network (RAN) is the also considered. In the RAN case, the assumed underlying technology is mobile access at bands around 26 GHz where the LoS probability represents an approximation of coverage availability. For such applications, the assessment is for LoS validity to slow moving or static user equipment (UE) at heights of $\sim$1.5 m for pedestrians on the pavement and $\sim$5 m for fixed wireless access (FWA) terminals affixed to roadside buildings. In the TN case, the role of macro cell sites as wireless transport hubs for future dense network deployments is examined. Here, the LoS probability to street level infrastructure sites such as lamp posts represent the opportunity of using mmWave links for backhaul / midhaul / fronthaul to a large number of new cooperative radio nodes close to the end user. In this scenario the macro site may provide a (first hop) wireless connectivity solution to either mmWave integrated access and backhaul (IAB) nodes [57] or conventional small cells / TRPs in a C-RAN architecture connected by dedicated high frequency transmission bands such as E-band, W-band or D-band. These fixed service bands promise a low latency high capacity wireless transport capability able to support fronthauling of lower layer functional split interfaces to new radio nodes [20]. A deployment topology where existing (or larger) macro cell sites evolve to become coordinating nodes (CU or DU locations) could be logically more favourable from a capacity, latency and synchronisation perspective over traversing large scale fronthaul connections deeper into the network. It is envisaged that such macro sites could offer favourable edge node aggregation points for emerging ultra dense network architectures

where the required processing and resource management capability for a multitude (cluster) of cooperative cells can be coordinated.

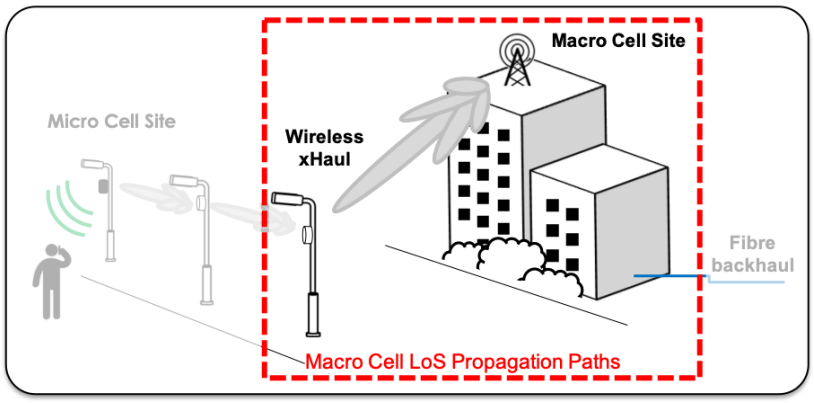

Figure 4.1: Macro cell LoS scenario.

To address these scenarios, the DSM environment is used to derive the LoS paths and the resulting statistical data sets. The primary objective of this chapter is the transport network use case detailing results for LoS between real lamp posts and macro cell masts in urban, suburban and rural cell types. These results are evaluated against recognised and published LoS probability models. Analysis of the radio access network use case is a by-product of the primary transport scenario but is nevertheless valuable in the context of real-world LoS probability analysis.

4.2 Macrocell Line-of-Sight Probability Models

Development of statistical channels models such as the LoS probability model has arisen through the need to treat the path loss exponents of LoS and NLoS cases differently. The LoS probability model describes the likelihood $\Pr_{\text{LOS}}$ of an endpoint being in clear LoS of the base station as a function of the two dimensional distance d_{2D} (in metres) between them. The probability for LoS or NLoS therefore depends on the various environmental factors, including building clutter, endpoint height, and distance as characterised in Chapter 3.

The model definitions adopted into standards are typically evolutions of the same form and are based on stochastic approaches inherited from historic 2D models which inherently do not consider the relative environmental clutter dimensions [59]. In recent years, most focus has been on the urban macro LoS scenario. The UMa LoS probability model was first adopted as part of the 3D channel model definition in 3GPP release 12 based on ITU and WINNER II definitions [37][60]. These definitions did not originally account for the influence of the endpoint height h_{UT} (in metres) which was subsequently introduced in the form of (4.1) in 3GPP TR 36.873 [61] and later 3GPP TR 38.900 / 38.901

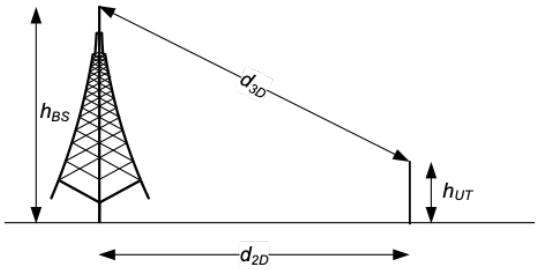

Figure 4.2: LoS probability scenario from [58].

[58]. These revisions were derived using ray-tracing techniques of a simulated urban environment with uniformly distributed building heights between 15 and 25 m, d_1 and d_2 fitting parameters together with a compensation term $C\prime(h_{UT})$ were included to account for inaccuracies in the base model above 13 m [62]. Significant effort has been applied to experimental verification and optimisation of the UMa case in recent years primarily resulting from a focused effort on feasibility of mmWave 5G mobile access where coverage characteristics are principally considered LoS dependent. Further revisions to the parametrisations of the UMa model, the 'd_1/d_2' model in (4.2) have subsequently been proposed [63] including the addition of a squared term modifier for increased resolution [64] in the New York University 'NYU squared' model (4.3). These proposals have been derived primarily from map based analysis or measurement campaigns of dense urban Manhattan grid style environments.

Conspicuous by its absence is a 3GPP recognised LoS probability model for the suburban macro (SMa) scenario which typically accounts for a higher proportion of cells in a European network as demonstrated in Chapter 3. The suburban case has a basic definition in the WINNER II channel model [60] although this was not brought forward into ITU recommendations or 3GPP guidelines.

While a dedicated rural macro (RMa) model is defined in 3GPP, there has been little development or experimental characterisation of the rural case since its adoption as part of the wider 3D channel model into 3GPP guidelines. The RMa LoS model was again adopted from historical ITU and WINNER empirical models based on relatively limited data sets and specific assumptions or approximations regarding the location of terrain and obstacles in the direct path. The result is the relatively simple definition in (4.4) which offers no fitting parameters or variables to account for endpoint height profile. These notable and recognised LoS probability models are outlined in Table 4.1 and assessed as part of the environmental simulation analysis in Section 4.4.

Table 4.1: Macro Cell Line-of-Sight Probability Models.

Model	Definition	Parameters
3GPP (UMa) [58]	$\Pr_{\text{LoS}} = \begin{cases} 1, d_{2D} \leq 18m \\ \left(\frac{d_1}{d_{2D}} + \exp\left(-\frac{d_{2D}}{d_2}\right)\left(1 - \frac{d_1}{d_{2D}}\right)\right) \\ \cdot \left(1 + C'\left(h_{UT}\right)\frac{5}{4}\left(\frac{d_{2D}}{100}\right)^3 \exp\left(-\frac{d_{2D}}{150}\right)\right), 18m < d_{2D} \end{cases}$ $Where$ $C'^{(h_{UT})} = \begin{cases} 0, h_{UT} \leq 13m \\ \left(\frac{h_{UT}-13}{10}\right)^{1.5}, 13m < h_{UT} \leq 23m \end{cases}$ (4.1)	$d_1 = 18$ $d_2 = 63$
d_1/d_2 (UMa) [63]	$\Pr_{\text{LoS}} = \min\left(\frac{d_1}{d_{2D}}, 1\right)\left(1 - \exp\left(-\frac{d_{2D}}{d_2}\right)\right) + \exp\left(-\frac{d_{2D}}{d_2}\right)\left(1 + C'\left(h_{UT}\right)\right)$ (4.2)	$d_1 = 20$ $d_2 = 66$
NYU Squared (UMa) [64]	$\Pr_{\text{LoS}} = \left(\min\left(\frac{d_1}{d_{2D}}, 1\right)\left(1 - \exp\left(-\frac{d_{2D}}{d_2}\right)\right) + \exp\left(-\frac{d_{2D}}{d_2}\right)\left(1 + C'\left(h_{UT}\right)\right)\right)^2$ (4.3)	$d_1 = 20$ $d_2 = 160$
3GPP (RMa) [58]	$\Pr_{\text{LoS}} = \begin{cases} 1, d_{2D} \leq 10m \\ \exp\left(-\frac{d_{2D}-10}{1000}\right), 10m < d_{2D} \end{cases}$ (4.4)	None

4.3 Simulation Environment

In order to assess the large scale LoS statistics representative of a national network, a deterministic simulation approach is developed built on the 3D DSM environment. The DSM is complemented with 3D projections of local authority street lighting and lamp post sites at their native heights collected throughout the 1875 sq km study area and within coverage of the 2154 macro cell sites. Only lamp post and street infrastructure sites within the Borough of London Westminster are excluded (withheld) from the analysis. As the DSM is a re-sampled model of a range of distinct LIDAR surveys with resolutions of 0.25 m, 0.5 m and 1 m some

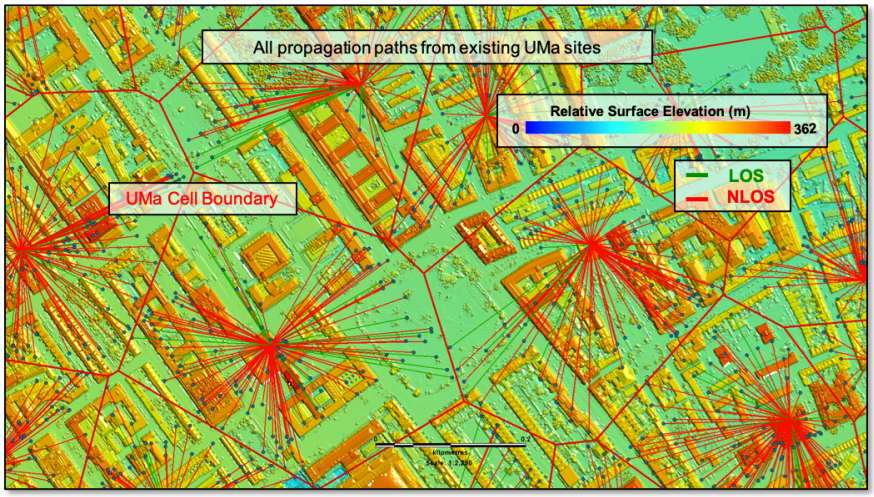

Figure 4.3: DSM 2D graphical representation of urban London.

areas represent lower resolution than others. Typically the highest resolution areas are those covered by significant geographic features, rivers and floodplains with lowest resolution being used in sparsely populated rural areas. As a result, any LoS propagation analysis is assumed to have a worst-case error margin in areas covered exclusively by the 1 m resolution LIDAR surveys where it is assumed to be no more than +/- 0.5 m, this accounts for 52% of the DSM model area. A total of 41% of the model area is covered by 0.5 m resolution and 7% by the highest 0.25 m resolution. A basic ray tracing technique is utilised for the LoS propagation path analysis where vector lines are constructed between each macro site and all lamp posts within its Voronoi coverage area where it is assumed to be the best server. The propagation path between base station height and each corresponding lamp post height is only validated where no pixels in the propagation path are intersected by the underlying surface model (i.e. buildings / terrain etc) as in Fig. 4.3. Whether validated as LoS or nLoS, all path properties including 2D and 3D distance are recorded.

4.4 Lamp Post Endpoints

In total, LoS validation was carried out between existing macro sites and over 250,000 lamp posts to evaluate the validity of the published LoS models for a real UK network. The distribution profiles of lamp post height properties are highlighted in Fig. 4.5 and the proximity to their serving cell in Fig. 4.6. The utilisation of lamp post data in this study is key, not only does it provide insight into the viability of wirelessly aggregating backhaul or fronthaul from new low power street cells to macro sites as discussed in Section 4.1 and highlighted in Fig.

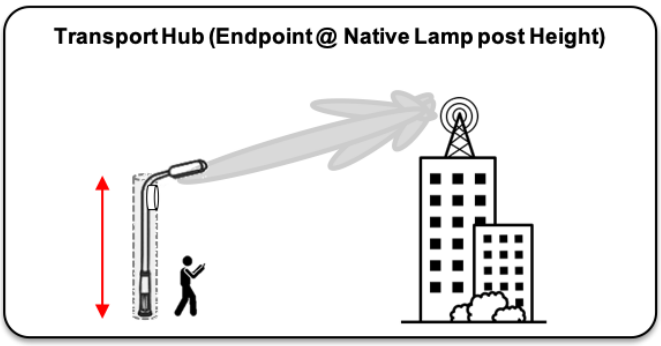

Figure 4.4: Transport hub scenario between macro cell roof top and lamp post.

4.4, but the lamp posts also act as a credible proxy for many alternative mmWave use cases. Characterisation of the height characteristics of the lamp post dataset in Fig. 4.5 provide understanding of the likely heights at which a new small cell radio could potentially be installed for each cell classification. In addition, the proximity to its nearest existing cell site in Fig. 4.6 provides a useful approximation of the variation in link lengths that may be required if such a cell were to be connected via a wireless link to an existing cell site. Furthermore, small variations in the spatial properties of this dataset allow the lamp post locations to be used as an accurate and representative sample point across the coverage environment for evaluation of the radio access network use cases also considered in Section 4.1.

For the radio access network case, the endpoints can be considered representative of an outdoor user distribution (although not user density distribution) since these data points are logically equivalent to the flow of outdoor mobile user terminals in a real network. As such, any associated theoretical modelling of the outdoor mobile user scenarios could also be aligned to the distributions describing the proximity of lamp posts to the serving cell in Fig. 4.6 rather than assumed random and uniformly distributed as per ITU and 3GPP simulation guidelines.

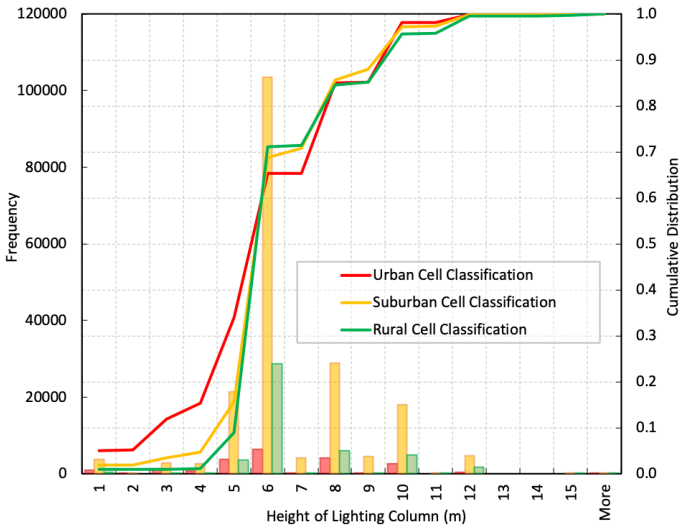

Figure 4.5: Lamp post native height distribution.

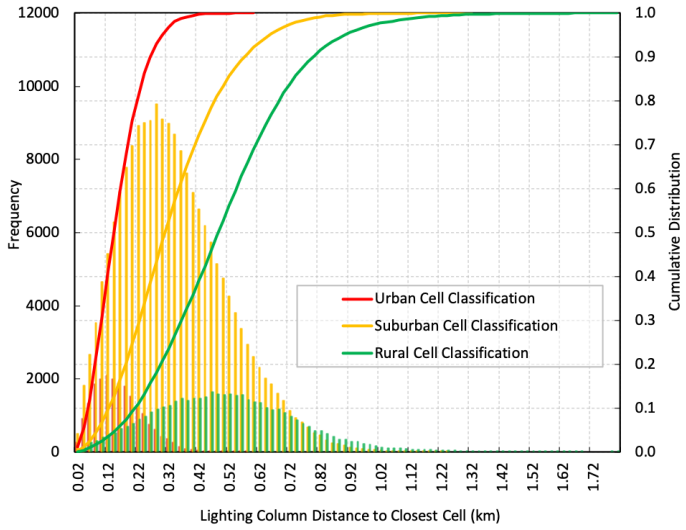

Figure 4.6: Lamp post proximity to nearest cell distribution.

Examination of the height distribution of the real lamp posts in Fig. 4.5 shows that 99.9% of the data points are below a height of 13 m. This is significant as the existing LoS probability models outlined in Table 4.1 would have no contribution from the height profile term $C'^{(h_{UT})}$ for data points below 13 m. As a result, the LoS probability for the entire lamp post dataset, regardless of individual height, would remain solely a function of the distance from the base station.

4.4.1 Urban Scenario

Firstly, the results for LoS probability across all urban classified cells are considered. All urban classified paths are aggregated and the probability of achieving a clear LoS as a function of the distance to the serving macro cell outlined in Fig. 4.7. In order to maintain statistical relevance for any distance intervals with a lower number of data points, a uniform data point count sampling approach is used across the x-axis as opposed to uniform distance sampling. The published models relevant to the UMa scenario from Table 4.1 are also overlaid using both the recommended values for the parameters d_1 and d_2, as well as optimised values achieved through minimisation of mean squared error (MSE) to the DSM data which are also summarised in Table 4.2. Optimisation of the existing model fitting parameters result in the same probability distribution for each model where $d_1 = 0$ and $d_2 = 44$, this is to be expected as these models are based on the same fundamental derivation.

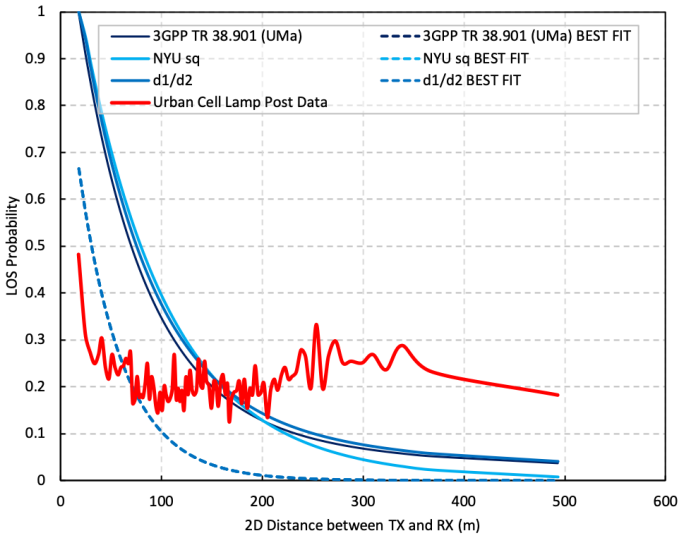

Figure 4.7: LoS probability of urban lamp posts.

Table 4.2: Urban Macro Line-of-Sight Probability Results.

Model	Parameters		MSE
3GPP UMa [58]	Default	$d_1 = 18$ $d_2 = 63$	3.88
	Best Fit	$d_1 = 0$ $d_2 = 44$	0.54
d_1/d_2 [63]	Default	$d_1 = 20$ $d_2 = 66$	4.57
	Best Fit	$d_1 = 0$ $d_2 = 44$	0.54
NYU (Squared) [64]	Default	$d_1 = 20$ $d_2 = 160$	5.05
	Best Fit	$d_1 = 0$ $d_2 = 44$	0.54

In all cases, existing model definitions show poor agreement with the calculated data set which demonstrate a much lower LoS probability towards the cell centre (within ∼150 m) with a peak probability of only 0.48 within 20 m. Results also demonstrate a much flatter profile across the remaining cell radius rather than the exponential decay of existing models. On average 22% of urban lamp posts within the towns and cities analysed could achieve LoS to their serving macro site. These findings are significant as they emphasise that any subsequent modelling or deployment analysis based solely on the recognised model definitions would be inaccurate or invalid for a typical UK urban environment.

4.4.2 Suburban Scenario

The equivalent LoS probability results for suburban cells are highlighted in Fig. 4.8 and the tabulated results with parameter fitting detailed in Table 4.3. No formal LoS model for suburban macro cell is recognised in 3GPP or ITU recommendations and so data results have been evaluated against the equivalent urban models in Table 4.1. As with urban results the suburban case demonstrates a poor fit against the published models even after optimisation. This further highlights the need for a formally recognised definition which can better describe the statistical properties of real network deployments. Overall, the suburban environment provided the highest probability of achieving clear light of sight with 34% of lamp posts successful across the entire DSM study area.

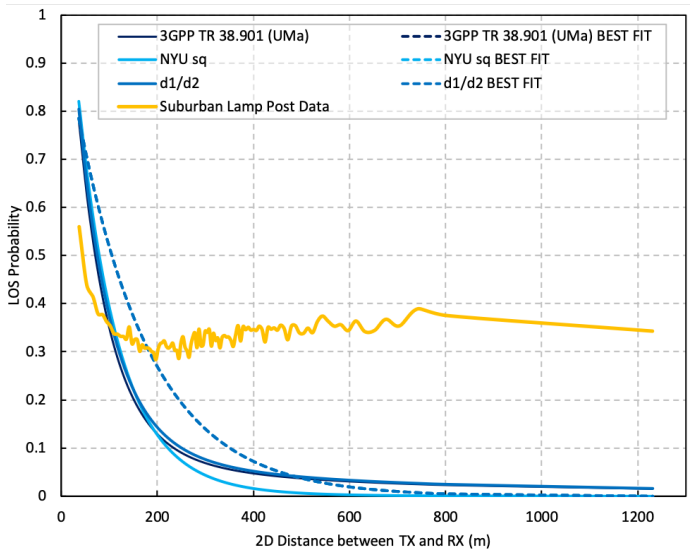

Figure 4.8: LoS probability of suburban lamp posts.

Table 4.3: Suburban Macro Line-of-Sight Probability Results.

Model	Parameters		MSE
3GPP UMa [58]	Default	$d_1 = 18$ $d_2 = 63$	1.38
	Best Fit	$d_1 = 0$ $d_2 = 153$	0.69
d_1/d_2 [63]	Default	$d_1 = 20$ $d_2 = 66$	1.25
	Best Fit	$d_1 = 0$ $d_2 = 153$	0.69
NYU (Squared) [64]	Default	$d_1 = 20$ $d_2 = 160$	1.54
	Best Fit	$d_1 = 0$ $d_2 = 305$	0.69

4.4.3 Rural Scenario

Rural cell results are shown in Fig. 4.9 and tabulated in Table 4.4. There are no optimisation parameters available for curve fitting in the RMa model resulting in a best case MSE of 9.19 and an overall LoS probability of 28% across the rural dataset. As such, the results for the rural scenario represent the most inaccurate model definition relative to the dataset. These finding further highlight the importance of following a deterministic approach in this work rather than reliance on system level simulations based on stochastic model approximations which have been shown to be unreliable for the UK environment.

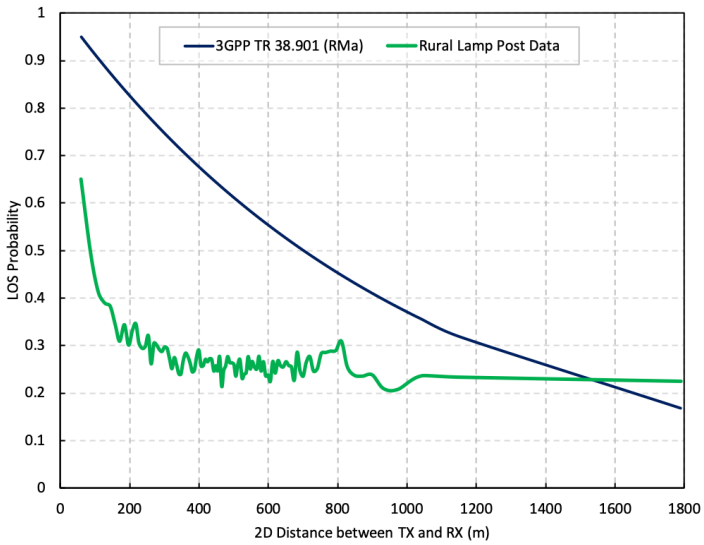

Figure 4.9: LoS probability of rural lamp posts.

Table 4.4: Rural Macro Line-of-Sight Probability Results.

Model	**Parameters**		**MSE**
3GPP RMa [58]	Default	None	9.19

4.4.4 Experimental Measurement Verification

The results highlighted in Section 4.4.1 - 4.4.3 are simulated results based on the DSM environment. To further understand the reliability of these results a measurement campaign aimed at validating LoS prediction accuracy from the DSM environment is also undertaken. A total of 68 measurement points were assessed over two live suburban cell site locations included within the study area during scheduled outage periods. The two sites where the measurements were taken were covered by a 0.5 m resolution area in the DSM. Two measurement methodologies were assessed: a 1-way LoS verification and a 2-way LoS verification. In the 1-way case, the LoS verification is conducted from the base station end with a telephoto camera towards a surveyor with a LoS spotting lamp at the 'terminal' end. In the 2-way case, cameras and spotting lamps were utilised at each end of the link as in Fig. 4.10. The majority of measurements 66%, were completed with the 1-way setup as this was deemed to be sufficiently accurate based on initial measurements and permitted more time for additional data points to be collected. In both scenarios, measurements are conducted at the localised height of the base station antenna and at 5 m at the 'terminal' end using a pole mounted camera and LoS spotting lamp. In total, 94% of the measurement locations distributed around the cell sites agreed with the DSM prediction. In the majority of the

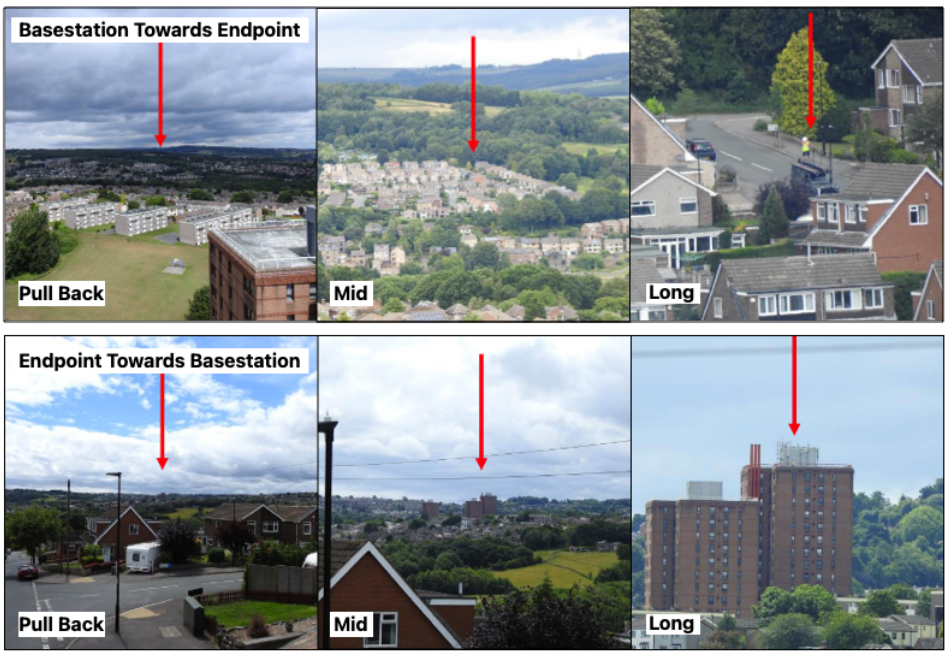

Figure 4.10: The 2-way LoS validation measurement.

incorrectly predicted locations the measurement team cited localised blockages close to either end of the propagation path as the primary factor. Such blockages were likely either blockages below the resolution of the DSM or foliage growth which has occurred between the LIDAR survey date and the measurement date (approximately 18 months). In addition, 15% of the measurement locations were also flagged as subjectively having the potential for Fresnel zone blockage for lower mmWave bands (namely 26 GHz). While these paths would likely not present an issue at higher fixed service transmission bands foreseen as promising fronthaul connectivity solutions (71 GHz E-band to 174 GHz D-band) findings do emphasise the suitability of the modelling methodology when considering frequency bands or link distances where the required Fresnel zone clearance approaches the assumed error margin in the deployment model.

4.5 Generalised Endpoint Height

Here, the generalised LoS case is considered in order to determine the influence of the endpoint height on LoS probability. This is achieved by reconfiguration the same lamp post dataset within the DSM but with modifications to the 3D height profiles. In the generalised case, all endpoint locations are reconfigured for a consistent height at increments between 1.5 m and 10 m above ground as

highlighted in Fig. 4.11. The objective of analysing the full spread of endpoint heights is to form a statistical view of how the end point height influences the LoS likelihood in environments where the clutter information is already defined in Chapter 3. The lowest height considered is 1.5 m which is representative of end user equipment applicable to mobile access use cases and the upper bound of 10 m represents the maximum height at which ITU / 3GPP consider a micro cell to be installed.

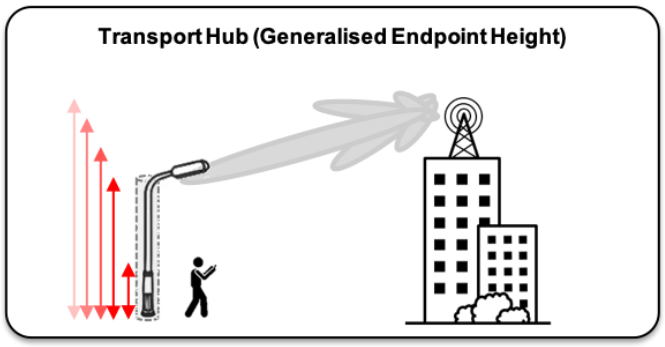

Figure 4.11: Transport hub scenario between macro cell and a specific height endpoint.

The resulting (height specific) LoS probability curves for UMa cells is shown in Fig. 4.12 with the corresponding SMa and RMa scenarios in Fig. 4.13 and Fig. 4.14 respectively. For each cell classification, the significance of endpoint height is evident through the spread of results. This further emphasises the need for a model that accurately reflects such end point height variation at street level which are absent in existing models for heights below 13 m. In addition, the absence of a recognised SMa definition and an over simplified RMa definition suggest integration of deployment scenarios in to a common model definition is feasible and could further streamline future refinements. Consequently, a new model is proposed in (4.5) based on heuristic parameter estimation and minimisation of the mean squared error curve fitting of the DSM results. The resulting predictions are overlaid in Fig. 4.12 - 4.14 with the mean squared error results and associated parameter optimisation values summarised in Table 4.5. The 'BT LoS' model definition in (4.5) follows the 3GPP LoS model form built on the product of two probability components but with modified parametrisation to account for the different deployment scenarios (a_1, a_2, a_3, c_1, c_2, d_1, d_2) and linear scaling variables $C'^{(h_{UT})}$ and $D'^{(h_{UT})}$ in each component to account for end point height variation. Analysis is currently confined to, and validated for, endpoint heights up to 10 m as this is the antenna height assumed by 3GPP for urban micro cell (UMi) deployments. The proposed model demonstrates good agreement for all h_{UT} up to 10 m albeit with reduction in accuracy for cell edge probabilities as endpoint height increases.

$$\begin{aligned}\mathrm{Pr}_{\mathrm{LoS}} = &\left(\frac{D'\left(h_{UT}\right)}{d_{2D}} + \exp\left(-\frac{d_{2D}}{a_1}\right)\left(1 - \frac{D'\left(h_{UT}\right)}{d_{2D}}\right)\right) \\ &\cdot \left(0.4 + C'\left(h_{UT}\right)\frac{5}{4}\left(\frac{d_{2D}}{a_2}\right)^3 \exp\left(-\frac{d_{2D}}{a_3}\right)\right) \\ &Where \\ &C'\left(h_{UT}\right) = \left(c_1 h_{UT}\right) + c_2 \\ &D'\left(h_{UT}\right) = \left(d_1 h_{UT}\right) + d_2\end{aligned} \tag{4.5}$$

Analysis of the DSM dataset crucially highlight distinct characteristics of increased probability and a local maximum toward the cell mid-point for endpoint heights 5 m and above. This is a property evident in all cell classification types resulting in the probability distribution functions becoming more clearly bi-modal rather than the assumed negative exponential form in current models. This characteristic is attributed to the point at which the endpoint height approaches that of the building height profile of the surrounding environment as building heights reduce with proximity to the cell centre. The clutter properties including the building height, size and density distribution profiles in the equivalent areas covered by the DSM have previously been analysed in Chapter 3. Crucially, these earlier findings further explain the higher variability observed in the urban LoS probabilty profile in Fig. 4.12 relative to the other cell classifications.

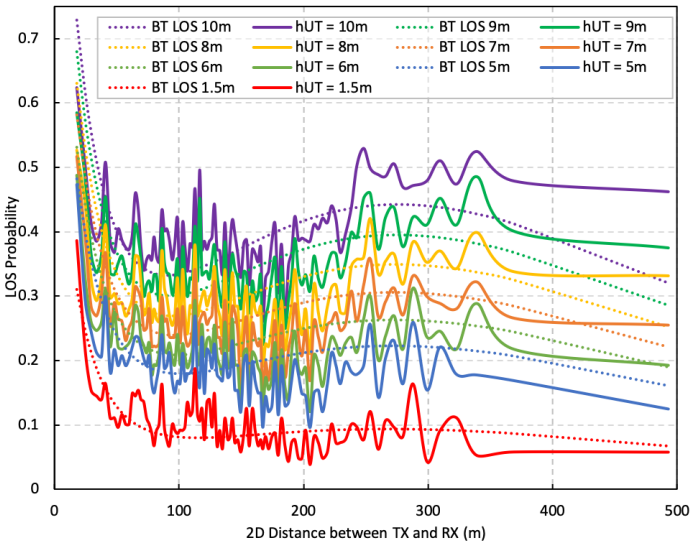

Figure 4.12: Urban height dependent LoS probability.

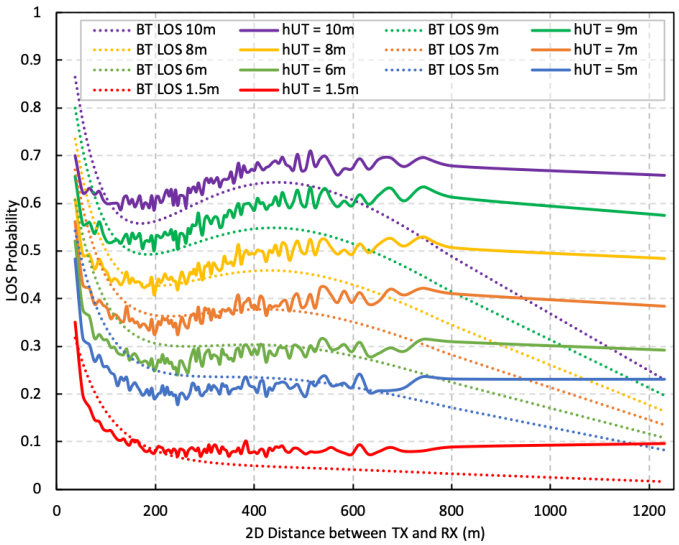

Figure 4.13: Suburban height dependent LoS probability.

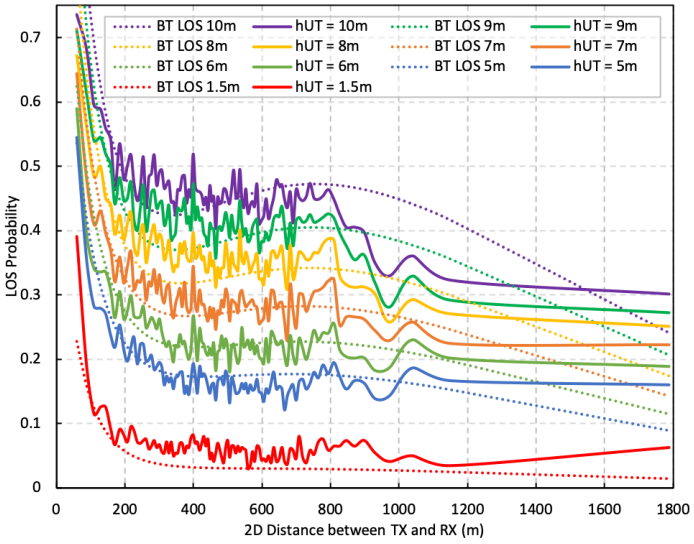

Figure 4.14: Rural height dependent LoS probability.

Table 4.5: Parametrisation of the BT Macro Cell Line-of-Sight Probability Model.

Model	Parameters	Height	MSE
BT LoS (UMa)	$a_1 = 20$	$h_{UT} = 1.5m$	0.07
	$a_2 = 95$	$h_{UT} = 5m$	0.08
	$a_3 = 150$	$h_{UT} = 6m$	0.09
	$c_1 = 0.013$	$h_{UT} = 7m$	0.10
	$c_2 = 0.38$	$h_{UT} = 8m$	0.13
	$d_1 = 3.69$	$h_{UT} = 9m$	0.52
	$d_2 = 5.47$	$h_{UT} = 10m$	0.19
BT LoS (SMa)	$a_1 = 70$	$h_{UT} = 1.5m$	0.03
	$a_2 = 192$	$h_{UT} = 5m$	0.18
	$a_3 = 257$	$h_{UT} = 6m$	0.17
	$c_1 = 0.039$	$h_{UT} = 7m$	0.11
	$c_2 = 0.21$	$h_{UT} = 8m$	0.08
	$d_1 = 14.26$	$h_{UT} = 9m$	0.10
	$d_2 = -3.49$	$h_{UT} = 10m$	0.12
BT LoS (RMa)	$a_1 = 60$	$h_{UT} = 1.5m$	0.07
	$a_2 = 235$	$h_{UT} = 5m$	0.02
	$a_3 = 440$	$h_{UT} = 6m$	0.04
	$c_1 = 0.01$	$h_{UT} = 7m$	0.06
	$c_2 = 0.09$	$h_{UT} = 8m$	0.11
	$d_1 = 20.86$	$h_{UT} = 9m$	0.15
	$d_2 = -12.21$	$h_{UT} = 10m$	0.15

4.6 Chapter Summary

In this chapter, the LoS statistical channel model is evaluated using a representative 3D environmental model of a mobile network in the UK. Existing LoS probability models were assessed against the digital surface model using real lamp post locations and heights as representative outdoor data points distributed throughout the coverage environment of the network. The primary deployment architecture represented in this chapter is the use of macro cell sites as potential aggregation hubs for wireless transport systems. In this scenario, each macro site could support onward densification of the radio access network through proliferation of lower power street level small cells where the ability to achieve a LoS path to a lamp post represents a potential high frequency transport link to a street level small cell.

Results have demonstrated that existing industry recognised LoS probability models are unsuitable for LoS predictions for all cell types when applied to a real network topology and geographic topography. As a result, the use of existing LoS probability models is insufficient for evaluation of use cases such as mmWave transport solutions between existing macro sites and new street infrastructure locations which may underpin future cell densification or deployment architectures. These findings are further supported with experimental verification

of the methodology used, implying a revised statistical model suitable for such theoretical deployments is required. By extending the analysis to account for height dependency of the endpoint, a new model is proposed which accounts for height attributes of the endpoint below 10 m (absent in existing model definitions). In addition, the newly proposed model integrates urban, suburban and rural deployment scenarios into one common definition. The proposed 'BT LoS' model demonstrates good agreement for all scenarios allowing a wide range of use cases to be analysed at scale. The findings contribute insight into the fundamental propagation characteristics of real mobile networks including large scale parameter assignment for LoS and NLoS propagation conditions.

With the potential to extend the existing macro cell transport network to street level using high frequency system now characterised, the opportunity to further extend the footprint of the transport network at street level can be assessed. Results in this chapter suggest the use of macro cells could be of value as a first hop transport link if onward wireless meshing or multi-hop wireless solutions to further extend reach are feasible. This scenario can be characterised using a complimentary micro cell LoS probability model investigated in the next chapter.

Chapter 5

Micro Cell Line-of-Sight

This chapter aims to understand the large scale feasibility of high frequency wireless transport distribution at street level and within street canyons. To understand this scenario the same a high resolution 3D DSM model is used to conduct large scale ray-tracing of direct propagation paths between neighbouring lamp posts. These paths serve as a representation of mmWave multi-hop, relay or self-backhauling small cells nodes. The statistical properties of the propagation paths are assessed against recognised line-of-sight probability models for the micro cell scenario. Contributions as outlined in this chapter again have application in analytical studies aiming to understand the statistical characteristics of unobstructed high frequency 'access' links between micro cell sites and end users as well as 'transport' xhaul links between neighbouring micro cell sites in a multi-hop or mesh street canyon deployment.

5.1 Introduction

As discussed previously, capacity growth through increased cell density may improve spectral efficiency but is often challenging from a cost perspective when considering conventional roof top or tower top macro cell deployments. This is particularly the case in urban / metropolitan environments [65]. For this reason, it is recognised that the use of low power street level small cells close to the end user allows for improved signal quality and spectral reuse is beneficial (owing to the limiting street canyon propagation characteristics). Use of street level infrastructure sites to locate new cells also offers the potential for simplified and lower operational costs resulting from fewer landlords and greater choice of locations - i.e. local authorities who may own suitable street infrastructure sites such as lamp posts.

The application of shorter range mmWave FR2 5G access bands (24.25 – 52.6 GHz) in mobile networks fits well with the street level deployment model referred to in 3GPP and ITU as urban micro cell (UMi) [37]. In particular, analytical models

such as the line-of-sight probability model, although frequency independent, align well with the challenging propagation characteristics of mmWave bands which are predominately characterised by the unobstructed line-of-sight component [66]. The marrying of these characteristics make application of mmWave access small cells a good fit for the UMi deployment environment.

In addition, transport technology developments in 5G NR such as integrated access and backhaul (IAB) allow for simplified deployment of micro cells through the standardisation of a self-backhauling multi-hop architecture aimed at reducing the cost and complexity of street level deployments. Such an approach addresses the backhaul requirement whilst also removing dependence on costly new street level fibre connectivity where often the necessary road closures and street works are cost and time prohibitive. Similar initiatives such as LTE relay have previously been standardised in 3GPP release 9 [67] but have failed to gain traction primarily due to limited capacity (especially within a half-duplex multi-hop scenario) in bands below 6 GHz. The standardisation of mmWave FR2 bands make the IAB specification a more credible solution for multi-hop and self-backhauling small cells [68].

As part of the IAB specification, each IAB node is built on two distinct radio interface functions; a 'transport' function known as Mobile Termination (MT) which is used to maintain a wireless 3GPP F1 midhaul interface towards an upstream a IAB donor cell, and an 'access' function or Distributed Unit (DU) for maintaining a 3GPP Uu interface towards connecting user equipment (UE) or downstream MTs of other IAB nodes [57]. The line-of-sight probability model is valuable in analytical deployment studies of such multi-hop wireless transport technologies as an accurate line-of-sight probability description can provide a theoretical analysis of a mmWave IAB node access coverage as well as transport.

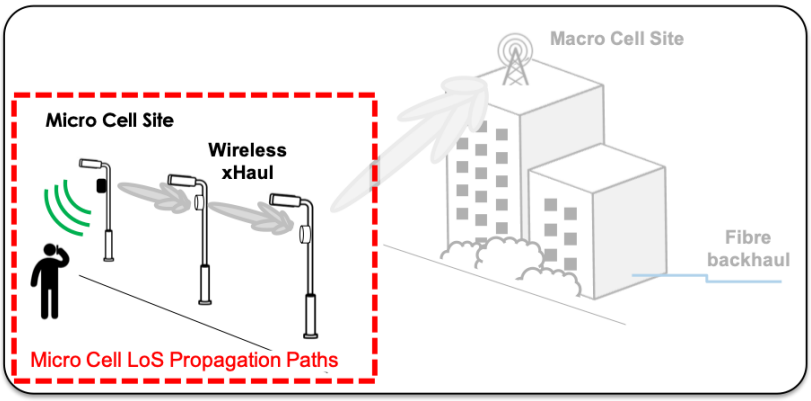

Figure 5.1: Micro cell LoS scenario.

In this chapter, the line-of-sight probability functions representative of lamp post mounted wireless transport nodes in a 3D UK urban environment are

constructed. The line-of-sight statistics of simulated high frequency xhaul nodes mounted on real lamp posts are outlined for the transport function scenario where endpoints are other multi-hop or mesh nodes mounted on the top of neighbouring lamp posts. As with the approach described in Chapter 4, the LoS path discovery in such analysis remains frequency independent and as such has application in any high frequency (LoS dependent) use case. In addition, and because of the commonality with the transport case, the access node scenario statistics are also derived representative of a lamp post hosting a mmWave small cell or RU but where the endpoint is a UE at a height of 1.5 m rather than a neighbouring lamp post. Both access and transport scenarios are assessed against recognised micro cell LoS probability models such as those adopted by 3GPP.

5.2 Micro cell Line-of-Sight Probability Models

The UMi LoS probability model definition is a derivative of the urban macro cell (UMa) case but where the base station antenna height is below the height of the surrounding buildings. In the 3GPP definition this is applicable to scenarios where the base station or transmitter is 10 m or below. The currently recognised 3GPP LoS probability model (5.1) makes up part of the 3D channel model definitions in [61] and is based on the two-dimensional ITU UMi model in [37]. Unlike the UMa definition, early ray-tracing simulations of simulated city environments suggested little impact to the LoS probability from the UMi endpoint height [69] and so the UMi definition does not include provision for endpoint height variation.

A number of revisions to the 3GPP base model have been subsequently proposed principally built on optimisation of the curve fitting parameters d_1 and d_2. The 'd_1/d_2' model (5.2) proposed by the 5G Channel Model Group in [63] revises the 3GPP fitting parameters to $d_1 = 20$ and $d_2 = 66$ based of minimisation of the mean squared error (MSE) for a range of measurement campaigns contributed by the authoring research groups. In addition, the 'NYU Squared' model (5.3) in [64] is often cited in LoS probability studies where the same base model is updated with a squaring term which permits a greater resolution when fitting to measurement data, here the default fitting parameters proposed are $d_1 = 22$ and $d_2 = 100$.

Unlike the macro cell scenario, no channel models are recognised for the suburban or rural micro cell deployment. This is fundamentally due to the historical assumption that micro cells would be a requirement exclusively for urban environments where demand, and so resulting density, is highest. As such, the larger suburban and rural environments would be expected to transition towards an urban definition as ISD decreases before there is a requirement for micro cell deployment. As a result, there are no recognised SMi (suburban micro cell) or RMi (rural micro cell) models to assess the DSM based LoS characteristics with. Despite this, these scenarios are studied in this chapter and new definitions derived

because they are still valid deployment scenario when considering future C-RAN and CF-mMIMO architectures where large scale distributed RU deployment is not economically sustainable using macro cell infrastructure such as tower tops and roof tops alone.

Each of the published LoS probability models in 3GPP and recognised derivatives are outlined in Table 5.1 and are assessed as part of the environmental simulation analysis in Section 5.4 (transport scenario) and 5.5 (access scenario).

Table 5.1: Micro Cell Line-of-Sight Probability Models.

Model	Definition	Parameters
3GPP (UMi) [58]	$\mathrm{Pr}_{\mathrm{LoS}} = \begin{cases} 1, d_{2D} \leq 18m \\ \left(\frac{d_1}{d_{2D}} + \exp\left(-\frac{d_{2D}}{d_2}\right)\left(1 - \frac{d_1}{d_{2D}}\right)\right), 18m < d_{2D} \end{cases}$ (5.1)	$d_1 = 18$ $d_2 = 63$
d_1/d_2 (UMi) [63]	$\mathrm{Pr}_{\mathrm{LoS}} = \min\left(\frac{d_1}{d_{2D}}, 1\right)\left(1 - \exp\left(-\frac{d_{2D}}{d_2}\right)\right) + \exp\left(-\frac{d_{2D}}{d_2}\right)$ (5.2)	$d_1 = 20$ $d_2 = 39$
NYU Squared (UMi) [64]	$\mathrm{Pr}_{\mathrm{LoS}} = \left(\min\left(\frac{d_1}{d_{2D}}, 1\right)\left(1 - \exp\left(-\frac{d_{2D}}{d_2}\right)\right) + \exp\left(-\frac{d_{2D}}{d_2}\right)\right)^2$ (5.3)	$d_1 = 22$ $d_2 = 100$

5.3 Simulation Environment

Analysis of the LoS propagation paths between all lamp posts in the DSM model (over 250,000) is computationally very time consuming for complete analysis.As a result, smaller representative areas of urban, suburban and rural locations are utilised for the micro cell case. In the urban scenario (UMi), Central London was chosen as a representative urban environment where the 3D DSM was augmented with real base station sites at their correct height as well as lamp post locations also at their correct height gathered from local authorities. Across the environmental model, all sites with an inter-site distance of 500 m or less were isolated as 'urban' cells and the propagation paths between lamp posts within these urban coverage areas analysed as a deterministic dataset to understand the UMi LoS probability distribution. A ray-tracing methodology was again used where all the possible direct propagation paths between each urban lamp post and any surrounding lamp posts within a 200 m radius (the inter-site distance assumed by 3GPP for UMi

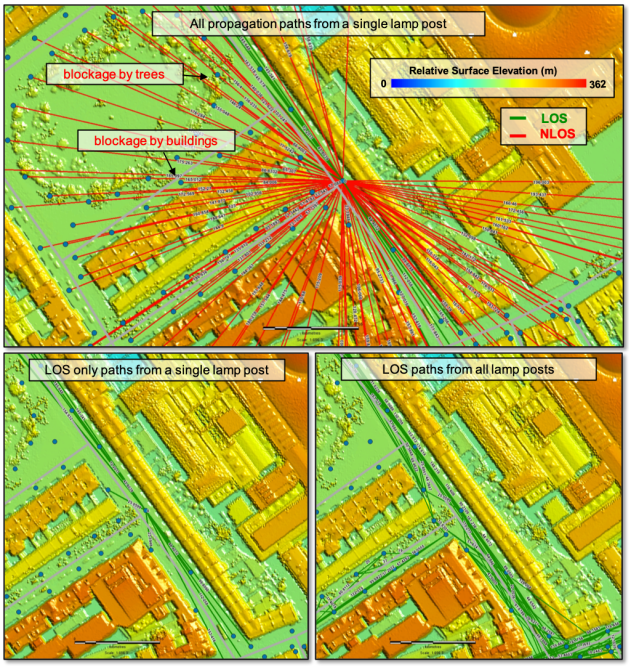

Figure 5.2: DSM LoS discovery for the micro cell scenario.

cells) analysed. In total, 837,687 direct propagation paths from 17,698 lamp posts were studied across the central London (urban) environment. Fig. 5.2 outlines a 2D view of the model as LoS and non-LoS paths are classified for a single lamp post and then iterated for the full data set to build an adjacency database of valid LoS paths and path distances between all lamp posts. In the suburban case, cells with ISD of between 501 m and 1299 m were identified primarily around the outskirts of Manchester. A total area of 18.86 sq km was used consisting of over 9858 suburban lamp posts with a total of 369,898 propagation paths analysed for LoS or NLoS paths. In the rural case, areas covered by rural macro cells (between 1300 and 1732 m ISD) were identified primarily around north Yorkshire which covered an area of 38.86 sq km with a total of 13,492 rural lamp posts. This allowed for analysis of 383,661 rural micro cell propagation paths.

5.4 Line-of-Sight Probability - Transport Node

In the transport node scenario, where the LoS path represents an xhaul transmission link between neighbouring nodes, the LoS paths are calculated between the maximum heights of individual lamp posts as in Fig. 5.3. The typical height of the lamp posts in different cell types is previously highlighted in Chapter 4 Fig. 4.5 where for urban sites the mean height is 5.5 m with a statistical mode of 6 m, for suburban a mean of 6.6 m and mode of 6 m and for rural mean of 6.6 m and mode

of 6 m. The LoS probability distribution function (PDF) is constructed by binning all propagation paths over the entire study area by path distance. For each x-axis bin, a constant number of paths is maintained resulting in a non-uniform x-axis sample interval rather than a uniform sampling approach in order to avoid any path distance intervals with statistically too few samples. Each constant sample interval is a ratio of the number validated LoS paths over the 3D DSM to non-LoS paths blocked by obstructions in the micro cell environment.

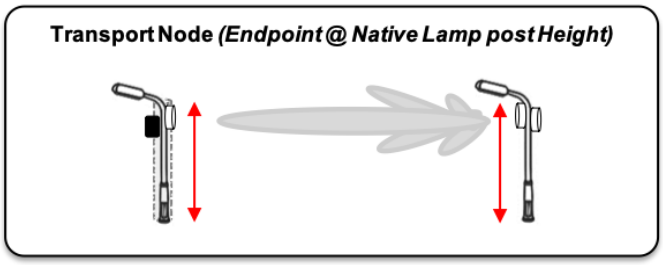

Figure 5.3: Transport node scenario between street infrastructure.

Results for LoS probability across all lamp post sites in each cell site classification within study area are outlined in Fig. 5.4 - 5.6. The existing published models relevant to the UMi scenario from Table 5.1 are also overlaid using both the recommended values for the parameters d_1 and d_2, as well as optimised values achieved through minimisation of mean squared error (MSE) to the DSM data which are also summarised in Table 5.2. Although there are no models directly comparable for the suburban and rural scenarios, the urban UMi definitions are used as a baseline reference. Whilst the default d_1 and d_2 parameters for each model demonstrate a poor fit to the simulation data set, the optimised fitted values for each urban, suburban and rural datasets are able to achieve good agreement with a MSE of 0.13 or lower. This highlights the fact that the fundamental base model on which all the models definitions are derived is sound and appropriate not only for the UMi LoS probability curve but also SMi and RMi definitions in a real UK environment. In the urban case, the 3GPP definition demonstrates a higher MSE relative to the other models primarily due to the upper bounding constraint of d_{2D} below 18 m. Investigation of short propagation paths have shown there are still a significant number of non-LoS paths within this range in urban settings typically resulting from road corner junctions and foliage blockage. In the suburban and rural cases there are statistically fewer neighbouring sites within the 18 m upper bound and so this effect is less evident. In general, the upper bounding condition of the d_1/d_2 and NYU Squared models reduce this bounding effect below 18 m providing a more appropriate fit to the underlying data. Statistically, 16% of all micro cell transport neighbour propagation paths in a urban environment are LoS, 32% in a suburban and 40% in a rural setting.

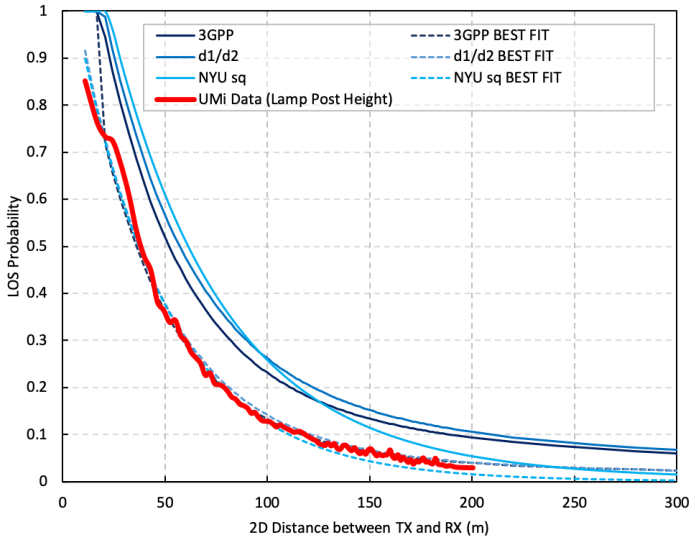

Figure 5.4: Urban transport LoS probability.

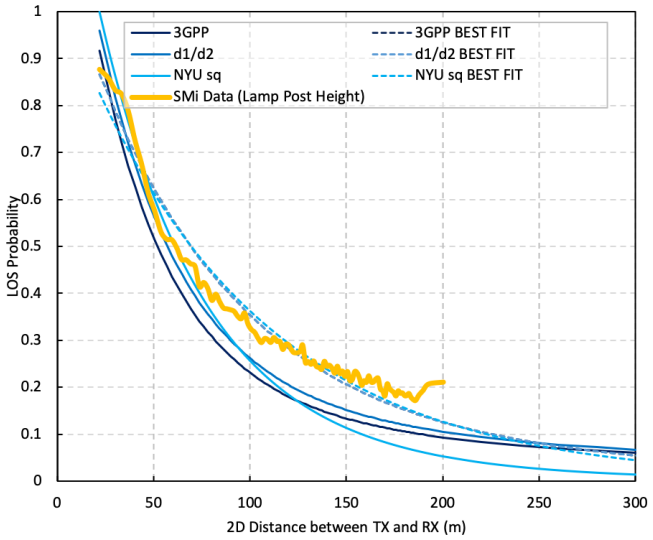

Figure 5.5: Suburban transport LoS probability.

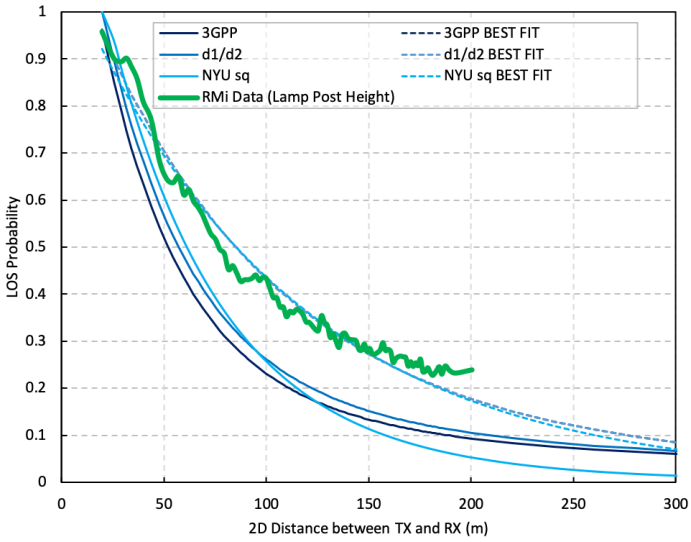

Figure 5.6: Rural transport LoS probability.

Table 5.2: Micro Cell Line-of-Sight Results - Transport Node Scenario.

		Urban		Suburban		Rural	
Model		**Params**	**MSE**	**Params**	**MSE**	**Params**	**MSE**
3GPP (UMi) [58]	Default	$d_1 = 18$ $d_2 = 36$	1.04	$d_1 = 18$ $d_2 = 36$	0.83	$d_1 = 18$ $d_2 = 36$	2.50
	Best Fit	$d_1 = 7$ $d_2 = 37$	0.10	$d_1 = 10$ $d_2 = 79$	0.11	$d_1 = 15$ $d_2 = 91$	0.09
d1/d2 (UMi) [63]	Default	$d_1 = 20$ $d_2 = 39$	1.66	$d_1 = 20$ $d_2 = 39$	0.46	$d_1 = 20$ $d_2 = 39$	1.75
	Best Fit	$d_1 = 7$ $d_2 = 39$	0.03	$d_1 = 10$ $d_2 = 79$	0.11	$d_1 = 15$ $d_2 = 91$	0.09
NYU Squared (UMi) [64]	Default	$d_1 = 22$ $d_2 = 100$	1.67	$d_1 = 22$ $d_2 = 100$	0.89	$d_1 = 22$ $d_2 = 100$	2.30
	Best Fit	$d_1 = 6$ $d_2 = 86$	0.03	$d_1 = 4$ $d_2 = 187$	0.13	$d_1 = 11$ $d_2 = 208$	0.10

■ No formal model definition available, UMi model used for reference.

5.5 Line-of-Sight Probability - Access Node

In the access node scenario, the LoS PDF where the endpoint is user equipment at a height of 1.5 m close to the lamp post data point as shown in Fig. 5.7 is considered. The same methodology as that used in the transport scenario is applied with the same dataset, the transmitter end of the propagation path is still at the native height of each lamp post but the receiver end is reconfigured for a constant height of 1.5 m above ground. This configuration represents the 3GPP Uu interface of

an IAB node which is servicing mobile terminals in the street where it is assumed that the inter lamp post propagation paths are broadly representative of LoS end user coverage.

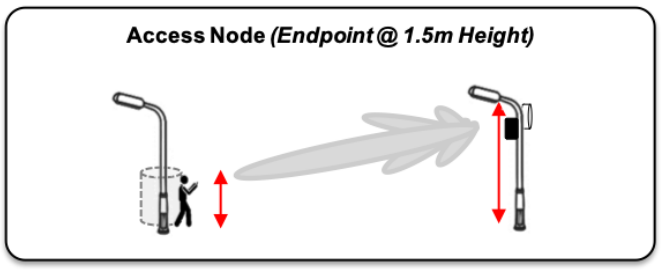

Figure 5.7: Access node scenario between street infrastructure.

The simulation results are presented in Fig. 5.8 - 5.10 and again the existing published UMi models in Table 5.1 overlaid. Although the access scenario (where the propagation path represents a street level base station to UE path) is the primary scenario considered in published models they again demonstrate a relatively poor fit to the results data with the default d_1 and d_2 parameter values. The decay profile does however align well with the simulation data set and a very good agreement ≤ 0.11 MSE can be achieved through optimisation of the fitting parameters for each scenario. A summary of the results are highlighted in Table 5.3 which again shows the d_1/d_2 and NYU Squared definitions providing best fit when new parametrisation is adopted. In total 12% of the propagation paths were classified as LoS in the micro cell access node scenario in an urban environment, 16% for suburban and 22% for rural.

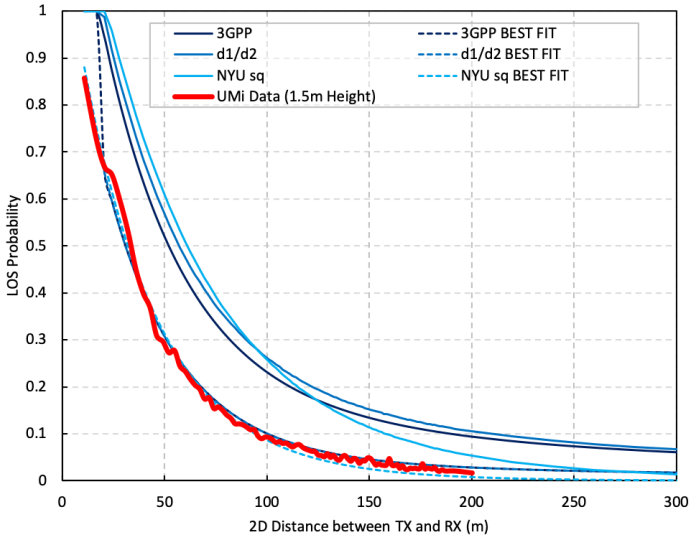

Figure 5.8: Urban access LoS probability.

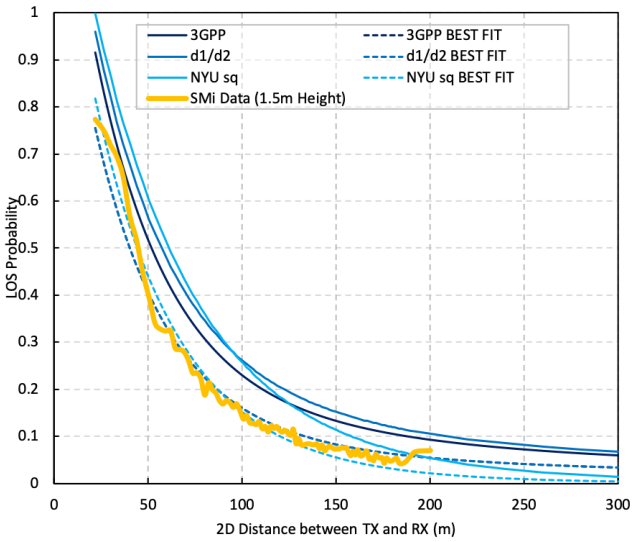

Figure 5.9: Suburban access LoS probability.

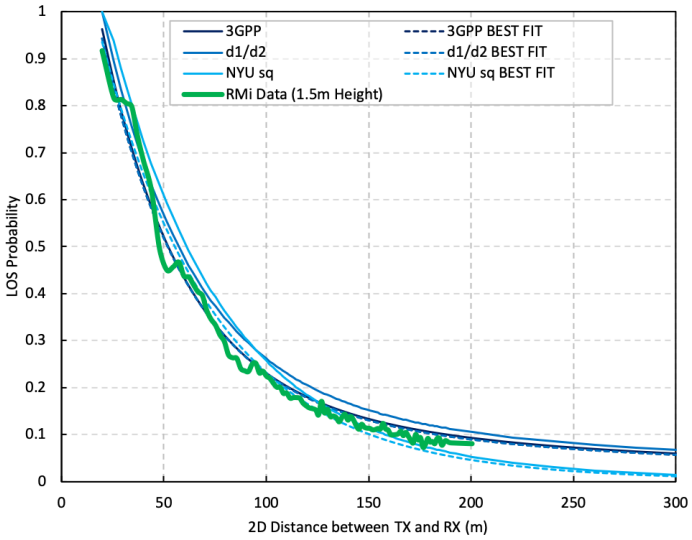

Figure 5.10: Rural access LoS probability.

Table 5.3: Micro Cell Line-of-Sight Results - Access Node Scenario.

Model		Urban		Suburban		Rural	
		Params	**MSE**	**Params**	**MSE**	**Params**	**MSE**
3GPP (UMi) [58]	Default	$d_1 = 18$ $d_2 = 36$	1.94	$d_1 = 18$ $d_2 = 36$	0.55	$d_1 = 18$ $d_2 = 36$	0.06
	Best Fit	$d_1 = 5$ $d_2 = 34$	0.11	$d_1 = 10$ $d_2 = 37$	0.06	$d_1 = 17$ $d_2 = 38$	0.06
d1/d2 (UMi) [63]	Default	$d_1 = 20$ $d_2 = 39$	2.79	$d_1 = 20$ $d_2 = 39$	1.03	$d_1 = 20$ $d_2 = 39$	0.18
	Best Fit	$d_1 = 5$ $d_2 = 34$	0.02	$d_1 = 10$ $d_2 = 37$	0.06	$d_1 = 17$ $d_2 = 38$	0.06
NYU Squared (UMi) [64]	Default	$d_1 = 22$ $d_2 = 100$	2.79	$d_1 = 22$ $d_2 = 100$	0.99	$d_1 = 22$ $d_2 = 100$	0.19
	Best Fit	$d_1 = 6$ $d_2 = 72$	0.02	$d_1 = 13$ $d_2 = 83$	0.05	$d_1 = 16$ $d_2 = 104$	0.06

■ No formal model definition available, UMi model used for reference.

5.6 Impact of Street Level Endpoint Height

The results analysis of the transport and access node scenarios in Section 5.4 and 5.5 demonstrates similar exponential decay profiles but a clear distinction in the LoS PDF curve highlighting the need for different parametrisation. The origins of the UMi LoS probability model are based on similar ray-tracing methodologies which suggested little impact of endpoint height. The finding in this analysis suggest that when considering the model as a purely access orientated scenario (i.e. to UE terminals) where only small variations of UE height are expected this is still a valid assumption. However, when broadening the model application to cover alternative deployment scenarios such as the transport or inter-micro cell paths there is a need to defined parameter sets differently.

In the street canyon environment, the transmitting endpoint is considered to be below that of the surrounding building height and as such the difference between transport and access scenarios can be assumed independent of building properties. The use of common data points in this study also isolate any impact from the layout of the street canyons themselves. As such, the differences observed between LoS paths from the top and bottom of the lamp post can be attributed entirely to the impact of street level clutter such as foliage and other street furniture where this impact is low but not negligible. As such it is prudent to differentiate these two sub cases of the micro cell LoS probability model which can also be considered the upper and lower bounds of a general micro cell LoS probability model for the UK environment. In addition, comparisons of the cell deployment environment themselves have highlighted significant differences in the LoS probability distribution. Despite the spread of environmental and endpoint height variables a good fit has been achieved with existing models for each or

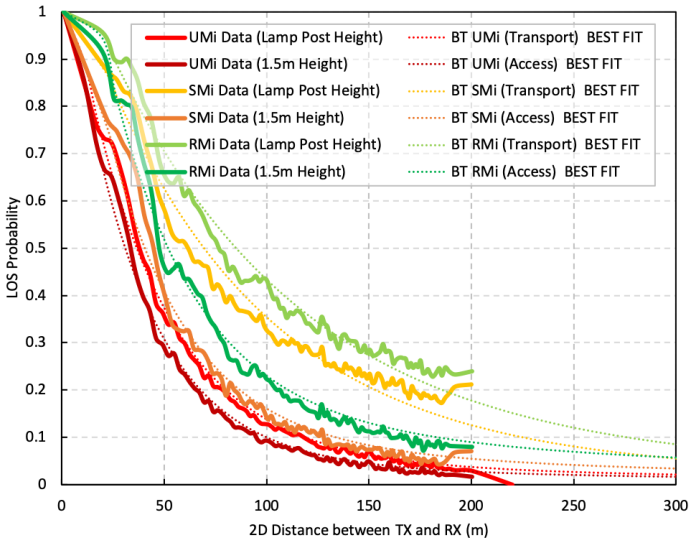

Figure 5.11: BT micro cell LoS probability model.

the urban, suburban and rural datasets. This emphasises that a common model definition is achievable that covers all scenarios as well as the height differences between the access and transport scenarios. As a result a 'BT LoS' definition of the micro cell LoS probability model is proposed in (5.4). This model is based on the d_1/d_2 definition but with revised parameters for the upper (transport) and lower (access) bounds of the model as well as the various deployment environments. The PDF of all curves against the DSM data sets are shown in Fig. 5.11 and the d_1 and d_2 optimisation parameters summarised in Table. 5.4. The proposed model aligns well with the DSM dataset achieving a MSE of 0.11 or less for every case.

$$\Pr_{\text{LoS}} = \min\left(\frac{d_1}{d_{2D}}, 1\right)\left(1 - \exp\left(-\frac{d_{2D}}{d_2}\right)\right) + \exp\left(-\frac{d_{2D}}{d_2}\right) \tag{5.4}$$

Table 5.4: Parameterisation of the BT Micro Cell Line-of-Sight Probability Model.

Model	Parameters		MSE
BT LoS (UMi)	Access	$d_1 = 5$ $d_2 = 34$	0.02
	Transport	$d_1 = 7$ $d_2 = 39$	0.03
BT LoS (SMi)	Access	$d_1 = 10$ $d_2 = 37$	0.06
	Transport	$d_1 = 10$ $d_2 = 79$	0.11
BT LoS (RMi)	Access	$d_1 = 17$ $d_2 = 38$	0.06
	Transport	$d_1 = 15$ $d_2 = 91$	0.09

5.7 Chapter Summary

In this chapter, the equivalent LoS statistical channel model for micro cell deployments in an each deployment environment classification is studied. Findings are built on a large scale deterministic methodology using a high resolution 3D environmental model with real lamp post locations. The results of a LoS propagation path analysis from urban, suburban and rural lamp post sites have shown that existing analytical probability models such as those adopted by 3GPP and ITU are not appropriate for characterising the statistical properties of a UK micro cell environment. Although existing model definitions have been shown to be suitable when optimised, the default fitting parameters result in a poor fit to the experimental dataset highlighting the need for a new model definition. As a result, an alternative model definition is proposed in this chapter based on the d_1/d_2 model but with new parameter values.

To date, published models have focused solely on the endpoint being a UE and have made no provision for variation in the height attributes of the endpoint. Crucially, in this analysis, the development of a high resolution environmental model sufficient to accurately model small scale street level blockages pertinent to high frequency mmWave propagation paths allow self-backhauling, mesh or multi-hop deployment architectures to be studied. Results have shown that the inter-micro cell (transport) propagation path between the tops of neighbouring lamp posts has a 2% higher LoS probability compared with the UMi to UE (access) propagation paths close to ground level. Parametrisation of these two scenarios are derived as part of the proposed BT micro cell LoS probability model which contributes new insight into the upper and lower bounds of the LoS probability for lamp post mounted radio equipment.

With a detailed street level LoS path analysis completed in the representative

study areas of the DSM model (and a statistical description available for extrapolation on a national based) a LoS path topology map is now available for studying high frequency multi-hop and mesh wireless xhaul solutions in dense network deployments. This dataset complements earlier macro cell analysis which, when combined, allows all the LoS paths between potential infrastructure sites to be identified and characterised in the context of wireless transport connectivity as discussed in the next chapter.

Chapter 6

Wireless Multi-hop Deployment Characterisation

This chapter presents mobile network deployment analysis aimed at understanding the use of high frequency wireless xhaul to realise dense cell centralised network architectures. An urban sample area is selected from the existing 3D DSM to model new cell deployments where the previously discovered line-of-sight propagation paths between potential infrastructure locations are used to simulate wireless xhaul paths across the urban environment. Analysis is carried out for a number of deployment scenarios in order to quantify the number of new lamp post mounted micro cell base stations that could be xhauled using a generic LoS multi-hop wireless transport solution. Findings aim to outline the fundamental requirements that such a multi-hop wireless transport solution must meet in order to maximise its potential as a lower cost and time-to-market alternative to a fully fibred network. As such, this chapter focuses on understanding the necessary deployment characteristics of the transport network environment from a deployment perspective rather than link performance.

6.1 Introduction

The concept of small cell or street level inclusive heterogeneous mobile networks have been the long term goal of network operators since the adoption of single frequency networks. While many reasons may be attributed to the relatively low volumes of micro cell deployments over the last twenty years, the principal draw back to large scale network densification is often the deployment cost associated with securing, backhauling and maintaining such a large volume of infrastructure sites [70]. The analysis in Chapter 3 has shown that <1% of cells in an established network have an inter-site distance (ISD) <200 m - the ISD considered by 3GPP to represent sub-macro cell density (Urban Micro cell UMi) [58].

When considering the capacity and spectral efficiency targets anticipated in

a mature 5G deployment, a ubiquitous fibre backhaul network represents the most desirable means of delivering the new centralised radio access network [71], distributed MIMO [72] and cell-free massive MIMO [73] architectures discussed in earlier chapters. The practical constraints in network planning and design however, mean that alternative transport technologies often represent a more achievable footprint at cost and scale [74]. To date the most widely deployed alternative to street level fibre backhaul has been with multi-hop wireless solutions as shown in Fig. 6.1 i.e. exploiting propagation paths such as those discovered in Chapter 4 and Chapter 5. For conventional backhaul applications (high layer functional splits with less demanding performance requirements), a large choice of wireless multi-hop frequency bands and technology solutions are possible. Whilst considerable effort has been placed into the wider study of wireless multi-hop backhaul both in terms of optimal path selection [75] and performance [76], such studies have largely been constrained by use of simulated or environmental approximations. Before detailed theoretical approaches are employed, it is important to bound the xhaul network deployment in an accurate real-world environment using deterministic methodologies such as those used in this chapter.

The recognition of the deployment challenges with small cell densification have been particularly evident in recent years with the standardisation of new RAN architectures such as IAB within the 3GPP Release 16 specifications [57]. The IAB objective is to minimise the deployment complexity and cost associated with backhauling new street level cells into the network [77]. While the initial standardisation efforts are primarily envisaged for higher layer functional splits and re-encapsulation of 'child node' midhaul / backhaul onto mmWave (>24 GHz) access bands, they do not address the same deployment barriers for more forward looking fronthaul based RAN architectures. Centralised / cloud RAN approaches seeking to benefit from centralised signal processing of a multitude of geographically separated access points will be dependent on the more stringent lower-layer (fronthaul based) protocol splits. Whilst the deployment scenarios considered in this chapter do not explicitly consider the performance requirements of the xhaul interface for new cells, this is assumed to be fronthaul as this not only maximises the opportunity for coordination and cooperation in a C-RAN architecture but simplifies the hardware requirements present at each cell site. This is particularly important when trying to minimise the footprint and aesthetics of street cell infrastructure sites.The fronthaul interface must therefore be capable of supporting extremely high capacity, low latency transmissions between a centralised processing unit and a low complexity radio head. Such transport requirements are unlikely to be compatible with 3GPP FR2 channel bandwidths or those available in traditional microwave transport bands (6-42 GHz) [20] and so any wireless based fronthaul transport solution will likely be underpinned by dedicated higher frequency bands such as E-band (71.125 - 83.125 GHz) W-band (92 - 114.24 GHz) or D-band (130 - 174.8 GHz). In D-band, the available channel bandwidths

and propagation characteristics align well with the capacity and ISD requirements of ultra-dense networks [78]. As discussed in Chapter 2, there are many initiatives seeking standardisation of new lower layer functional split transport interfaces such eCPRI [11] the O-RAN Alliance and the Small Cell Forum. It is these efforts which ultimately set the requirements on the transport solution. If the long term ambitions of fully coordinated cell-free architectures are to be realised in the face of practical considerations, it is important to understand the viability of a generic wireless xhaul deployment scenario and the extent to which ideal high frequency LoS wireless transport can support such RAN architectures.

In this chapter, two contributions are presented aimed at understanding the real-world deployment requirements of wireless multi-hop transport in realistic dense network deployments. In Section 6.3 a cell site demand model is proposed which seeds the 3D environmental model outlined in Section 6.2 with new lamp post based street level cells. Here, findings aim to highlight the maximum cell density that could be achieved in a given urban environment before selection of suitable lamp post infrastructure sites become sub-optimal. In Section 6.4 the LoS paths of the newly built dense cell topology for different deployment scenarios are analysed. The objective of a deployment / topology orientated analysis is to characterise the necessary radio link properties of a high capacity multi-hop transport solution that could feasibly connect the new sites to existing or new fibre aggregation locations as shown in Fig. 6.1.

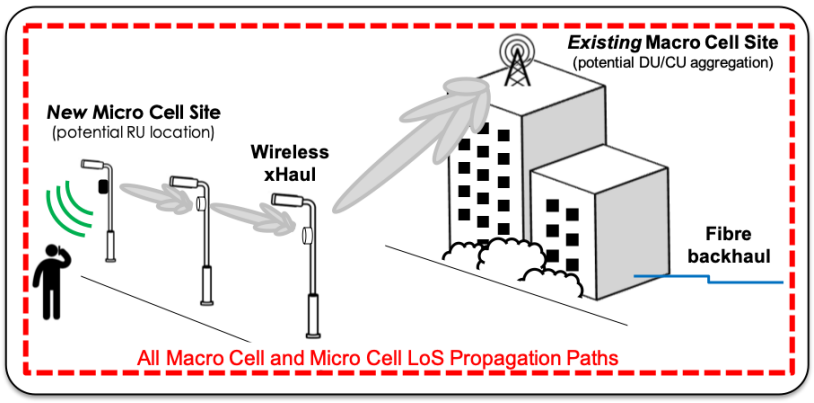

Figure 6.1: Wireless multi-hop xhaul scenario.

6.2 Deployment Study Area

To understand the ideal characteristics of street level wireless multi-hop transport in ultra-dense RAN deployments, a study area is selected from the larger DSM model. Here, central London is chosen as a representative urban environment where the resolution of the 3D environmental model is 0.5 m. This provides

sufficient resolution to capture detailed urban features such as foliage and street canyon obstructions crucial to accurate mmWave blockage / propagation analysis (Fig. 6.2 - 6.3).

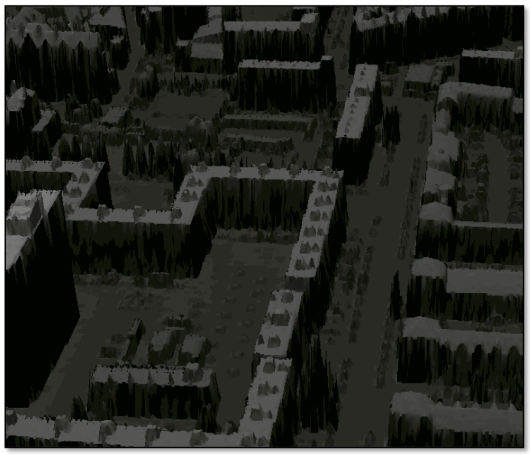

Figure 6.2: DSM 3D rendering of central London.

Figure 6.3: DSM propagation paths imported and visualised in Google Earth ©2022 Google.

A 2.5 sq km sample area of central London (centred on the British Museum) is chosen as the environment for all the subsequent deployment modelling which utilises the unobstructed LoS paths discovered from previous chapters. In combining the propagation analysis of earlier chapters, the study area contains all the possible propagation paths between lamp post sites and macro cell sites. In total 136,578 propagation paths between 2226 urban lamp posts (at their native height) as well as 35 existing roof top macro cell sites make up a wireless LoS xhaul topology map of the area. The resulting system model in Fig. 6.4 is a full mesh topology of potential LoS xhaul paths across the urban landscape which can be used to quantify the fundamental requirements of high frequency wireless transport solutions in future dense cell networks as discussed in Section 6.1.

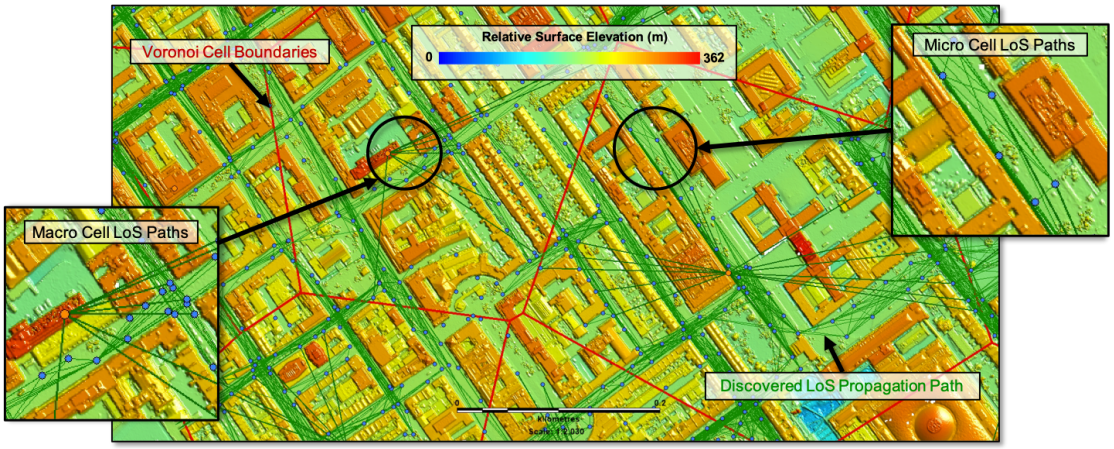

Figure 6.4: DSM LoS path full mesh topology.

6.3 Ultra Dense Cell Demand Model

Before any meaningful deployment scenarios can be investigated, the study area and its full xhaul path topology need to be seeded with the future expectation of new cell site locations and densities that could address the anticipated long-term capacity growth.A cell site demand model is subsequently proposed based on an arbitrary time series roll-out of new lamp post based cell site locations. Cells are sequentially added to the map at the lamp post location which maximises the reduction in the mean inter-site distance (ISD) of the area.The study area of central London is covered by the 35 existing macro cell sites where the site locations and Voronoi cell boundaries are shown in Fig. 6.6. This topology is the reference point for the dense cell demand model where the ISD distribution of these cells with a mean ISD of 305 m as shown in Fig. 6.5 represents the cell site density of the existing deployment with no new cells added. This serves as the starting point ($t_0 = 305m_{ISD}$) when adding new sites to the network topology in order to further densify the network.

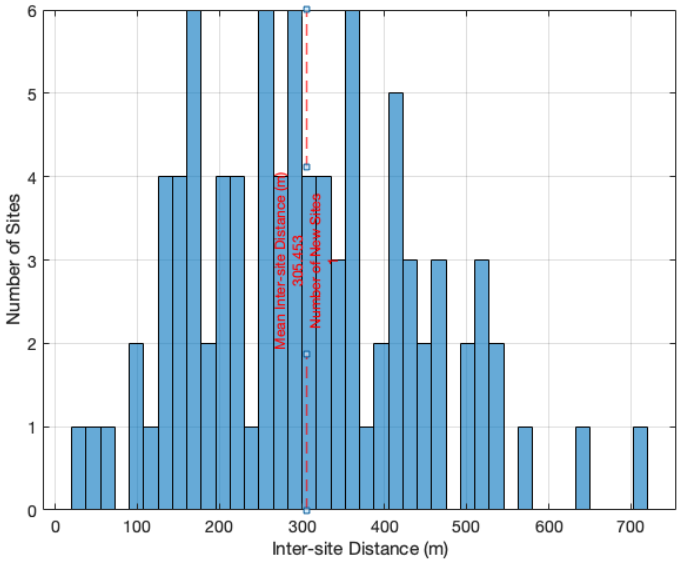

Figure 6.5: Existing mean ISD distribution of study area 305 m (no new sites added).

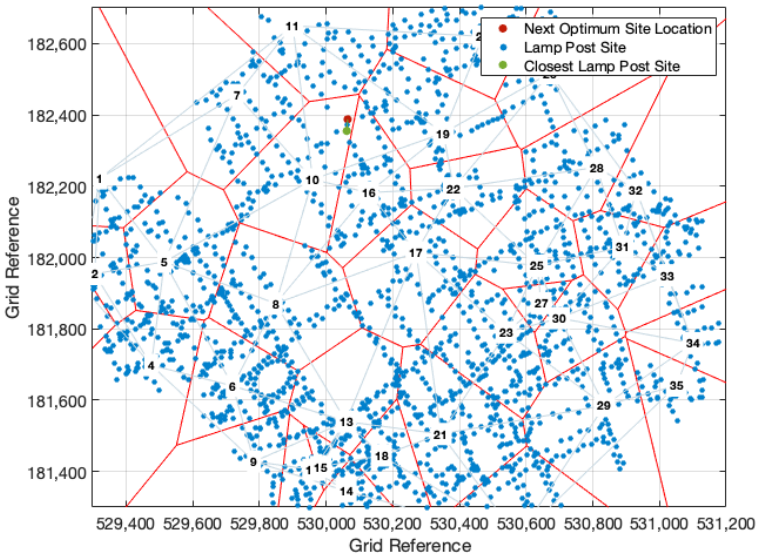

Figure 6.6: Existing mean ISD topology of study area 305 m (no new sites added).

A Delaunay triangulation graph is constructed based on the existing cell locations (at t_0 the graph is solely made up of existing macro cell roof top sites as in Fig. 6.6) where the triangulation edges represent the ISD between adjacent cells. The demand model is designed to sequentially add new street level micro cell sites to the lamp post nearest to the incentre of the largest Delaunay triangle. A greedy heuristic optimisation algorithm (Algorithm. 1) aims to maximise the

reduction in the current ISD distribution iterating one new cell at a time until the target ISD is met. During design of the demand model algorithm it was recognised that utilising the circumcentre of the largest Delaunay triangle for placement of each new cell would represent a more optimal solution (where the circumcentre is exactly equidistant from each of the two cell locations that it bisects) however, this has the potential to create boundary conditions at the graph edge where cells are placed outside the graphing area.

Algorithm 1: Ultra Dense Cell Demand Model

```
Data: Current_Sites; Potential_Lamp_Posts
while Current_ISD > Target_ISD do
    Let dt = Delaunay Triangulation of Current_Sites;
    Let optimal_cell_location = incentre of largest face in dt;
    Let optimal_lamp_post = closest point in Potential_Lamp_Posts to
      optimal_cell_location;
    if optimal_lamp_post has > 0 LoS paths then
        Current_ Sites ← Current_Sites + optimal_lamp_post;
        Potential_Lamp_Posts ← Potential_Lamp_Posts - optimal_lamp_post;
    else
        Choose next closest point to optimal_cell_location in Potential_Lamp_Posts;
    Current_ISD = ISD of Current_Sites;
```

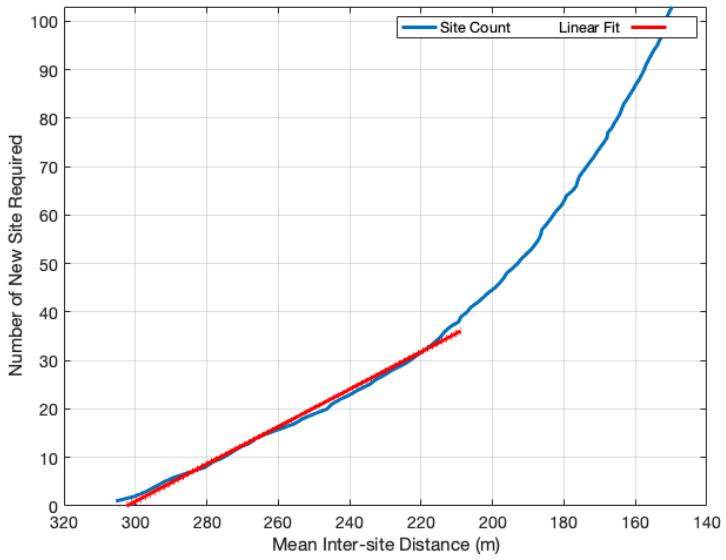

Figure 6.7: New cell sites required to meet the target ISD.

When the demand model is allowed to run until a very high density of cells is achieved e.g. 150 m ISD as shown in Fig. 6.7 (reversed x-axis) it can be seen that for an ISD orientated network deployment, the utilisation of street level lamp post

cells holds a near linear density growth only up to ∼209 m. A linear regression fit of the data maintains an R^2 value greater than 0.99 until approximately 209 m. Beyond 209 m the cell density enters a more exponential growth profile with diminishing gains for each new site built. This suggests that the use of lamp posts as small cell infrastructure sites is most cost effective for densities up to ∼209 m ISD after which, suitable lamp posts become limiting and cell placement is sub-optimal. As a result, an optimum ISD (from a build / cost perspective) rounded to 200 m is assumed for subsequent analysis. Coincidentally, an ISD cell density of 200 m also aligns with 3GPP UMi ISD deployment assumptions [58]. For a target ISD of 200 m, 45 new street level sites ($t_{45} \leq 200 m_{ISD}$) would be required in the study area as shown in the ISD distribution in Fig. 6.8 and the associated cell topology in Fig. 6.9. Modelling of the network growth through cell density rather than a more conventional geo-spatial user / traffic demand allows the underlying radio configuration of the sites as well as commercially sensitive traffic forecasting requirements to be abstracted away.

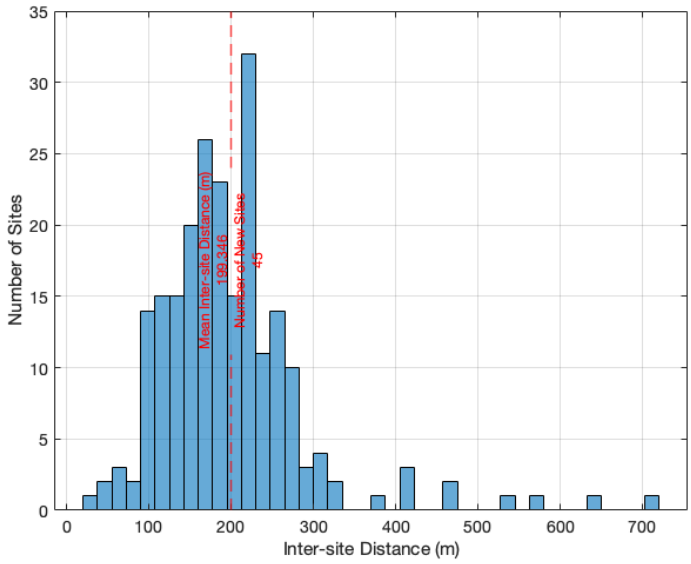

Figure 6.8: Mean ISD distribution built to 200 m (+45 new sites added).

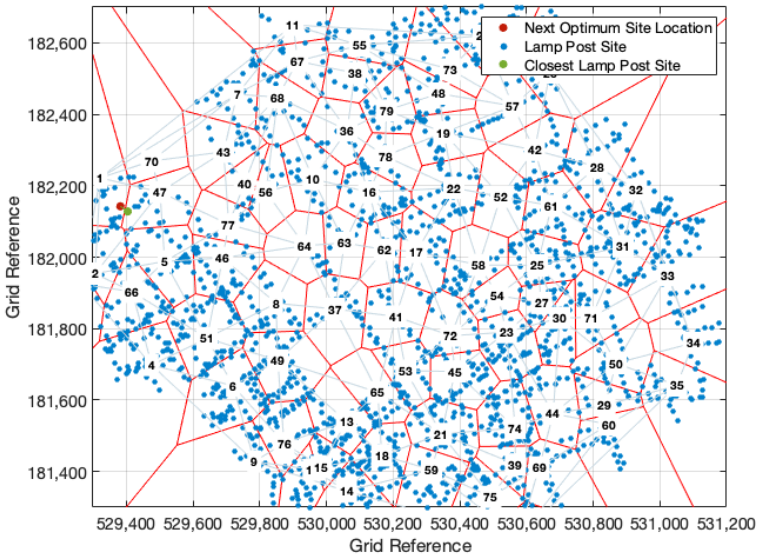

Figure 6.9: Mean ISD topology built to 200 m (+45 new sites added).

With the optimum density of lamp post based cells now identified, the 3D physical model can be rationalised into a 2D logical graph as shown in Fig. 6.10. Here, the vertices of the graph represent potential infrastructure locations and the undirected edges represent the discovered 3D LoS paths that join them and which could be used by a high frequency LoS wireless solution. The new cell demand sites represent nodes in the graph which require connectivity to a fibre aggregation point, the existing macro sites represent nodes already with such a connection. All other nodes in the graph are remaining lamp posts which may be passed through as 'relay' or 'multi-hop' nodes via the graph edges. For the purposes of this chapter, which is focused solely on ideal deployment characteristics, the graph edge weights equate to basic Euclidean distances. The edge weight however, can readily be equated to more meaningful performance based metrics such as capacity, latency or jitter when modelling specific xhaul interface requirements or wireless transport capabilities - these performance metrics are explored in the next chapter.

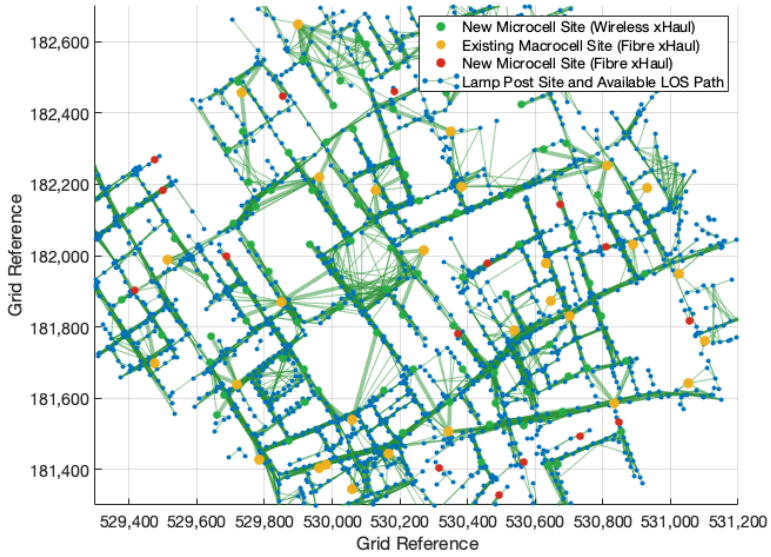

Figure 6.10: Logical 2D LoS topology and new cell site locations.

6.4 Deployment Scenarios

The extent to which wireless LoS xhaul could support the anticipated urban cell densification requirement is assessed through analysis of the undirected graph model built in Section 6.3 using a number of different deployment scenarios. Although there may be many approaches operators may take in order to build the transport necessary to support a dense cell deployment, the three scenarios covered in this work focus on the use of wireless transport as described in Table 6.1. In the following sections the analysis of traversing the graph edges (LoS paths) from each new lamp post based cell site added by the demand model toward the optimal network ingress point (i.e. an existing fibre site) is studied. A Dijkstra shortest path algorithm is utilised to select the optimal route between source and target nodes based on minimum hop count and minimum distance (in the event of multiple candidate routes), this approach represents a cost oriented deployment. For each scenario, the optimal multi-hop path properties are analysed at 25 m ISD intervals as site density increases to a 200 m maximum ISD as suggested by Section 6.3.

Table 6.1: Summary of Deployment Scenarios.

	Deployment Scenario	Modelling Description
Roof Top Only Wireless Extension	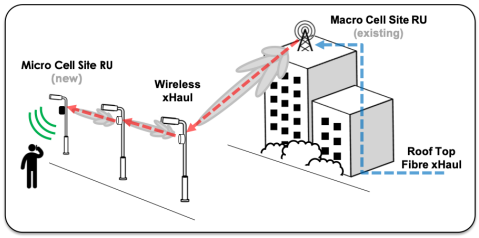	• Only existing macro cell sites are available as fibre points. • No new fibre sites are added, each new micro cell site can use an unlimited number of wireless hops to reach a fibre node.
Street Level Only Wireless Extension	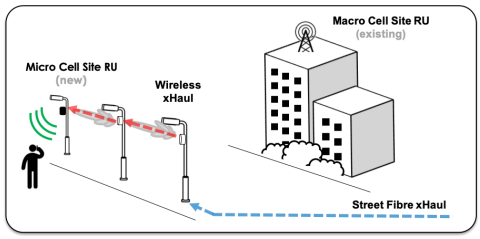	• The macro layer is considered isolated and is not used as a potential xhaul wireless hop or fibre point. • If a newly added micro cell cannot find an existing fibre point within 3 wireless hops the site becomes a fibre node.
Roof or Street Level Wireless Extension	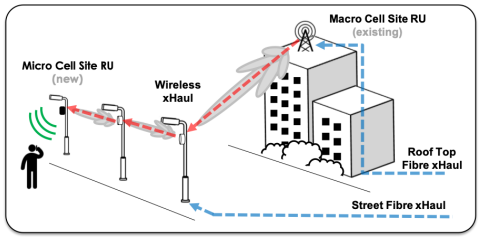	• New micro cell sites can be xhauled wirelessly to any available fibre point – either macro or micro site. • If no fibre site can be reached within 3 wireless hops the site becomes a fibre node.

6.4.1 Roof Top Only Wireless xHaul Extension

The 'roof top only' scenario represents a deployment where no new fibre points are added as the network expands. As a result, the cell densification is built entirely around wireless transport where only existing macro cell sites are used as xhaul aggregation points (potential DU / CU baseband hosting sites in a C-RAN evolution). This scenario aims to quantify the maximum potential of LoS wireless xhaul without new fibre installations. The new cell site locations added by the demand model together with all possible LoS paths are shown in map format in Fig. 6.11. The optimum xhaul path topology chosen when applying the shortest path algorithm across the LoS paths towards the new sites is shown in Fig. 6.12. Analysis of these shortest path LoS xhaul routes in terms of the required number of hops is outlined in the CDF in Fig. 6.13. This shows that a maximum of 5 and mean of 2.3 hops per site is observed when no constraints are placed on the number of hops possible.With an unconstrained hop count, 96% of new sites could potentially be connected with a LoS wireless link back to an existing macro cell site (82% within a more realistic 3 hop criteria). The CDF of associated link lengths required in given in Fig. 6.14 where for the highest cell density of 200 m ISD, a

maximum hop / link length of 237 m and mean of 107 m was required. These results suggest that building cell sites to a peak 200 m ISD density would require any existing fibre points (macro cell sites in this scenario) to support an additional 2.25 micro cell sites on average with the maximum observed being 4 additional micro cell sites and a transport solution capable of supporting links of up to 237 m. A summary of the deployment characteristics as density increases is given in Table 6.2.

Figure 6.11: Map of potential xhaul paths and sites for roof only scenario.

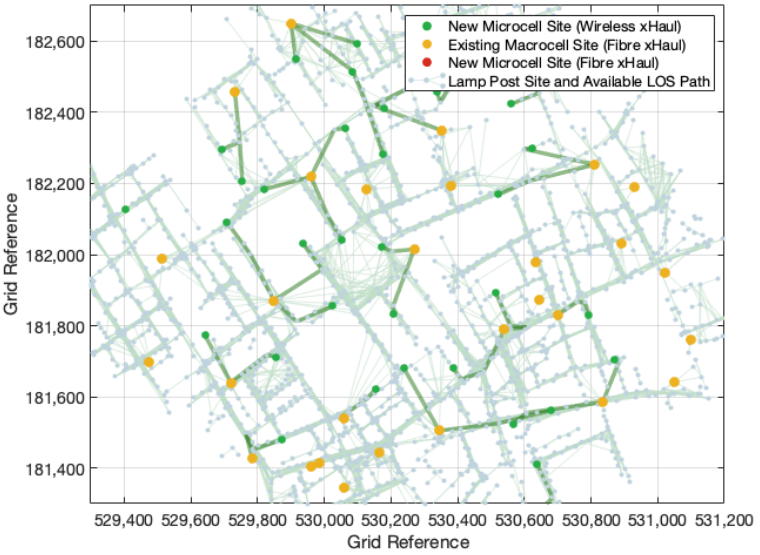

Figure 6.12: Optimal xhaul path determination for roof only scenario.

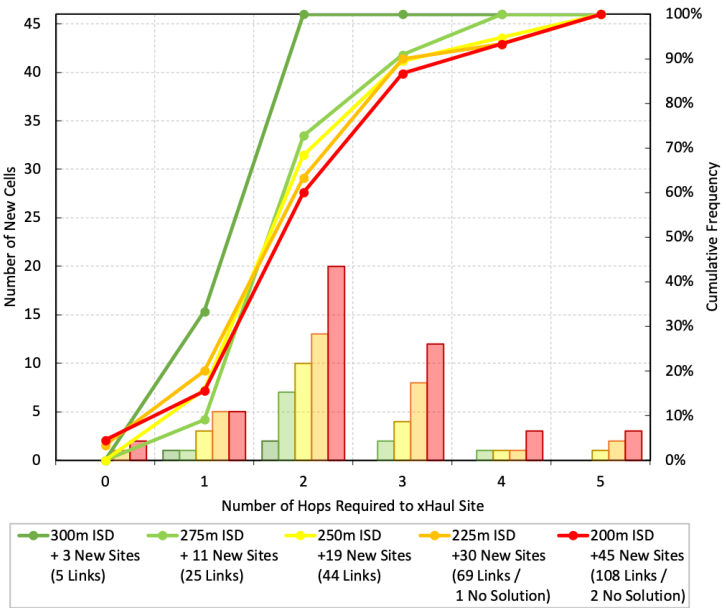

Figure 6.13: Hop count distribution for new cell sites for roof only scenario.

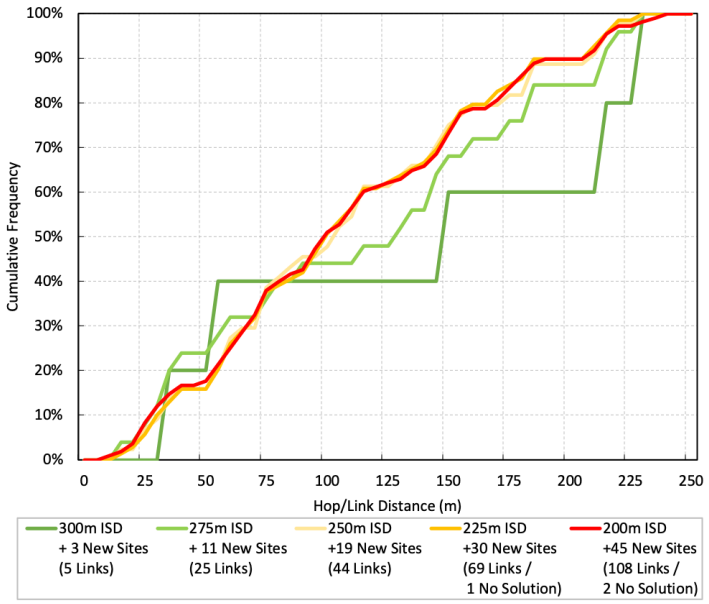

Figure 6.14: Hop length distribution for new cell sites for roof only scenario.

Table 6.2: Summary of xHaul Hop Characteristics for Roof Top Only Scenario.

Target ISD	**New Cells Required**	**New Fibres Required**	**New Wireless Links Required**	**Max Hop Length**	**% of New Sites Connected**
300 m	3	0	5 *(2 relay sites)*	230 m	100% Wireless *(100% ≤3 hops)*
275 m	11	0	25 *(14 relay sites)*	230 m	100% Wireless *(91% ≤3 hops)*
250 m	19	0	44 *(25 relay sites)*	230 m	100% Wireless *(89% ≤3 hops)*
225 m	30	0	69 *(40 relay sites)*	230 m	97% Wireless *(87% ≤3 hops)*
200 m	45	0	108 *(65 relay sites)*	237 m	96% Wireless *(82% ≤3 hops)*

6.4.2 Street Level Only Wireless xHaul Extension

In the 'street level only' scenario the micro cell layer is build out independently of the macro layer using only new street level fibre access. This scenario aims to simplify street level cell densification without dependency on existing macro cell infrastructure. When a new lamp post based cell is built, a wireless multi-hop solution is used providing it is within the transport interface performance budget (here simplified to 3 wireless hops). If a fibre point cannot be reached within 3 hops the site becomes a new fibred node. The resulting site locations and connectivity solution for this scenario are shown on the map in Fig. 6.15 and the optimal LoS link topology for wireless connections in 6.16.

Results show that at the peak 200 m ISD density this approach would require 57% of the sites added to be fibred of which there is a heavy weighting toward early deployed cells as summarised in Table 6.3. At this peak density, only 24% of fibre sites would be able to aggregate one or more additional new sites with a wireless LoS extension as in Fig. 6.17. A maximum hop / link length of 193 m was observed on sites able to exploit a LoS path to existing fibre locations as shown in Fig. 6.18 demonstrating a shorter link length requirement for this scenario relative to when rooftop sites are considered.

Figure 6.15: Map of potential xhaul paths and sites for street only scenario.

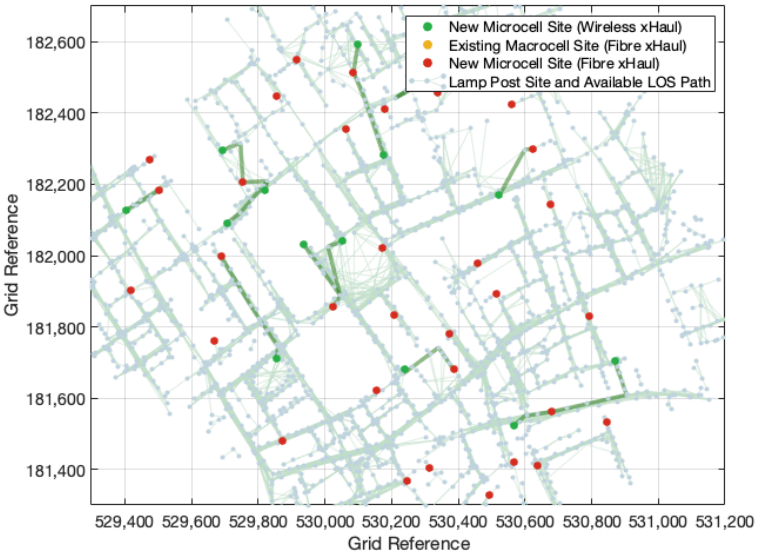

Figure 6.16: Optimal xhaul path determination for street only scenario.

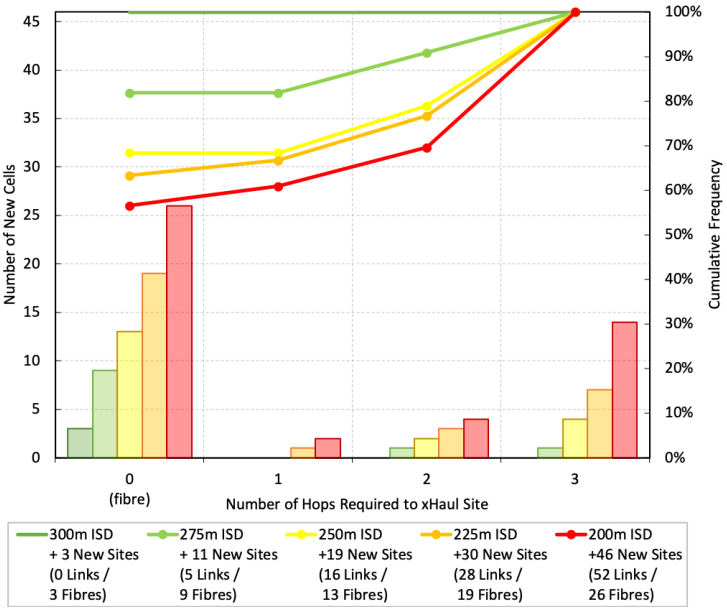

Figure 6.17: Hop count distribution for new cell sites for street only scenario.

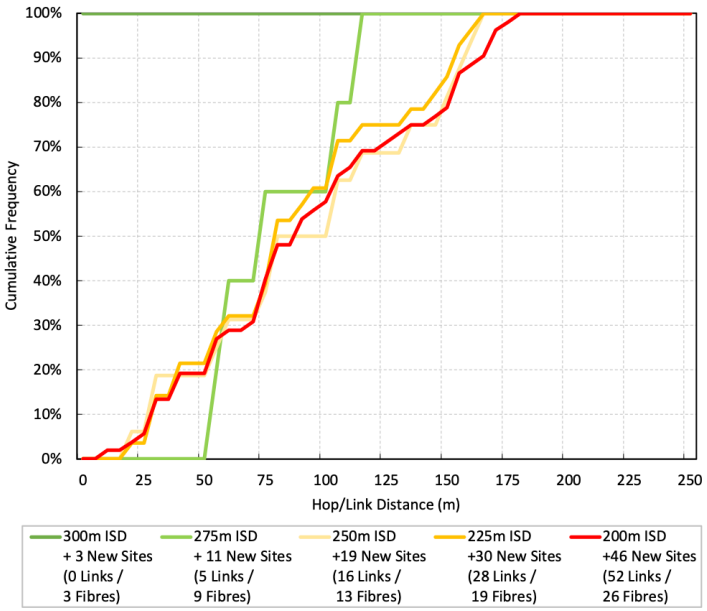

Figure 6.18: Hop length distribution for new cell sites for street only scenario.

Table 6.3: Summary of xHaul Hop Characteristics for Street Only Scenario.

Target ISD	**New Cells Required**	**New Fibres Required**	**New Wireless Links Required**	**Max Hop Length**	**% of New Sites Connected**
300 m	3	3	0 *(0 relay sites)*	183 m	100% Fibre 0% Wireless
275 m	11	9	5 *(3 relay sites)*	183 m	82% Fibre 18% Wireless
250 m	19	13	16 *(10 relay sites)*	193 m	68% Fibre 32% Wireless
225 m	30	19	28 *(17 relay sites)*	193 m	63% Fibre 37% Wireless
200 m	46	26	52 *(32 relay sites)*	193 m	57% Fibre 43% Wireless

6.4.3 Roof or Street Level Wireless xHaul Extension

In this scenario, new cell sites can be connected wirelessly to any available fibre location (either existing macro site or newly build street level fibre site). If a new site cannot reach an existing fibre point within the 3 wireless hop criteria the site becomes a new fibred node. This scenario aims to consider all options for wireless xhaul aggregation in urban environments whilst minimising the dependency on new fibre installations. Again the site locations and final connectivity solutions for this scenario is highlighted in Fig. 6.19 and the optimal path topology for any LoS wireless links in Fig. 6.20

Results in this scenario are similar to those of the 'roof top only' case where the majority of sites achieve xhaul connectivity via existing macro cell roof top sites. Only 13% of new sites required new street level fibre at the highest deployment density of 200 m ISD as in Fig. 6.21. As can be seen from Table 6.4 the proportion of wireless xhaul to new fibre sites remain reasonably consistent as the density increases. The link length characteristics are broadly in line with other deployment scenarios with a maximum hop / link length of 237 m and average of 113 m as highlighted in Fig. 6.22. Findings from this scenario are perhaps most relevant to the underlying research objectives as this represents the most flexible approach to use of wireless xhaul deployment. As such, these result likely represent the most realistic deployment characteristics and highest opportunity for wireless connectivity when performance or hop constraints are ultimately considered.

Figure 6.19: Map of potential xhaul paths and sites for roof or street scenario.

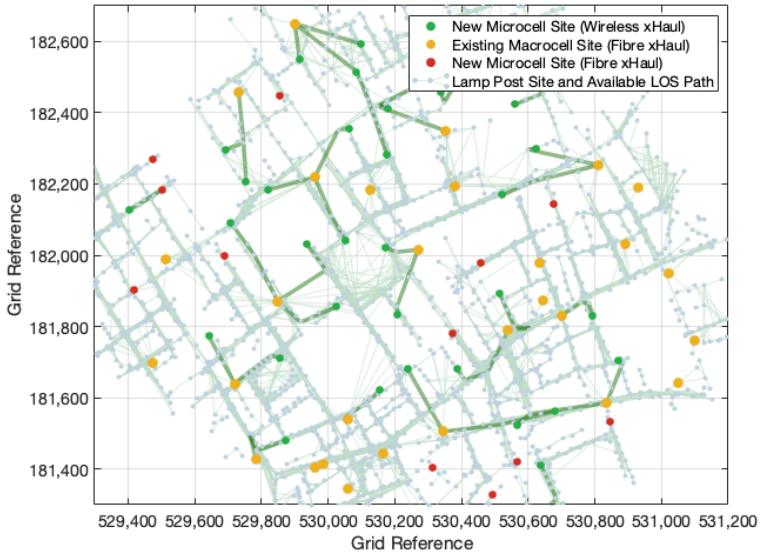

Figure 6.20: Optimal xhaul path determination for roof or street scenario.

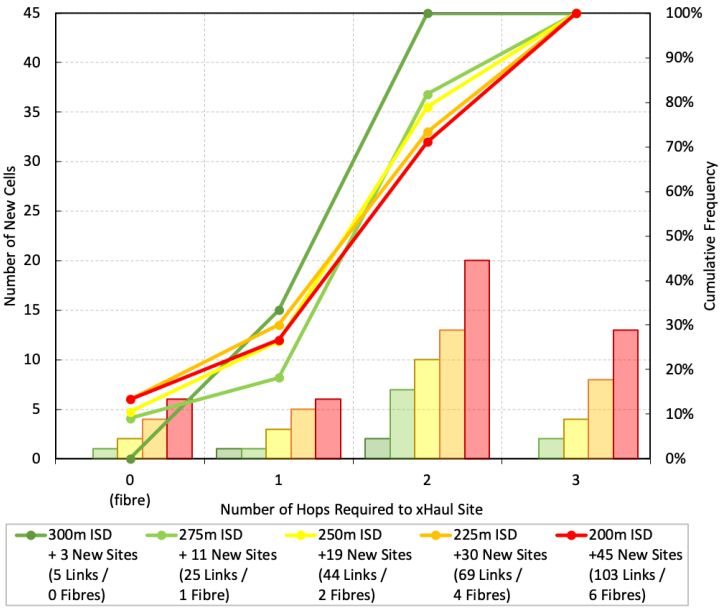

Figure 6.21: Hop count distribution for new cell sites for roof or street scenario.

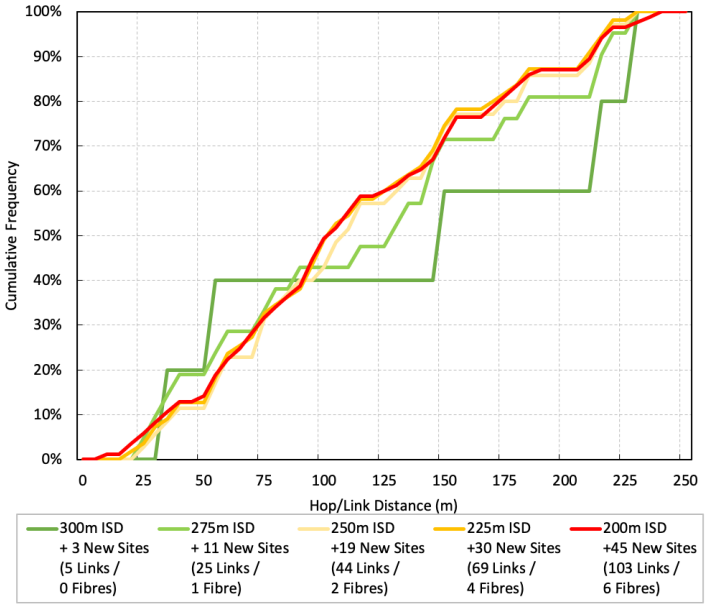

Figure 6.22: Hop length distribution for new cell sites for roof or street scenario.

Table 6.4: Summary of xHaul Hop Characteristics for Roof or Street Level Scenario.

Target ISD	**New Cells Required**	**New Fibres Required**	**New Wireless Links Required**	**Max Hop Length**	**% of New Sites Connected**
300 m	3	0	5 *(2 relay sites)*	230 m	0% Fibre 100% Wireless
275 m	11	1	25 *(11 relay sites)*	230 m	9% Fibre 91% Wireless
250 m	19	2	44 *(18 relay sites)*	230 m	11% Fibre 89% Wireless
225 m	30	4	69 *(29 relay sites)*	230 m	13% Fibre 87% Wireless
200 m	45	6	103 *(46 relay sites)*	237 m	13% Fibre 87% Wireless

6.5 Chapter Summary

In this chapter, the fundamental requirements of a wireless transport solution for a range of key deployment scenarios that could be adopted when densifying the mobile network are identified. A deployment rather than a technology led approach is considered utilising the a real-world 3D network topology built in earlier chapters to understand the ideal characteristics of a multi-hop urban transport solution.

Findings show that with sufficiently detailed environment planning data which allows accurate LoS path discovery, wireless transport could be a critical technology in reducing the dependency on street access fibre when deploying dense cell architectures. Although fibre roll out in the UK is increasing at a tremendous pace, the ability to utilise this for street infrastructure is very much location specific. In addition, many fibre infrastructure providers prioritise fibre roll-out on residential premises for the consumer broadband market leaving the provisioning of urban street access fibre still challenging from a cost perspective and complicated further by regulatory compliance.

Although analysis at this stage does not take into account the performance capability of any specific wireless transport solution nor the specific xhaul requirements of the cell, findings highlight the key deployment parameters or constraints (i.e. site counts, hops counts, link lengths etc.) in which such a solution would need to operate. For a dense cell deployment, results suggest that with an unconstrained hop count 93% of new street level sites in typical UK urban environments could be xhauled to an existing roof top site using a wireless multi-hop LoS solution. In a mixed roof top and street fibre deployment where fibre locations are used as xhaul aggregation hubs a 44% reduction in street level fibre could be achieved by using high capacity wireless transport. In the scenario where macro sites are not considered in the transport architecture

of new street level cell sites, the use of wireless multi-hop technology could reduce the dependency on street level fibre by as much as 43% relative to an all fibre transport network. The deployment modelling discussed in this chapter demonstrates the potential proportion of sites which could use high frequency wireless connectivity but this is predicated on the assumption that the performance of future wireless transport solution is able to support the minimum requirements of C-RAN transport interfaces. To understand these factors and identify the likely performance constraints in such a transport network the fronthaul interface requirements on which they are expected to be built must first be quantified, this is explored in the following chapter.

Chapter 7

Next Generation Transport Interfaces

The application of wireless backhaul is widely adopted in commercial mobile networks as a cost effective alternative to fibre. However, the practical use of wireless transport to support new centralised RAN architectures is not well studied. This chapter outlines the theoretical performance requirements of evolving fronthaul based functional split interfaces and experimentally measures the performance characteristics of the latest E-band (71 - 86 GHz) mmWave point to point wireless transport solution. The objective of this chapter is to define meaningful fronthaul performance requirements and the associated performance capabilities of potential wireless solutions that could be utilised in the DSM deployment model previously discussed. The theoretical performance metrics of promising new functional split implementations are first derived. A wireless fronthaul testbed is then built to characterise a state of the art E-band wireless solution and use the measurements to forecast the anticipated performance of future higher frequency W and D-band systems operating above 100 GHz. Finally a wireless fronthaul proof of concept is presented using an Open Air Interface (OAI) software base station fronthauled over the high capacity Ethernet based E-band radio link using the most challenging 3GPP option 8 fronthaul interface.

7.1 Introduction

The use of wireless backhaul is generally favoured where fibre optic connectivity is either absent or cost prohibitive. In fact, wireless transport solutions such as point-to-point microwave account for the majority of existing cell site backhaul installations worldwide [79]. However, the introduction of higher capacity 5G RAN and an architectural evolution towards disaggregated and centralised deployment models bring new performance challenges for wireless transport systems [20]. To address these new challenges, the next generation wireless transport solutions must

target new performance criteria suitable of offering a viable alternative to fibre. In response, a migration to millimetre-wave transmission bands, such as W-band (92-114.25 GHz) and D-band (130-174.8 GHz) [80] is being considered for future high capacity, low latency wireless xhaul scenarios [20].

Underpinning the new requirements placed on wireless transport is the specification of new 'functional splits' in 5G standards which aim to increase deployment flexibility of the RAN. Moreover, the adoption of alternative functional splits further facilitates the realisation of centralised and virtualised radio access network (C-RAN / vRAN) components [81], [82]. Functional splits allow for geographic separation and disaggregation of the traditional RAN cell site functions throughout the network [83], [84]. In such architectures, the radio unit (RU) is principally concerned with radio signal reception and transmission at the cell site whilst real-time signalling procedures are handled by the distributed unit (DU) and non-real-time higher layer protocol functions handled by the centralised unit (CU). C-RAN architectures are able to support a range of new deployment scenarios from consolidation and disaggregation of baseband capabilities to more efficient cell densification. Such architectures however, each necessitate new high capacity, low latency fronthaul based transport interfaces. As such, the challenge for wireless transport is whether it can meet the performance and deployment requirements necessary to support fronthaul based C-RAN architectures.

In recent years the theoretical requirements for fronthaul based transport interfaces have been well studied [83], [84]. Whilst each split point in the 5G protocol stack may be suited to a particular deployment scenario, the impact of the associated performance requirements are not well studied beyond the optical transport domain. Historically, it has been assumed that the benefits of C-RAN architectures could only realistically be achieved using large scale fibre transport networks [85]. As such fronthaul and C-RAN challenges for a wide range optical transport technologies including passive optical networks (PON) and wavelength division multiplexing (WDM) have been extensively studied [86] including the use of free space optics (FSO). It is however recognised that although technologies such as FSO alleviate some of the inherent inflexibility of fibre transport in the same way as radio, they also pose significant atmospheric availability challenges which in turn has resulted in research effort into optimisation of hybrid FSO and radio solutions for fronthaul networks [87]. Limited experimental studies around wireless fronthaul are evident from literature, a proprietary wireless transport solutions in [88] has however been demonstrated where findings suggest the latency requirements of low layer fronthaul splits could be met using 60 GHz and 70 GHz radio solutions.

In this chapter, the fundamental requirements of emerging fronthaul interfaces at key functional split points are considered and contrasted with current and anticipated performance characteristics of high frequency millimetre-wave and sub-THz wireless transport bands. The theoretical requirements of Ethernet based fronthaul interfaces are derived in Section 7.2. The suitability of existing E-band

mmWave wireless transport for the theoretical fronthaul interface requirements are characterised in Section 7.3 with results used to model the anticipated performance of future higher bandwidth transport solutions such as W / D-band. Finally a wireless fronthaul proof-of-concept is presented in Section 7.4 demonstrating the feasibility of the OAI option 8 implementation over E-band transport.

7.2 Fronthaul Requirements

Although historically significant effort has been applied to quantifying the advantages and disadvantages of each of the 3GPP split options (1-9) both from a performance and practical perspective [83], [89], [90], only the most credible splits with industry traction are considered in this work as highlighted in Fig. 7.1. All such definitions assume support from underlying carrier grade Ethernet transport networking where performance is maximised through application of a number of end-to-end time sensitive network technologies including class of service (CoS) priority markings (IEEE 802.1p), scheduling, shaping and pre-emption awareness (IEEE 802.1Qbv, IEEE 802.3br and 802.1Qbu) as well as synchronisation protocol support (IEEE 802.1as) at Ethernet layer 2. The generalised transport requirements of fronthaul based splits (below the MAC layer) can be broadly summarised in terms of datarate, latency, jitter and frame loss.

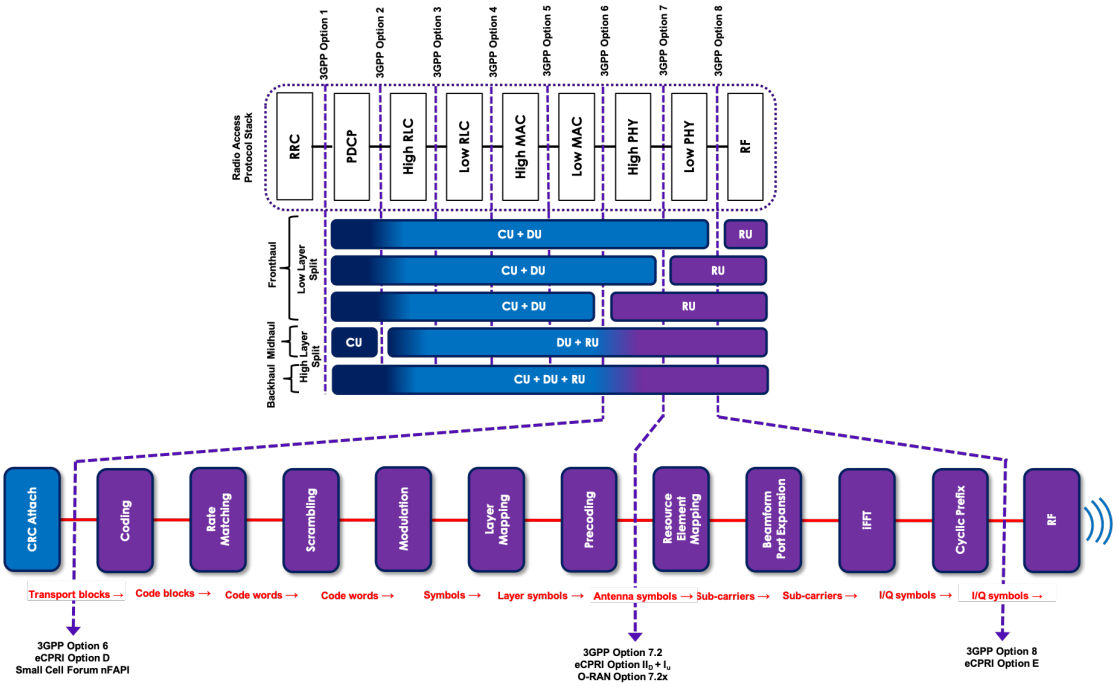

Figure 7.1: RAN functional split overview.

7.2.1 Datarate

7.2.1.1 Option 8 Split

The 3GPP option 8 split, whilst offering the lowest complexity RU and highest potential centralisation gains requires the most stringent capacity, delay and jitter requirements on the transport interface [91]. The radio interface I/Q is sampled and quantized allowing a constant bitrate (CBR) interface which scales with the number of antennas and channel bandwidth (FFT size). The PHY / RF option 8 split as specified in 3GPP TR 38.801 has conventionally been addressed with the CPRI implementation [12] necessitating dedicated fibre such as optical transport network (OTN) or wavelength division multiplexing. The evolutionary trend towards more cost effective Ethernet based fronthaul solutions however, make this split realisable with carrier grade Ethernet transport solutions through the use of eCPRI split E [11] or IEEE 1914.3 Radio over Ethernet (RoE) [15] encapsulation.

- The transport datarate requirement for conventional CPRI $\mathrm{D_{CPRI}}$ can be calculated as in (7.1). Where N_{Ant} is the number of antenna ports on the RU, fs is the sampling frequency - which is the product of the sub-carrier spacing and the FFT size (scaling with bandwidth), M which is the number of quantizer bits per I and Q (conventionally 15 bit), $\mathrm{CM_{CPRI}}$, the overhead of control and management words per CPRI frame (1/16) and $\mathrm{LC_{CPRI}}$, the overhead induced by line coding (either 10/8 for 8B/10B or 66/64 for 64B/66B coding for DC balance and clock recovery). For an Ethernet based option 8 split such as eCPRI $\mathrm{D_{eCPRI}}$ the line coding can be replaced with overheads resulting from Ethernet framing $\mathrm{OH_{ETH}}$ and eCPRI encapsulation $\mathrm{OH_{eCPRI}}$ as in (7.2) - subsequently timing and synchronisation aspects are addressed in alternative 'control plane' flows using established Ethernet based protocols discussed further in Section 7.2.3.

$$\mathrm{D_{CPRI}} = N_{ant} \cdot\ fs \cdot\ 2M \cdot\ \mathrm{CM_{CPRI}} \cdot\ \mathrm{LC_{CPRI}} \tag{7.1}$$

$$\mathrm{D_{eCPRI}} = N_{ant} \cdot\ fs \cdot\ 2M \cdot\ \mathrm{CM_{CPRI}} \cdot\ \mathrm{OH_{ETH}} \cdot\ \mathrm{OH_{eCPRI}} \tag{7.2}$$

7.2.1.2 Option 7.2 Split

As outlined in Chapter 2 there are a number of possible split options defined by 3GPP within the option 7 definition; 7.1 (low PHY), 7.2 (intra PHY) and 7.3 (high PHY). Whilst all these options have their relative merit, the fragmentation and interpretation of the option 7 splits have somewhat held back mainstream adoption to date. It is the effort of the O-RAN alliance over recent years in part driven my the operator community requirements for 'open' fronthaul interfaces which have enabled traction in the standardisation of the 7.2 variant known in O-RAN as 7.2x. The O-RAN 7.2x split is broadly aligned with eCPRI split II_D and I_U where

reduction in the required interface bandwidth (relative to option 8) is achieved through resource element mapping functions remaining within the RU. Whilst this split adds more complexity to the RU, it enables only user occupied resource elements to traverse the fronthaul interface. As a result the 7.2x split is the first split which allows for a variable bitrate interface. This however, does require the introduction of control plane overhead $\mathrm{OH_{CP}}$ needed to carry the resource block assignment and any antenna beamforming information in the downlink between DU and RU. As the control plane messaging is implementation specific, the data rate requirements for this split can vary between implementations. The O-RAN alliance suggest control plane overhead in the order of 10% [92].

- The transport data rate for O-RAN 7.2x implementation $\mathrm{D_{7.2x}}$ can be calculated as in (7.3) and (7.4) where the uplink and downlink are specified differently due to the lack of control plane overhead $\mathrm{OH_{CP}}$ needed in the uplink. At this split, the transport requirements can be reduced because transport data rates become a function of the MIMO layers N_{layers} in operation as well as the occupied resource block allocation N_{PRB} (where a utilisation scaling factor of 1 is assumed for peak data rate requirement). In the 7.2x split, it is assumed that some element of I/Q compression is employed for each resource block. In O-RAN, this is specified as a block floating point compression where each subcarrier $N_{SCperRB}$ I and Q samples are compressed to a signed bitwidth $M_{mantissia}$ and unsigned exponent $M_{exponent}$ (typically 9 bit and 4 bit respectively). The underlying layer 2 and layer 3 transport protocols for this split also introduce Ethernet framing $\mathrm{OH_{ETH}}$ and eCPRI encapsulation $\mathrm{OH_{eCPRI}}$ overhead.

$$\mathrm{D_{7.2x_{DL}}} = (N_{layers} \cdot \ N_{PRB}) \cdot \ (N_{SCperRB} \cdot \ 2M_{mantissa} + M_{exponent}) \cdot \ T_{SymPerSlot}^{-1} \cdot \mathrm{OH_{CP}} \cdot \ \mathrm{OH_{ETH}} \cdot \ \mathrm{OH_{eCPRI}} \tag{7.3}$$

$$\mathrm{D_{7.2x_{UL}}} = (N_{layers} \cdot \ N_{PRB}) \cdot \ (N_{SCperRB} \cdot \ 2M_{mantissa} + M_{exponent}) \cdot \ T_{SymPerSlot}^{-1} \cdot \mathrm{OH_{ETH}} \cdot \ \mathrm{OH_{eCPRI}} \tag{7.4}$$

7.2.1.3 Option 6 Split

The option 6 split separates the PHY and MAC layer in the protocol stack whereby all PHY related functions are carried out at the RU and the MAC layer and above are controlled at the DU. At this split the transport requirements can be reduced further as the fronthaul interface carries the MAC transport blocks which are a function of the individual channel coding rate and data rate of each user. This also means that relative to lower layer splits, the option 6 split has a higher proportion of control to user plane traffic as the MAC scheduling functions are transported to

the PHY layers at the RU. The most significant standardisation efforts for option 6 are driven through the Small Cell Forum where the nFAPI specification targets low cost, smaller capacity / coverage areas and indoor cell deployments where high order massive MIMO and advanced transmission schemes such as CoMP and M-TRPs are not envisaged.

- The transport datarate requirement for nFAPI split 6 implementation D_{6nFAPI} can be calculated as in (7.5) and (7.6)[1]. For a MAC / PHY split the fronthaul datarate requirements are dependent on the number of MIMO layers N_{layers} and transport block size TBS in use which in turn is dictated by the modulation and coding scheme index I_{MCS} being utilised on the radio interface together number of scheduled resource blocks N_{PRB}. For peak fronthaul datarates the maximum cell utilisation can be assumed (a utilisation scaling factor of 1 and the maximum MCS supported). In 4G LTE the derivation of TBS for each transmission time interval $N_{TTIperSec}$ is given by static lookup tables in 3GPP TS 36.213 [93]. For 5G NR, the TBS derivation per slot T_{slot} is made using specific formulas as defined 3GPP TS 38.214 [94] to account for the much larger combinations of modulation and coding scheme and resource block allocation[2]. The nFAPI option 6 implementation defines a message API between MAC and PHY layers and as such includes a nFAPI encapsulated control plane overhead OH_{CP}, an associated layer 4 transport overhead header OH_{nFAPI} in addition to the necessary layer 3 IP overhead OH_{IP} and layer 2 Ethernet framing overhead OH_{ETH} to carry the fronthaul flows.

$$D_{6nFAPI_{LTE}} = N_{layers} \cdot (TBS \cdot N_{TTIperSec}) + OH_{CP} \cdot OH_{ETH} \cdot OH_{IP} \cdot OH_{nFAPI} \quad (7.5)$$

$$D_{6nFAPI_{NR}} = N_{layers} \cdot (TBS \cdot T_{slot}^{-1}) \cdot OH_{CP} \cdot OH_{ETH} \cdot OH_{IP} \cdot OH_{nFAPI} \quad (7.6)$$

7.2.1.4 Fronthaul Datarate Comparison

An example of the anticipated fronthaul data rates for common cell configurations of a single RU are outlined in Table 7.1 and shown in Fig. 7.2. It is important to note that further scaling of fronthaul data rates is required for a typical macro cell site which may consist of up to three RU sectors and potentially multiple concurrent frequency bands. Calculations outlined agree well with similar industry

[1]Although both Frequency Division Duplexing (FDD) and Time Division Duplexing schemes are defined for 4G LTE and 5G NR, subsequent calculations are assumed to be the more typical scenario of FDD cell configuration for 4G LTE and TDD for 5G NR

[2]The derivation for 5G NR downlink and uplink transport block size used in calculations for this work can be found in Appendix A

led published analysis in [95] and are used in later dimensioning analysis to represent a single RU small cell or distributed MIMO RU in a C-RAN deployment.

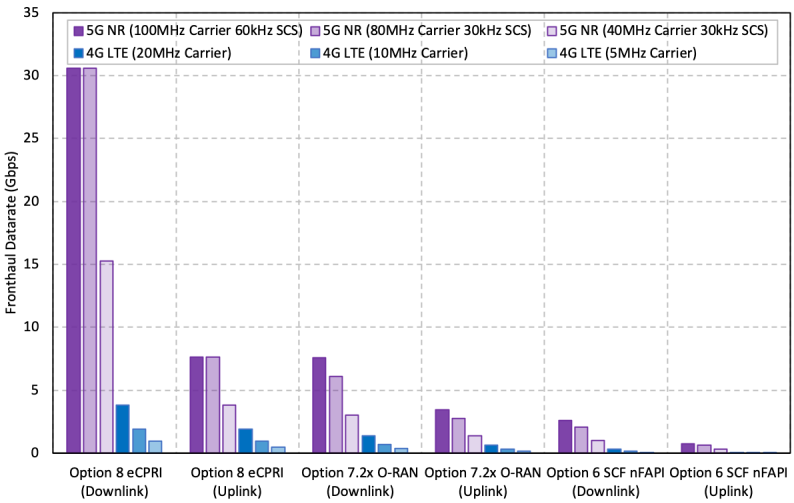

Figure 7.2: Example fronthaul datarates.

Table 7.1: Cell Configuration Used for Fronthaul Data Rate Calculations.

	4G LTE			**5G NR (FR1)**		
Channel Bandwidth (MHz)	5	10	20	40	80	100
SC Spacing (kHz)	15	15	15	30	30	60
SC Per RB [$N_{SCperRB}$]	12	12	12	12	12	12
RB Bandwidth (kHz)	180	180	180	360	360	720
Resource Blocks [N_{PRB}]	25	50	100	107	217	135
Subcarriers [N_{SC}]	300	600	1200	1284	2604	1620
Symbols per Slot [$N_{SymPerSlot}$]	14	14	14	14	14	14
Slot Length [T_{slot}] (ms)	0.001	0.001	0.001	0.0005	0.0005	0.00025
Sym Period per Slot [$T_{SymPerSlot}$] (μs)	71.4	71.4	71.4	35.7	35.7	17.9
FFT Size	512	1024	2048	2048	4096	2048
Sampling Frequency [fs] (MHz)	7.68	15.36	30.72	61.44	122.88	122.88
I/Q Quantizer Bits [M]	15	15	15	15	15	15
Mantissa Bits [$N_{mantissa}$]	9	9	9	9	9	9
Exponent Bits [$N_{exponent}$]	4	4	4	4	4	4
Antennas [N_{ant}] (UL/DL)	2/4	2/4	2/4	2/8	2/8	2/8
MIMO Layers [N_{layers}] (UL/DL)	2/4	2/4	2/4	2/4	2/4	2/4
Modulation Index [I_{MSC}] (UL/DL)	16/28	16/28	16/28	28/27	28/27	28/27

Reference cell configuration assumed in subsequent analysis

7.2.2 Latency

Unlike the fronthaul datarate requirements, the latency requirements (one way delay) of the different fronthaul lower layer functional splits are constrained by time bound closed loop processes higher in the protocol stack. As the fronthaul interface must support a range of cell configurations, the latency requirement becomes a function of the specific cell configuration, most notably whether the cell is 4G LTE or 5G NR radio.

- For 4G LTE based fronthaul (i.e. splits below the 4G LTE MAC layer - 3GPP option 6 and below) the packet delay constraint is underpinned by the total delay budget of the LTE HARQ (Hybrid Automatic Repeat Request) loop process which operates at the MAC layer – specifically the uplink HARQ loop process. In LTE, HARQ is asynchronous in downlink and synchronous in the uplink . In synchronous (uplink) HARQ, retransmission for each process occurs at predefined times relative to the initial transmission (every 8 subframes - equivalent to 8 ms or 8 transmission time intervals TTIs). This means that a HARQ process ID does not need to be signalled (saving downlink control information resource) and is instead inferred from the transmission timing. This also means that retransmissions must be scheduled at fixed, regular time intervals relative to the data subframe n (i.e. $n + 8$). In FDD mode, retransmission must occur within the 8 ms constraint so the UE must prepare the response as soon as it completes the decode of its data on subframe n and transmit it 4 ms (4 TTI) later. The UE must start its acknowledgement / negative-acknowledgement (ACK / NACK) transmission in the subframe $n + 4$ i.e. within the following 3 TTIs (3 ms) as in Fig. 7.3. In LTE, the physical HARQ indicator channel (PHICH) is a dedicated downlink channel to carry HARQ ACK / NACK for uplink traffic carried on the physical uplink shared channel (PUSCH).

  For LTE fronthaul specifications, a 100 μs maximum one-way delay is typically specified [12] [17] once the baseband processing delay of the HARQ procedure has been factored out. As this processing delay is implementation specific a more relaxed fronthaul delay budget is often quoted between 123 μs [96] and 250 μs [97] (where 2.5 ms is typically assumed for processing delay leaving 500 μs round trip delay or 250 μs one-way delay). It is however recognized that delay levels much beyond these figures have the potential for degraded UE performance as the HARQ process breaks down. For the nFAPI split 6 interface, the Small Cell Forum specifies signalling to allow HARQ interleaving and deferral of HARQ buffer emptying, this allows for higher 250μs latency fronthaul links to be tolerated.

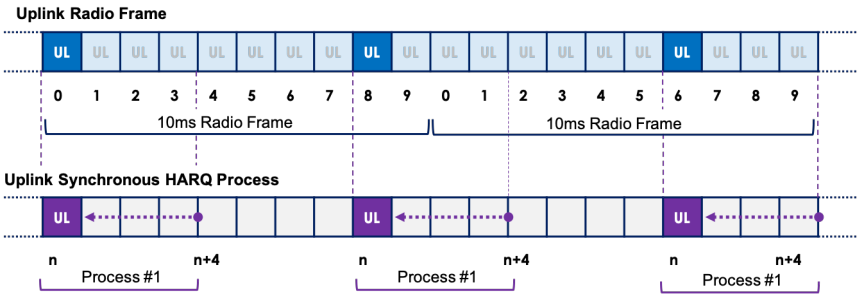

Figure 7.3: Delay constraints in 4G LTE fronthaul.

- In 5G NR, asynchronous HARQ is used in the uplink as well as downlink meaning that fronthaul splits at MAC layer and below are not constrained by the HARQ loop process in the same way as 4G LTE. In asynchronous HARQ, retransmissions can occur at any time, a HARQ process ID is signalled to correctly match any retransmission with the corresponding initial transmission. Although asynchronous HARQ adds overhead relative to synchronous HARQ it benefits from increased flexibility in scheduling and thus delay budget constraints. For Ethernet based 5G NR fronthaul, the transport latency requirements are instead driven by the next closed loop protocol timing constraint which is the configuration of the response window function in the random access procedure. In order to attach to the network a UE decodes the random access channel (RACH) configuration found in the cell broadcast information. This determines the time, frequency, preamble identity and repetition information to use when initiating the attach procedure (sending of a PRACH preamble) to the gNB (*MSG1*) as in Fig. 7.4. If *MSG1* is received correctly by the gNB, it transmits a random-access response (RAR) message to the UE (*MSG2*). The UE will monitor the physical downlink control channel (PDCCH) for the RAR message for a defined monitoring period. This monitoring period is set by the *raResponseWindow* parameter in system information block 1 (SIB1) which has a configurable value (defined in number of slots in 5G NR [98] not subframes as it is in 4G LTE). In 5G NR the subframe length of 1 ms can be divided into 1, 2, 4, 8, 10, 20, 40, 80 slots (rather than TTI in 4G), lasting a maximum of 1 ms or minimum of 12.5 μs [99]. As such the configured *raResponseWindow* is defined by the operator's configured numerology and the anticipated coverage and mobility of the cell. If the UE does not receive *MSG2* within the window it assumes a RACH failure and start over, thus fronthaul latency outside this delay budget directly impacts the ability for UEs to join the network. For a conventional 40 MHz or 80 MHz sub 6 GHz 5G RAN running 30 kHz sub carrier spacing such as in Table. 7.1 there are 2 slots per 1 ms subframe , this equates to a minimum configurable RA window size (and one way delay budget) of 500 μs and maximum of 4 ms.

For a typical 100 MHz carrier running 60 kHz sub carrier spacing there are 4 slots per subframe equating to a minimum configurable window size (and one way delay budget) between 250 μs and 2 ms.

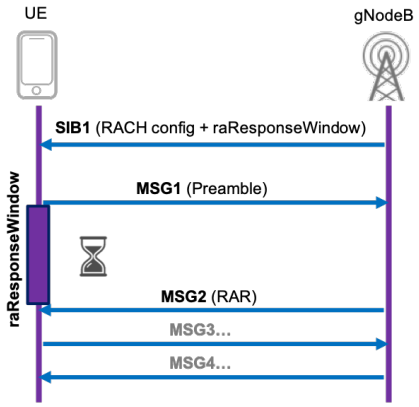

Figure 7.4: Delay constraints in 5G NR fronthaul.

To account for the variability in delay budget created by 5G NR specific configurations as well as the HARQ feedback loop constraint in 4G LTE (or 4G+5G in non-stand-alone deployments), fronthaul transport specifications such as 802.1CM, O-RAN and eCPRI define a range of latency classes between 25 μs for URLLC (5G ultra reliable low latency communication) use cases to 500 μs for large latency deployments incorporating longer transport propagation delay or switching delay in multi-hop transport networks. It should be noted however that complimentary specifications such as IEEE 802.1CM and O-RAN are ultimately based on underlying eCPRI specification requirements.

The control (and management) plane traffic flows for fronthaul splits necessary for scheduling and beamforming commands typically have greater tolerance in the transport delay budget. As these commands are typically vendor specific they are treated with more generalised requirements ranging from between 1 ms for 'fast' or 'near-real-time' control traffic to 100 ms for 'slow' or non-real-time' control traffic. A summary of Ethernet based fronthaul latency requirements and associated priority classes outlined by the relevant industry specification and standardisation bodies is given in Table. 7.2.

7.2.3 Jitter/Sync

The evolution toward Ethernet and packet based fronthaul means that synchronisation information is no longer transmitted by the specific fronthaul protocol (i.e eCPRI, O-RAN or nFAPI) but instead is addressed with existing and well established timing and synchronisation protocols such as Synchronous Ethernet (SyncE) or Precision Timing Protocol (PTP).

Table 7.2: Summary of Fronthaul Latency Requirements.

	eCPRI[100]	O-RAN [92]	IEEE [17]	One-way Delay Requirement	4G LTE User Plane	4G LTE Control Plane	5G NR User Plane	5G NR Control Plane	Application
High Priority	High25	High25	Class2	25μs			✓		Full NR Ultra-low latency performance
	-	High75	-	75μs			✓		Full NR performance with fibre lengths in the 10km range
	High100	High100	Class1 /Class2	100μs	✓		✓		Full E-UTRA or NR performance
	High200	High200	Class2	200μs			✓		Installations with fibre links lengths in the 40 km range
	High500	High500	Class2	500μs			✓		Large latency installations
Medium	Medium	Medium	Class2	1ms		✓	✓	✓	User Plane (slow), C and M Plane (fast)
Low	Low	Low	Class2	100ms		✓		✓	C and M Plane (slow)

■ Reference cell configuration assumed in subsequent analysis

- For legacy option 8 based fronthaul, synchronous interface protocols such as CPRI specify a 65 ns maximum variation in delay (jitter) of 2 sample periods Ts [12]. This is based on a 20 MHz 4G LTE carrier where the sampling frequency fs is 30.72 MHz. As a result a more relaxed delay variation tolerance is theoretically possible for smaller channel bandwidths e.g. 130 ns for 10 MHz and 260 ns for a 5 MHz carrier.

- For packet based fronthaul networks the maximum delay variation (jitter) constraints are fundamentally tied to the timing error budget requirements of the RAN. For packet based fronthaul interfaces, existing timing and synchronisation protocols such as PTP and associated PTP profiles such as G.8275.1 [101] are utilised to meet the relevant 3GPP time alignment error (TAE) specifications [102], [103]. As such it is the 3GPP feature set supported by the RAN which dictate the required TAE and resulting timing accuracy between DU and RU or clustered RUs. There are two distinct timing requirements for the RAN as shown in Fig. 7.5; an absolute time error requirement referenced to a primary reference time clock (PRTC) or telecom grandmaster (T-GM) clock and a relative time error requirement measured between any two elements in the cluster e.g RUs running telecom

time synchronous clocks (T-TSC) or intermediate telecom boundary clocks (T-BC). The time error budget requirements to meet the 3GPP TAE targets are derived in 802.1CM [17] and presented in Table 7.3. For an example typical FR1 5G RU as outlined in Table 7.1 supporting intra-band contiguous carrier aggregation a maximum delay variation between elements of 190 ns is specified [92], [100], [104].

Table 7.3: Summary of Fronthaul Timing Error Requirements

Category	**Time Error Requirements**		**3GPP Time Alignment Error between Antennas**	
	Integrated T-TSC [3]	**Non-integrated T-TSC**		
A+ (relative)	-	20 ns	65 ns	e.g. MIMO or Transmission Diversity
A (relative)	60 ns	70 ns	130 ns	e.g. FR2 Intra-band contiguous carrier aggregation
B (relative)	190 ns	200 ns	260 ns	e.g. FR1 Intra-band contiguous carrier aggregation
C (absolute)	1100 ns [4]	1100 ns	3 μs	e.g. TDD and dual-connectivity

■ Reference cell configuration assumed in subsequent analysis

[3] Figures assume the use of an 'enhanced' T-TSC in the RU where the time error budget contribution is lower (35 ns) compared with 'regular' T-TSC integrated with the RU (80 ns).

[4] O-RAN specifications define a wider range of absolute time error requirements (between 1320 ns and 1425 ns) based on a range of primary reference timing clock standards each with differing time error budget contributions (30 ns to 100 ns).

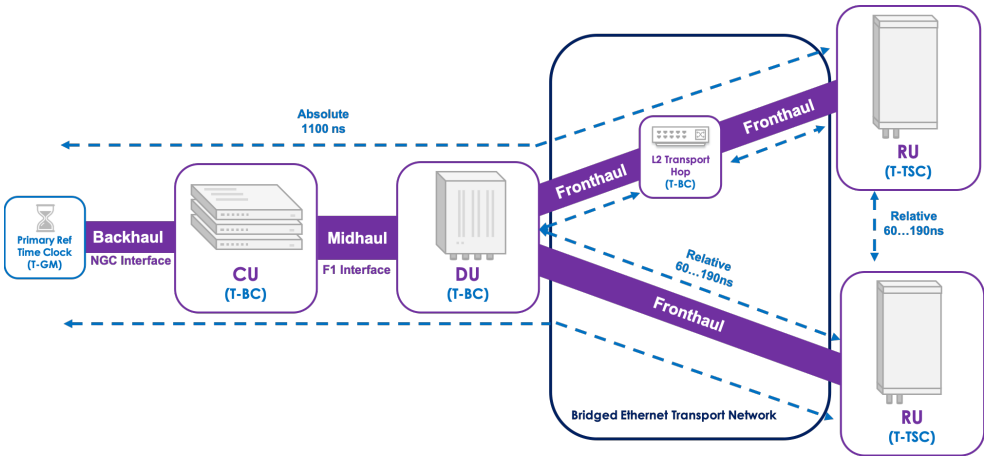

Figure 7.5: Example timing and synchronisation fronthaul architecture (integrated T-TSC).

7.2.4 Frame Loss

In a bridged Ethernet fronthaul network the frame loss ratio is specified as the limit which can be tolerated by the interface. As a result, the frame loss does not meaningfully characterise the service availability or resulting network performance. In a similar way to latency requirements, frame loss tolerance is specified per traffic flow (where priority classes are the same as in Table 7.2) with a common definition and specification across the various standardisation groups; eCPRI, O-RAN and IEEE as summarised in Table 7.4.

- The maximum tolerable frame loss ratio between edge ports of an I/Q based fronthaul data flow for the most stringent 'high' and 'medium' class of service (CoS) is 10^{-7}. A more relaxed frame loss tolerance of 10^{-6} for 'slow' / 'non-real-time' control flows is specified [92].

Table 7.4: Summary of Fronthaul Frame Loss Requirements.

Priority	**Application**	**Frame Loss Ratio**
High (High25 - High500)	User Plane (fast)	10^{-7}
Medium	User Plane (slow), C and M Plane (fast)	10^{-7}
Low	C and M Plane (slow)	10^{-6}

■ Reference cell configuration assumed in subsequent analysis

7.3 Wireless Transport Testbed

In order to examine the feasibility of wireless fronthaul, and verify the theoretical performance criteria of new functional split interfaces derived in Section 7.2, a wireless fronthaul testbed is built. The experimental setup is depicted in Fig. 7.6. The testbed is comprised of two network functions; the radio access network, built on the inherent flexibility offered by the opensource software libraries of OpenAirInterface5G (OAI5G) [105], and the transport network provided by an E-band mmWave point-to-point radio link. The testbed is designed to address two key aspects of the wider research thesis; firstly to understand the real world performance of a state-of-the-art commercially available wireless transport system, and secondly, to demonstrate a working end to end implementation of wireless fronthaul based centralised RAN deployment.

7.3.1 OpenAir Interface System Model

The RAN aspects of the fronthaul testbed comprises of a core network connected to an end-to-end LTE system from eNodeB to commercial-off-the-shelf (COTS) User Equipment (UE). A 4G system is utilised in this study which has a comparable

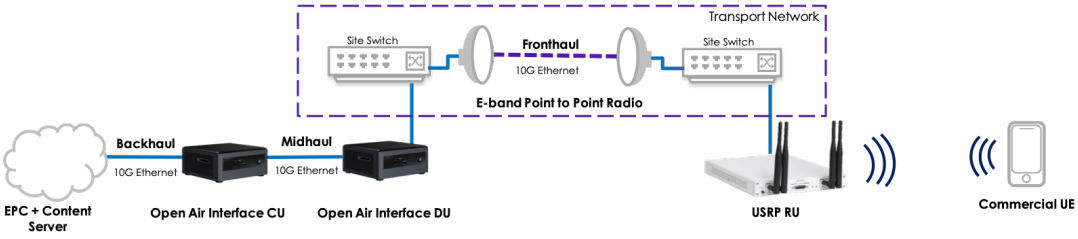

Figure 7.6: Wireless fronthaul testbed setup.

radio interface to 5G but offers a more mature and stable solution at the time of writing. The functionalities of the protocol stack are implemented in the eNodeB via OAI5G. The OAI CU and DU software is installed on machines with 16 GB of RAM memory and Intel Core i7 CPU @ 3.2 GHz and 10 Gbps Ethernet interfaces. The DU machine is connected to an Ettus Universal Software Radio Peripheral (USRP) X310 device over 10 Gbps Ethernet link acting as the RU. OAI5G was installed and configured on the machine with minimal modifications. However, it is acknowledged that the processing capability of hardware used in this study is below the recommended specification for operation of eNodeB channel bandwidths above 10 MHz. As a result, the radio interface configuration under study is kept in a basic 5 MHz or 10 MHz channel bandwidth operating at 2.6 GHz (3GPP band 7) with single input single output (SISO) antenna configuration. The CU is connected to an Athonet core network built for lab environment testing which is a complete virtual Enhanced Packet Core (vEPC). The commercial UE device used for verification of end user performance testing was a Samsung Galaxy Tab S6.

7.3.2 mmWave Transport Network

The wireless fronthaul transport link under test in this study is a point-to-point E-band mmWave link as shown in Fig. 7.7. The link represents commercially available carrier grade equipment configured for use in the 'self-co-ordinated' lightly licensed portion of the band in the UK (73.375-75.875 GHz / 83.375-85.875 GHz). For peak capacity the link operates with 2 GHz channel bandwidth at 128 QAM for a physical layer data rate of 10 Gbps limited by the optical port interfaces. The system can operate with a maximum transmit power of upto 10 dBm and antenna gain of 46.6 dBi. The link spans a short 255 m distance between rooftops at BT's R&D headquarters in Martlesham, UK. Longer link performance is simulated through modification of the operating modulation rate.

7.3.3 Benchmarking Results

The theoretical fronthaul requirements discussed in Section 7.2 are first assessed against the capability of the E-band link with a benchmarking exercise of the

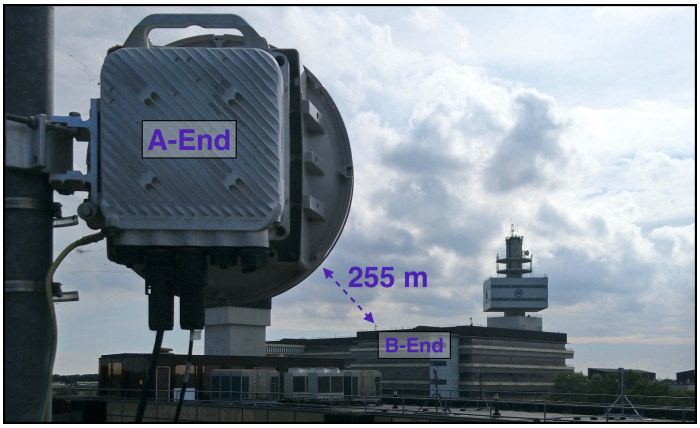

Figure 7.7: E-band testbed transport link.

testbed transport network (TN) outlined in Fig. 7.6. Each transport performance metric criteria (as outlined in Section 7.2) is assessed with alignment to RFC 2544 [106] test procedures for 0% frame loss and with ± 10 ns accuracy.

In the benchmarking exercise, the test traffic payload is aligned with the OAI option 8 implementation which is broadly equivalent eCPRI overhead. The Ethernet framing headers accounts for an additional 14 bytes per 1514 byte Ethernet frame. Rather than a standardised RoE or eCPRI Ethertype header, an IP and UDP encapsulation is used accounting for an additional 28 bytes and an available fronthaul data payload of 1472 bytes. The capacity, latency and jitter characteristics of the wireless fronthaul are measured at three different channel bandwidths B_{GHz} of the E-band radio; 0.5 GHz, 1 GHz and 2 GHz (the maximum possible with the equipment and spectrum available). The performance expectations of different length links are assessed through manual configuration of each modulation rate supported. Based on the measured results the anticipated performance of a higher capacity 5 GHz channel is also modelled with the aim of representing the future capability of a D-band or aggregated E+W band solution.

7.3.3.1 Datarate Measurements and Modelling

The maximum available capacity measured over the E-band transport link with a 1472 byte fronthaul payload was 9589.9 Mbps, this is the highest measured point shown in Fig. 7.8. This was achieved at the highest modulation rate of 128 QAM (7 bits per symbol) and maximum available channel bandwidth of 2 GHz for the equipment under test. The measured capacity for other lower channel bandwidths (1 GHz and 0.5 GHz) and modulation configurations (2-8 bits per symbol) is also presented in Fig. 7.8. In addition to the measured results, the theoretical (predicted) capacity for each modulation rate (in bits per symbol BPS) and higher channel bandwidths B_{GHz} representative of future W or D-band

systems is calculated from (7.7) where the Reed-Solomon data stream coding RS_{OH} and Trellis coding rates TC_{OH} are aligned with ETSI fixed radio system examples [107]. In addition, the Ethernet framing overheads ETH_{OH} outlined in Section 7.3.3 are accounted for. Whilst the coding and overheads assumptions in Table. 7.5 may not necessarily be representative of all commercially available mmWave transport systems, the modelling calculations, which are also overlaid in Fig. 7.8, fit well to the measured results providing confidence in the forecast capacities for 5 GHz channels possible in bands above 100 GHz.

$$\text{TN\_Capacity}_{\text{Gbps}} = (\text{BPS} \cdot B_{GHz}) \cdot \text{RS}_{\text{OH}} \cdot \text{TC}_{\text{OH}} \cdot \text{ETH}_{\text{OH}} \tag{7.7}$$

Table 7.5: Wireless Transport Capacity Model Coding and Overhead Assumptions.

Transport Link Modulation	**QPSK**	**8PSK**	**16 QAM**	**32 QAM**	**64 QAM**	**128 QAM**	**256 QAM**
PHY Symbol Rate [BPS]	2	3	4	5	6	7	8
PHY Coding	RS (255/243)	RS (255/243)	16TCM-4D (4/3.5) + RS (255/243)	32TCM-2D (5/4.5) + RS (255/243)	64TCM-4D (6/5.5) + RS (255/243)	128TCM-4D (7/6.5) + RS (249/243)	256TCM-4D (8/7.5) + RS (249/243)
Reed-Solomon Overhead [RS_{OH}]	0.953	0.953	0.953	0.953	0.953	0.976	0.976
Trellis Coding Overhead [TC_{OH}]	-	-	0.875	0.900	0.917	0.929	0.938
Ethernet Overhead [ETH_{OH}]	0.968	0.968	0.968	0.968	0.968	0.968	0.968

In addition to the measured and forecast capacity of the link, data rates for each of the functional split requirements discussed in Section 7.2 are also overlaid on Fig. 7.8 in red. The fronthaul requirements for the 'reference cell' configuration in Table. 7.1 (5G NR with 100 MHz carrier) serve as reference for later fronthaul dimensioning where the necessary performance requirement can be met.

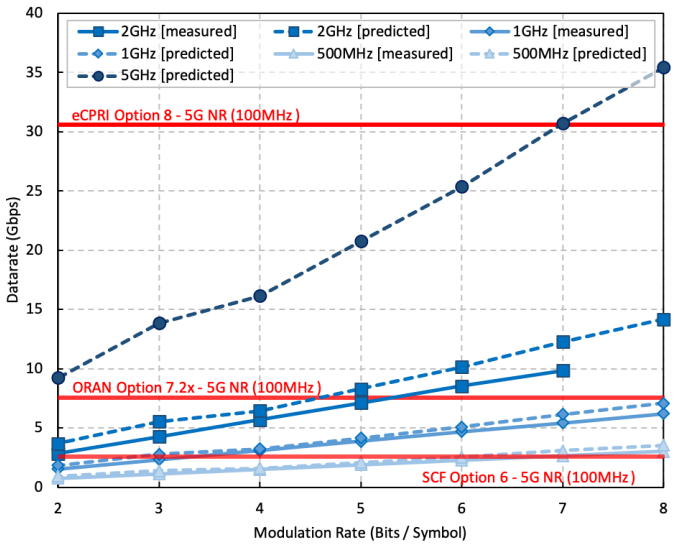

Figure 7.8: Wireless transport capacity (1472 byte).

7.3.3.2 Latency Measurements and Modelling

The latency characteristics of the commercial E-band link are also recorded for a range of modulation schemes and channel bandwidths in Fig. 7.9. These transport network characteristics also include any delay contribution through the two site switches and represent an ideal deployment where there is no other traffic aggregation, prioritisation or queuing present on any of the Ethernet ports in the path. The transport network elements in this particular scenario do not support the ideal end-to-end IEEE time-sensitive network (TSN) protocols which have the to potential to further optimise performance for priority fronthaul traffic flows.

The minimum one-way delay measured for a 1472 byte fronthaul payload was of 40.6 μs achieved at the highest capacity configuration of 2 GHz and 128 QAM. The measured results demonstrate a clear correlation with the available link capacity allowing a prediction model to be derived for equivalent higher capacity links. A curve fitting approach is used for the predicted 5 GHz channel latency characteristics because although the latency characteristics are fundamentally a function of the available bandwidth, the queuing, buffer and processing delay contributions of the hardware will be implementation specific and thus not easily modelled for future D-band hardware performance. As a result the latency prediction model in (7.8) is derived solely from the measurement data channel bandwidth B_{GHz} and modulation rate BPS and extrapolated for the 5 GHz channel bandwidth case. The predicted latency characteristics are overlaid with measured results in Fig. 7.9 which demonstrate good agreement providing confidence that use of the proposed latency model in wider deployment modelling will provide realistic results grounded in real-world experimental measurements. The one-way

delay threshold for the 'reference cell' configuration in Table 7.1 and 7.2 (High 100) is again shown in red representing the upper latency limit for link configurations used in later dimensioning and deployment analysis.

$$\text{TN\_Latency}_{\mu s} = (138 \cdot B_{GHz}^{-0.8}) \cdot \text{BPS}^{(0.23 \cdot ln(B_{GHz}))-0.52}, \quad 0.5 \leq B_{GHz} \leq 5 \tag{7.8}$$

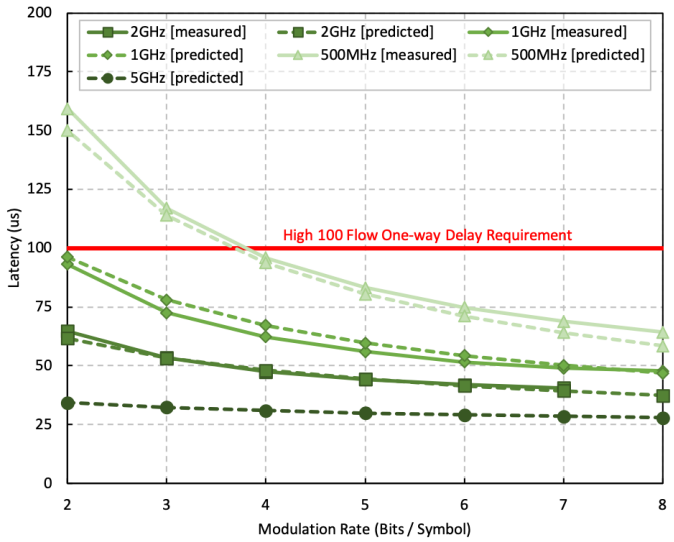

Figure 7.9: Wireless transport latency (1472 byte).

7.3.3.3 Jitter Measurements and Modelling

The measured jitter characteristics for the E-band transport network are shown in Fig. 7.10 where the minimum achievable jitter of 20 ns was measured at the highest capacity configuration. The measured jitter values represent a wireless transport network leg where there is no traffic prioritisation or management implemented. In practice, delay variation in the transport network could be optimised through application of TSN Ethernet technologies where effective queue and buffer management could potentially reduce or eliminate jitter at the cost of increased fixed one-way delay [108]. A jitter model is also constructed based on the channel bandwidth B_{GHz} and modulation rate BPS of the measurement data of the testbed radio link to predict likely jitter characteristics of wider channel solutions in (7.9). The jitter prediction model shows a good fit to measurement data at higher modulation schemes but reduced accuracy at lower modulation schemes with smaller channel sizes. This again demonstrates that the proposed jitter model is a reliable mechanism to predict realistic jitter characteristics of simulated links constructed in later deployment feasibility studies.

$$\text{TN\_Jitter}_{\text{ns}} = (1424 \cdot B_{GHz}^{-0.7}) \cdot \text{BPS}^{(-0.43 \cdot B_{GHz})-0.82}, \quad 0.5 \leq B_{GHz} \leq 5 \tag{7.9}$$

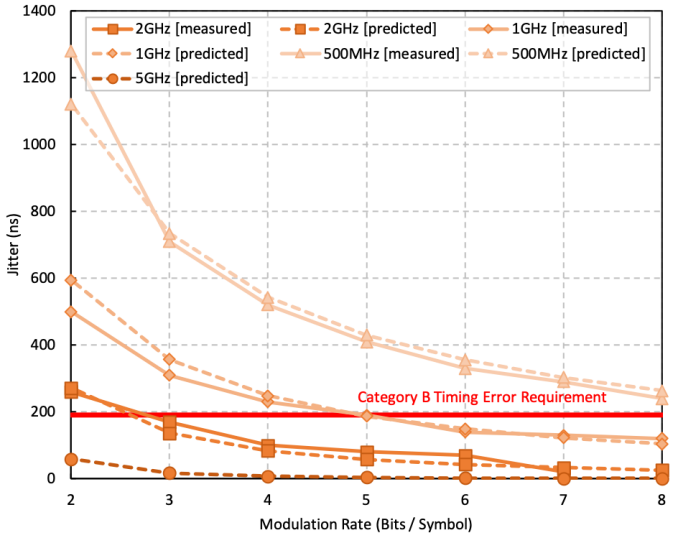

Figure 7.10: Wireless transport jitter (1472 byte).

The relative timing requirement (Category B) used for the 'reference cell' fronthaul interface as highlighted in Table 7.3 is also overlaid in red on Fig. 7.10. This represents the maximum permissible timing error in a fronthaul traffic flow (without optimised TSN timing and synchronisation support) for subsequent dimensioning and feasibility analysis.

7.4 Wireless Fronthaul Proof of Concept

With the benchmarked performance metrics of the mmWave transport network characterised, the operational performance of the OAI fronthaul is measured where the wireless transport network is deployed between DU and RU entities. The transport interfaces of the DU and RU are monitored in real-time using packet traces from mirrored Ethernet ports on the sites switches. As outlined in section 7.3.1 the performance capabilities of the hardware used in the testbed limit the RAN configurations possible for experimental measurements. As such rather than the ideal 'reference cell' example configuration highlighted in section 7.2 and used in later (Chapter 8) dimensioning and deployment modelling, a basic low capacity 4G eNB is configured for operational validation and proof-of-concept.

7.4.0.1 Verification of Occupied Bandwidth

The occupied fronthaul bandwidth for the option 8 CPRI over Ethernet OAI implementation is assessed and compared to the theoretical bandwidth (calculated from (7.2) and the eNodeB radio interface parameters in Table 7.6). For the two baseline configurations of a 5 MHz and 10 MHz 4G LTE single antenna eNodeB

the expected data rate was a CBR 256 Mbps and 511 Mbps respectively between DU and RU.

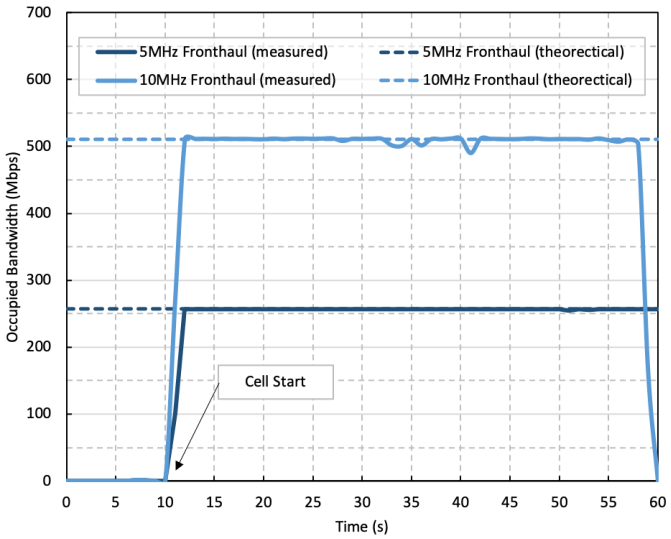

Figure 7.11: Occupied fronthaul bandwidth of 5 / 10 MHz eNodeB.

Table 7.6: Theoretical and Measured Fronthaul Datarates.

LTE Channel Bandwidth (MHz)	**5**	**10**
SC Spacing (kHz)	15	15
Resource Blocks	25	50
Subcarriers	300	600
FFT Size	512	1024
Quantizer Bits $[M]$	15	15
Sampling Freq $[fs]$ (Msamples)	7.68	15.36
Antennas $[N_{ant}]$	1	1
Theoretical OAI Datarate $[\mathrm{D}_{\mathrm{CPRI}_{\mathrm{ETH}}}]$ (Mbps)	**256**	**511**
Theoretical OAI Latency (μs)	**100**	**100**
Theoretical OAI Jitter (ns)	**260**	**130**
Measured OAI Datarate (Mbps)	**257**	**510**

Firstly, the fronthaul traffic is monitored with the testbed transport network operating at maximum capacity (2 GHz bandwidth and 128 QAM modulation). The measured option 8 CBR datarate is shown in Fig. 7.11 and summarised in Table 7.6 and show very good agreement with theory when factoring in the OAI packetisation overheads. The measured data rates for the 5 MHz configuration was 257 Mbps and 510 Mbps for a 10 MHz configuration (within 1 Mbps of the theoretical value) which validates that the theoretical derivations of datarate requirements can be reliability used for later dimensioning and deployment

analysis. The operational performance of the wireless fronthaul link is verified by successful connection of the UE to the eNodeB and EPC and completing an end to end traffic speed test.

7.4.0.2 Operation with Lower Performing Links

To further verify the theoretical requirements and viability of wireless fronthaul, the same measurements are repeated (still using a 2 GHz channel bandwidth) but for each modulation scheme supported by the E-band link in line with the benchmarked configurations in Section 7.3.3 to simulate lower performing longer distance transport links. Based on the benchmarking results it was expected that the both capacity and latency characteristics of the wireless fronthaul transport for all modulation settings would be sufficient for the basic 5 MHz and 10 MHz OAI eNodeB operation.

Because the OAI option 8 implementation represents a packetised version of legacy synchronous fronthaul akin to CPRI over Ethernet, the delay variation tolerance is equivalent to 2 sample periods i.e 130 ns for a 10 MHz carrier and 260 ns for a 5 MHz carrier. For jitter tolerance, benchmarking measurements would suggest that performance of the transport network would fall outside of theoretical 10 MHz carrier 130 ns specification below 16 QAM (4 bits / symbol) as highlighted in Fig. 7.10. In testing, the 5 MHz eNodeB carrier configuration was able to maintain full operational performance across all the fronthaul transport link modulation schemes tested. For 10 MHz operation however, the fronthaul interface could not be reliably sustained at the 32 QAM level where the transport jitter performance was still expected to be sufficient and failed completely at all lower modulation settings (summarised in Table 7.7). It is believed that the fronthaul interface failed earlier than anticipated in the 10 MHz configuration (at 32 QAM rather than below 16 QAM) due to unquantifiable jitter contributions in the DU processing stage. While these failure scenarios may be attributed to sub-optimal hardware performance in this particular setup, results do highlight the sensitivity, particularly to jitter variation, for option 8 Ethernet based fronthaul in practical deployments. Such findings however are still promising. As previously discussed, the implementation of key Ethernet TSN transport technologies is absent in this particular experiment. The sensitivity to packet delay variation (jitter) can potentially be addressed with appropriate buffer and queue management optimisations albeit at the expense of increased fixed offset delay (latency). As can be seen from the benchmark results in section 7.3.3, the one-way latency budget for such high capacity mmWave systems provides sufficient overhead to compensate for some level of delay variation absorption in an optimised solution.

Table 7.7: Wireless Fronthaul Operational Results Summary.

Transport Link Modulation	**128QAM**	**64QAM**	**32QAM**	**16QAM**	**8PSK**	**QPSK**
5MHz eNodeB FH Operation	OK	OK	OK	OK	OK	OK
10MHz eNodeB FH Operation	OK	OK	NOK	NOK	NOK	NOK

7.5 Chapter Summary

The fronthaul interface requirements necessary to realise the evolving concepts of Ethernet based mobile fronthaul are derived in this chapter. The characteristics of key, industry led, fronthaul functional split standardisation efforts are explored and their requirements assessed in the context of wireless transport. A high capacity wireless transport testbed is also established in order to experientially verify the performance characteristics of the latest E-band commercial radio system and to model the potential performance characteristics of higher bandwidth future systems such as W-band and D-band. The testbed is further utilised to validate the theoretical fronthaul requirements through demonstration of a proof-of-concept wireless fronthaul C-RAN based on OAI components. The proof-of-concept study has demonstrated promising results where even the most stringent requirements of the 3GPP option 8 fronthaul interface could feasibly be supported over existing high capacity mmWave transport solutions such as E-band. Although findings have highlighted limitations on the current cell configurations possible, the viability of wireless fronthaul has nevertheless been experimentally demonstrated. The findings highlighted in this chapter serve as fronthaul performance criteria for the deployment models established in previous chapters. The results represent a single hop wireless fronthaul link which can be used in combination with the DSM based LoS deployment models in Chapter 6 to form a performance orientated deployment feasibility analysis in the following chapter.

Chapter 8

Wireless Fronthaul Deployment Feasibility

Each of the topics supporting the underlying research questions outlined in this work are brought together in this chapter. In attempting to understand the role of wireless transport in future centralised mobile network architectures, the deployment model, fronthaul interface requirements and wireless transport capability findings from previous chapters are finally combined in a dimensioning and feasibility exercise. In applying a link by link performance orientated assessment of the existing deployment model and using representative wireless transport performance and realistic functional split requirements, this chapter aims to highlight the extent to which wireless fronthaul can be used to support C-RAN deployments. The analysis in this chapter considers combinations and permutations of technology options to highlight the optimal choice of fronthaul interface, spectrum band and deployment scenario which could maximise the opportunity to utilise wireless transport in C-RAN based deployment architectures.

8.1 Introduction

In this chapter, the fundamental requirements of emerging fronthaul interfaces at key functional split points (options 8, 7.2x and 6) are applied and combined with the performance characteristics of mmWave and sub-THz wireless transport bands (E, W and D-band). The fronthaul dimensioning analysis of a representative 5G small cell RU configuration with candidate wireless transport bands is used as a pre-requisite for wider deployment feasibility analysis based on fronthaul performance capability. These contributions aim to provide new insight into the feasibly of deploying 5G small cells or remote RUs in environments such as urban street canyons using wireless fronthaul. Crucially, analysis is based on industry standardised fronthaul interfaces and spectrum bands targeted for global harmonization.

Some studies considering the performance criteria of fronthaul interfaces have previously been considered for wireless transport from a theoretical perspective. In [109] and [110] a number of promising enabling technologies such as fronthaul compression and line-of-sight MIMO are considered as a means of meeting fronthaul performance criteria with wireless transport. Analysis suggests that reliable fronthaul performance can be achieved using line-of-sight MIMO at 80 GHz in order to meet the necessary spectral efficiency. In [111] it is recognised that the flexibility of wireless transport solutions offer cost and time benefits over the more ideal optical transport. A number of candidate mmWave bands are also explored where it is concluded that the requirements of upper-layer fronthaul split interfaces could be met with existing bands below 100 GHz whilst suggesting lower layer splits would need to be addressed with higher capacity spectrum bands above 100 GHz due to the more demanding latency requirements. The data rate requirements of various fronthaul splits are also calculated for a range of realistic 5G cell configurations in [112]. Here, the data rate requirements are compared with simulation results of the available capacity from various channel bandwidths operating at 105 GHz and 220 GHz sub-THz bands. Results suggest that the lowest option 8 and 7.1 splits are not a suitable split option for sub-THz fronthaul transport where link distance of least 100 m is required.

While literature to date suggests the concept of wireless fronthaul could be realised to some extent both theoretically and experimentally, research has generally been focused on narrow performance criteria such as data rates or latency and without consideration for where or how such links may be deployed. To address these literature gaps and understand the viability of wireless fronthaul, a wider analysis is required considering all the transport requirements and technology capabilities together with real-world environmental data such as that offered by the DSM deployment model developed in this work. As Ethernet based fronthaul interfaces start to become a reality due to standardisation efforts, the question of wireless fronthaul feasibility also becomes more evident and whether there is an opportunity for emerging wireless transport solutions to accelerate the adoption of commercial C-RAN deployments.

In this chapter the deployment opportunity for wireless fronthaul is studied. Representative system parameters for candidate wireless transport spectrum bands are studied in Section 8.2 where the anticipated operational link budget and performance of candidate bands are derived. This is subsequently combined in a dimensioning exercise in Section 8.3 with the various fronthaul interface requirements for the reference 5G cell configuration outlined in Chapter 7. These final inputs serve as the capability profiles of an adapted deployment model now based on the performance criteria proposed in Section 8.4. Results from the performance-led deployment model for a range of deployment scenarios are discussed in Section 8.4.1 - 8.4.3 with the aim of highlighting the potential of high frequency transport bands to deliver candidate fronthaul interfaces splits

over wireless transport in real-world deployment scenarios.

8.2 Wireless Transport Link Budget

To support the performance profiles and predictions in Chapter 7 the link budget for each candidate wireless fronthaul transport band (E, W and D-band) is characterised. The system configuration assumptions for the wireless transport options are detailed in Table 8.1. For simplicity, a single carrier, single polarization, FDD system is assumed in each case. Many configurations are possible in these bands however each follow a 250 MHz channel raster aligned with ITU specifications. For E-band the maximum channel size currently specified by the ITU is 2 GHz with a duplex spacing of 10 GHz. Assumptions about channel operating frequency and maximum channel bandwidths possible for W-band and D-band are aligned with current industry expectations [78] pending channel arrangement harmonisation in these bands [80]. The channel rasters for W and D-band also follow a 250 MHz spacing where 2 GHz channel size is assumed for W-band with an FDD duplex separation of 11.55 GHz (sub-channel arrangement 'M' [25]) and 5 GHz for D-band with an FDD duplex spacing of 15.50 GHz (sub-band arrangement 'b/c' [26]).

Other key parameters directly influencing the total system gain and resulting link budget include the achievable transmit power and antenna gains. For E-band, the transmit power of commercial solutions such as that utilised in the testbed is in the order of +10 dBm. For W-band, the frequency range and channel bandwidths are broadly in line with E-band for which they are expected to be based on similar transistor and fabrication technologies and thus similar transmit power. For D-band, literature would suggest that alternative fabrication technologies are more suitable for higher frequencies but equivalent power output is nevertheless achievable [113] and so the assumed transmit power has been scaled with channel bandwidth accordingly. For antenna gain, the 30 cm 46.6 dBi parabolic antenna used in the testbed environment does not represent a solution suitable for urban street level deployments. Recent advancements in compact flat panel phased array antenna systems offer the potential for automatic beam alignment techniques and a more appropriate compact solution - albeit with reduced peak gains. As such the link budget analysis assumes antenna gain in the order of 35-40 dBi based on early prototype studies [32] [114].

The minimum received signal level required for each modulation scheme $\mathrm{RSL_{mod}}$ is aligned with ETSI TR 101 854 v2.1.1 [107] in (8.1) when considering the channel bandwidth B_{MHz}, typical noise figure NF, industrial margin $\mathrm{IM_F}$ and theoretical signal-to-noise ratio $\mathrm{SNR_{mod}}$ necessary for each modulation rate (in bits per symbol BPS). While ETSI examples do not provide data for receiver noise figures above 86 GHz, examples of prototypes and laboratory measurements in

Table 8.1: Summary of Wireless Transport System Parameters.

	E-band		**W-band**		**D-band**	
	A-End	**B-End**	**A-End**	**B-End**	**A-End**	**B-End**
Frequency (MHz) [f_{MHz}]	72125	82125	95325	103125	143625	158625
Channel Bandwidth (MHz) [B_{MHz}]	2000	2000	2000	2000	5000	5000
Water Vapour Attenuation (dB/km) [γ_w]	0.25	0.32	0.43	0.54	1.09	1.59
Gaseous Adsorption (dB/km) [γ_o]	0.20	0.06	0.03	0.04	0.02	0.02
Polarization	V	V	V	V	V	V
Rain Rate 99.99% Availability (mm/hr)	25	25	25	25	25	25
Rain Attenuation (dB/km) [γ_R]	10.62	11.30	11.90	12.07	12.51	12.74
Tx Radiated Power (dBm)	10.00	10.00	10.00	10.00	6.02	6.02
Tx Antenna / BF Gain (dBi)	40	40	35	35	35	35
Rx Antenna / BF Gain (dBi)	40	40	35	35	35	35
Rx Chain Losses (dB)	1.00	1.00	1.00	1.00	1.00	1.00
Rx Noise Figure (dB) [NF]	13.00	13.00	13.00	13.00	13.00	13.00
Industrial Margin (dB) [$\mathrm{IM_F}$]	4.00	4.00	4.00	4.00	4.00	4.00
Min Rx Sensitivity (dBm)	**-63.99**	**-63.99**	**-63.99**	**-63.99**	**-60.01**	**-60.01**
Max System Gain (dB)	**152.99**	**152.99**	**142.99**	**142.99**	**135.03**	**135.03**

literature would suggest a noise figure in the order 10 dB [115] or lower [116] is nevertheless possible in D and W-band using SiGe semiconductor technology. As these figures do not likely represent a commercialised solution at cost, a more conservative noise figure of 13 dB is assumed. The resulting link budget calculations in are within 1 dB of the manufacturers quoted specifications for the E-band testbed link and thus deemed a suitable approximation for future commercialised systems operating at W and D-band.

$$\begin{aligned} \mathrm{RSL}_{mod} &= -174 + 10 \cdot (\log_{10} B_{MHz}) + \mathrm{NF} + \mathrm{IM_F} + \mathrm{SNR}_{mod} \\ &\text{Where} \\ \mathrm{SNR}_{mod} &= 10 \cdot \left(\log_{10}\left(2^{BPS}\right) - 1\right) \end{aligned} \tag{8.1}$$

The environmental conditions necessary to meet a 99.99% atmospheric availability target in the link budget calculations for each candidate frequency f_{MHz} are modelled using ITU atmospheric adsorption modelling recommendations ITU-R P.676-11 [31]. Water vapour attenuation γ_w and gaseous (dry air) adsorption γ_o contributions in dB/km are calculated based on a representative UK atmospheric pressure of 101.3 kPa, a temperature of 15 °C and a water vapour density of 7.5 g/m^3. For peak rainfall losses γ_R factored in to the link margin, a 25 mm/hr rain rate in dB/km is assumed (ITU rain zone F for the UK) where calculations are aligned with ITU-R P.838-3 [30] for a vertically polarized, 0° path elevation link. The total path loss calculation PL at distance d_{km} is given in (8.2).

$$\mathrm{PL} = 32.4 + (20 \cdot (\log f_{MHz})) + (20 \cdot (\log d_{km})) + (d_{km} \cdot (\gamma_w + \gamma_o + \gamma_R)) \tag{8.2}$$

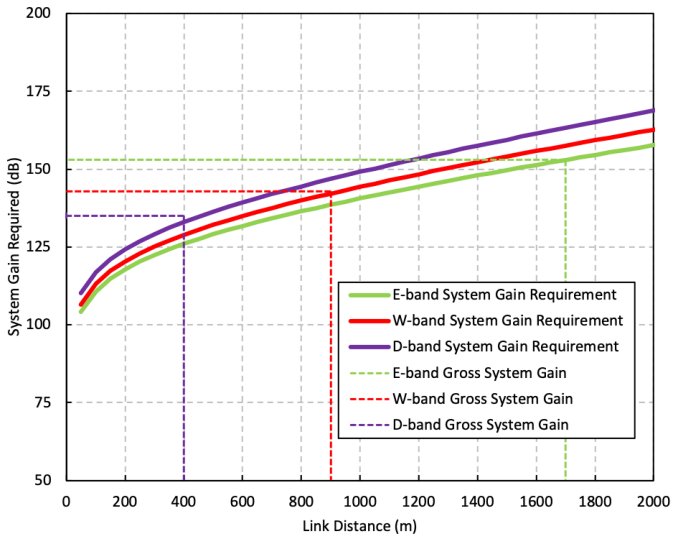

Figure 8.1: System gain requirements for single hop wireless transport.

The resulting path loss profile in terms of total system gain requirements (based on a maximum 256 QAM modulation and minimum QPSK) can be seen in Fig. 8.1. The link budget definition in terms of system gain requirement allow for the fronthaul interface performance metrics to be calculated for each modulation rate and ultimately determine operational link lengths that can be used in the deployment model. This is discussed in the following section.

8.3 Reference Cell Dimensioning

To understand the deployment feasibility of wireless fronthaul the performance measurements and predictions from Section 7.3.2 and the link budget analysis from Section 8.2 are combined. The resulting data rate, latency and jitter characteristics of each candidate spectrum band as a function of link distance is calculated and shown in in Fig. 8.2, 8.3 and 8.4.The cell configuration used in the dimensioning exercise is the 100 MHz 5G reference cell highlighted in Tables 7.1, 7.2 and 7.3 which aim to be representative of a typical 5G small cell or distributed RU. The requirements of the reference cell for each of the standardised functional split interfaces considered (eCPRI option 8, O-RAN option 7.2x and SCF nFAPI option 6) are also overlaid in red on the link budget capability graphs in Fig. 8.2, 8.3 and 8.4. These key performance indicator (KPI) budgets serve as the limit for wireless fronthaul dimensioning. These link budget performance KPIs are combined into the routing cost metrics to be used when adding new cell sites to the deployment model. Here, the total KPI budget may be consumed by one or more hops between potential infrastructure sites in the deployment topology graph.

When considering each of the data rate, latency and jitter requirements it can be seen that only D-band could feasibly support an option 8 split fronthaul interface due to capacity constraints in the other bands. While the reference cell configuration employing an option 7.2x or 6 split could be supported on all candidate transport bands, only D-band could support these interfaces over the full link budget of the system (upto 350 m). The O-RAN option 7.2x split becomes data rate limited with E-band and W-band after 850 m and 350 m respectively whilst the lower data rate SCF nFAPI option 6 becomes jitter limited in E-band beyond 1250 m and 550 m in W-band. In all candidate transport bands the dimensioning analysis suggests adequate latency budget for each fronthaul split interface across the full operation link length. Although the data rate requirements of an option 8 fronthaul interface demonstrates a limited deployment potential, the operating regions for option 7.2x and 6 in these high frequency transport bands still suggest good alignment with the dense urban cell inter-site distances and link lengths characterised in Chapter 6.

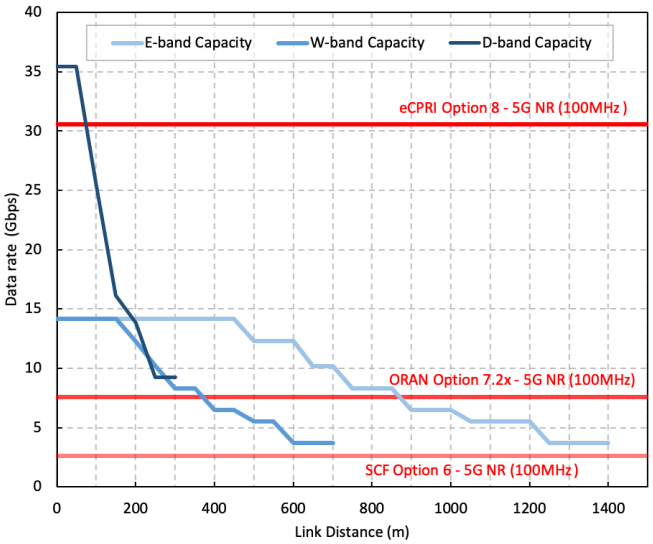

Figure 8.2: Operating regions for reference cell (single-hop) fronthaul capacity requirement.

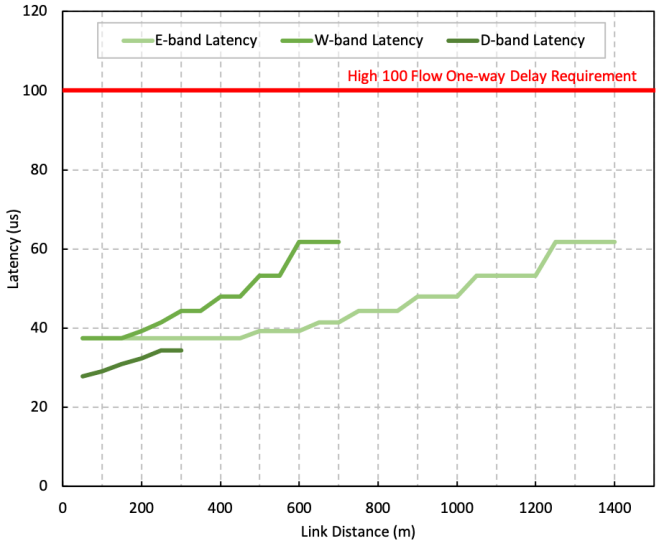

Figure 8.3: Operating regions for reference cell (single-hop) fronthaul latency requirement.

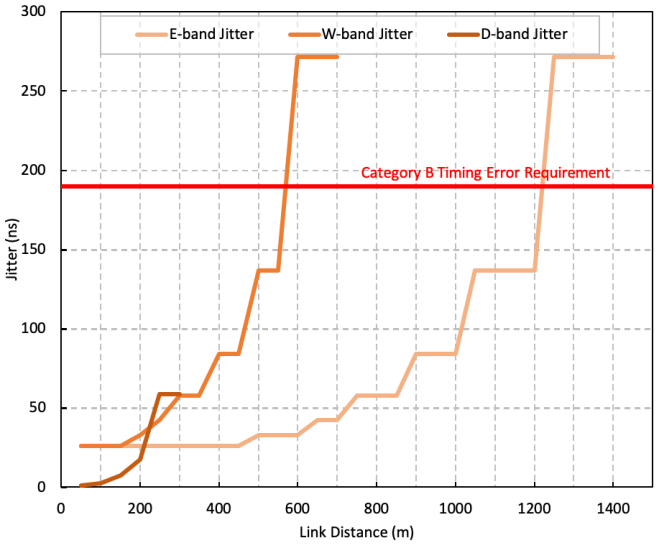

Figure 8.4: Operating regions for reference cell (single-hop) fronthaul jitter requirement.

8.4 Performance-Led Deployment Model

With all the necessary dependencies of the wireless fronthaul concept now identified, input profiles both in terms of fronthaul performance requirements and wireless transport solution capabilities are incorporated into the main

deployment model. The input profiles are utilised to extend the generic LoS based environmental deployment model of Chapter 6 to allow for a performance-led deployment analysis - summarised in Fig. 8.5. In this approach rather than the generic LoS transversal between potential infrastructure sites in the model, each link is now modelled as if it were an E, W or D-band transport solution with the associated performance characteristics as derived in Section 8.3. In addition, the propagation and availability characteristics can be applied from Section 8.2 of this chapter such that the link budgets, availability targets and link distances and are reflective of real-world conditions.

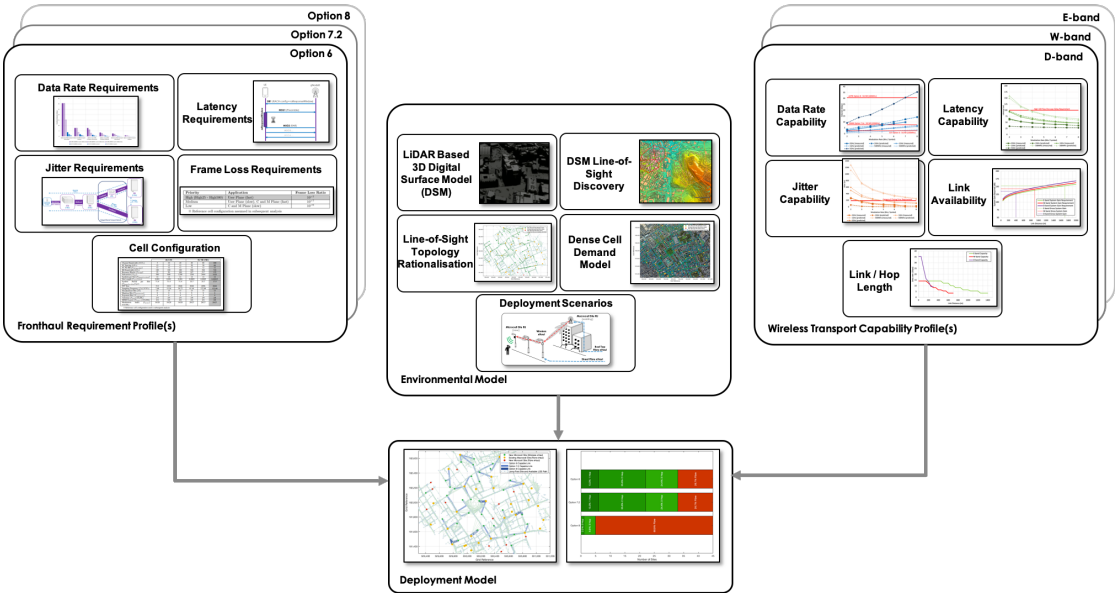

Figure 8.5: Performance-led deployment model.

The cell demand / growth model remains the same (as outlined in Chapter 6) whereby cells are placed into the model environment to minimise the overall inter-site distance. The target site density is again set to 200 m ISD however in the performance-led approach, rather than assuming a generic cell end point placement, the cell is assumed to be the 100 MHz 5G reference RU requiring a fronthaul connection with the associated fronthaul performance criteria as outlined in Chapter 7 (either eCPRI option 8, O-RAN option 7.2x or SCF nFAPI option 6). In this approach the target routing metric necessary to traverse each link in the model is the corresponding fronthaul interface requirement (a function of the cell configuration and fronthaul split options selected) and each path cost metric is the calculated capability of the link between each node in the graph.

The objective of the performance-led deployment analysis is to firstly understand the feasibility of wireless fronthaul in a real-world multi-hop urban environment and secondly to identify the most appropriate technology selection

(i.e. technology enablers) which would maximise the use of wireless transport in urban C-RAN based cell densification scenarios. As with the generic deployment characteristic study in Chapter 6, the same deployment scenarios as described in Table 6.1 are retained with either; a) utilisation of existing roof top site fibre points only, b) complete exclusion of the roof top macro site network and use of newly built street level fibre only, and c) a hybrid approach where any available fibre point can be exploited. The only differences to the deployment scenarios of Chapter 6 is that the hop count constraint is removed and the ability to aggregate fibre points and new site locations is based purely on whether wireless transport links can be constructed between them that can fulfil the fronthaul transport requirement. The high level algorithm is described in Algorithm. 2. In all the scenarios it is assumed that the DU / CU host site is at the fibre aggregation point in the model.

Algorithm 2: Performance-Led Deployment Model

```
Data: Current_Sites; Potential_Lamp_Posts; Ref_Cell_Fronthaul_Requirements
while Current_ISD > Target_ISD do
    Add new site to graph (Call Algorithim 1(return(new_site));
    Let Source_Site = new_site;
    Let Target_Site_List = All Current_Sites with fibre;
    foreach Target_Site in Target_Site_List do
        Potential_path(s,t) ← Find shortest path (Source_Site, Target_Site);
        foreach Fronthaul_Split [option 8, option 7.2, option 6] do
            foreach Spectrum_Band [D-band, W-band, E-band] do
                Potential_path(s,t).edge().path_loss ← Eqn 8.2;
                Potential_path(s,t).edge().rx_signal_level ← Eqn 8.1;
                Potential_path(s,t).edge().capacity ← Eqn 7.7;
                Potential_path(s,t).edge().latency ← Eqn 7.8;
                Potential_path(s,t).edge().jitter ← Eqn 7.9;
                if Potential_path(s,t).total_capacity & Potential_path(s,t).total_latency
                  & Potential_path(s,t).total_jitter ≤ Ref_Cell_Fronthaul_Requirements
                  then
                    Source_Site.fronthaul_transport = wireless;
                else
                    Source_Site.fronthaul_transport = fibre;
        Current_Sites ← Current_Sites + Source_Site;
```

8.4.1 Roof Top Only Wireless Fronthaul Extension

In the roof top only scenario, new sites can only be connected to the network via existing roof top macro cell sites which are assumed to be suitable DU / CU host sites. The performance-led deployment results for each candidate spectrum band and fronthaul split combination are outlined in Fig. 8.6 - 8.11 and tabulated in further detail in Appendix B. As no new fibre nodes are added to the topology

in this scenario, the percentiles in red represent new cell sites that cannot be connected (i.e. no fronthaul connectivity solution is possible).

Results in this scenario suggest the use of the option 8 fronthaul interface (eCPRI split E) would severely limit the potential to utilise wireless fronthaul between new sites and existing macro cell fibre sites. Only 11% of new sites were able to support an option 8 wireless fronthaul link using D-band. No sites at all were able to supported option 8 using either W or E-band transport. The detailed analysis in Appendix B further highlights that all option 8 links unable to utilise a wireless solution failed due to capacity constraints reasons. This emphasises that the option 8 interface represents an unrealistic technology selection for the wireless transport implementations considered.

The fronthaul technology selection of options 7.2 (O-RAN 7.2x) and 6 (SCF nFAPI) however, is more promising. Analysis shows that as much as 71% of new sites could be connected by utilising a D-band solution and 47% if using either W or E-band. Notably, the results for option 7.2 and 6 for W and E-band combinations are identical. These results highlight that it is the link bandwidth which is fundamentally dictating support for these fronthaul interfaces. The link budget and atmospheric availability differences between these bands is not a determining factor on the ability to support fronthaul links. This emphasises that the link / hop distance requirements in these deployment scenarios are not the limiting factor and as these bands are configured with the equivalent channel bandwidth the deployment opportunity remains identical.

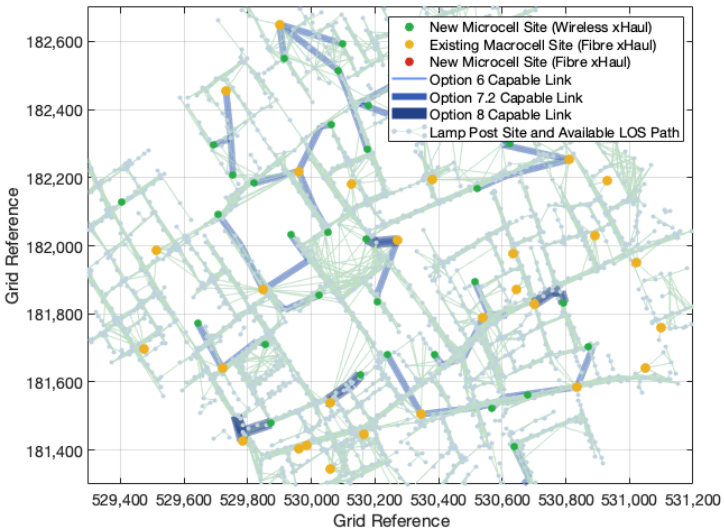

Figure 8.6: Roof top only deployment topology using D-band transport.

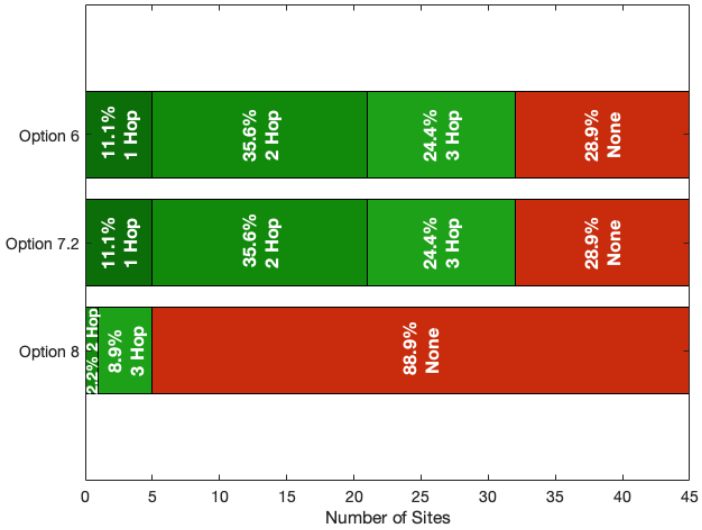

Figure 8.7: Roof top only deployment statistics using D-band transport.

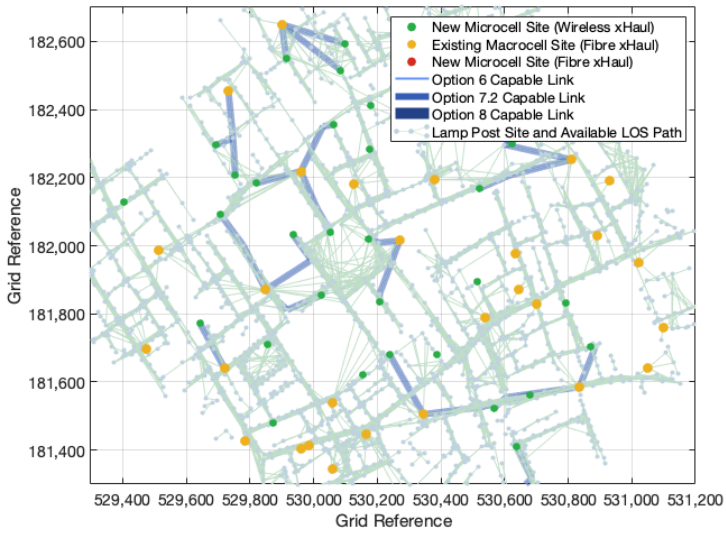

Figure 8.8: Roof top only deployment topology using W-band transport.

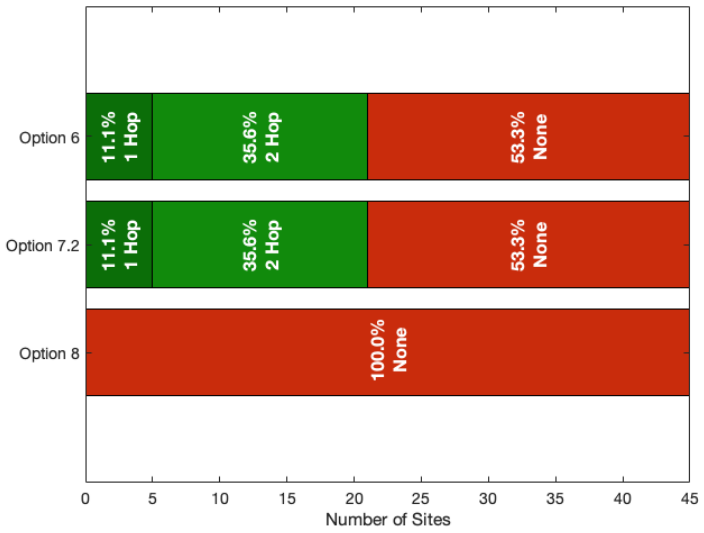

Figure 8.9: Roof top only deployment statistics using W-band transport.

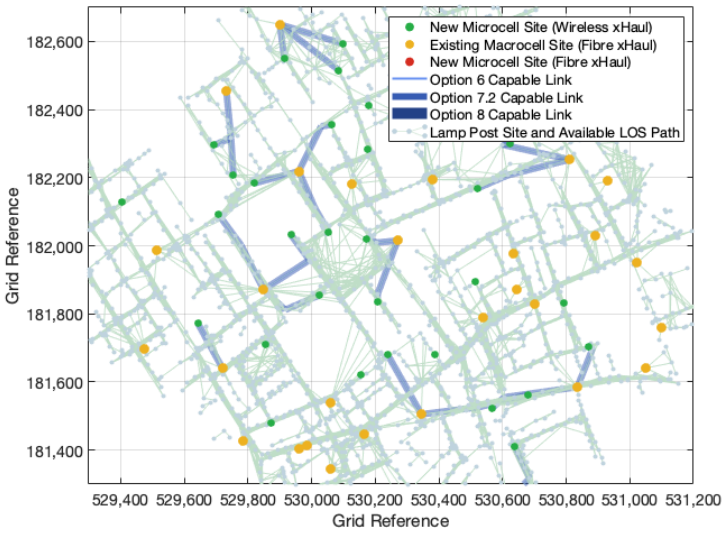

Figure 8.10: Roof top only deployment topology using E-band transport.

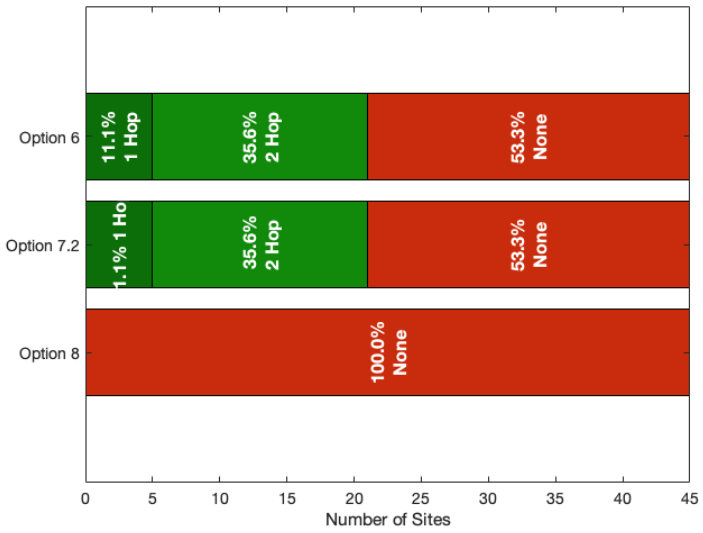

Figure 8.11: Roof top only deployment statistics using E-band transport.

8.4.2 Street Level Only Wireless Fronthaul Extension

In the street level only scenario, the macro cell layer is considered logically isolated from the small cell street level layer. This deployment model may be desirable from a design and operational perspective such that the different cell layers do not share an infrastructure interdependency. As a result, the LoS paths to roof top sites are not considered in this scenario and so do not exist in the graph topology. The fronthaul topology and connectivity result statistics from the performance-led deployment model for each band combination of and fronthaul interface combination are shown in Fig. 8.12 - 8.17.

Relative to the roof top only scenario the proportion of new sites able to exploit a wireless solution in this scenario is significantly lower. Again the capacity requirements of option 8 interface make the deployment of this interface without fibre unrealisable with results demonstrating a maximum opportunity of only 7% of sites when using the highest capacity D-band wireless solution.

The choice of a lower requirement fronthaul interface such a 7.2 and 6 shows more promise but again the performance differentiation between W and E-band is not evident. These combinations give equivalent results and only 13% of sites connected using a wireless fronthaul solution. The choice of D-band for these lower requirement interfaces does however improve the wireless connectivity to 30% of sites. As highlighted in Chapter 6 with the generic deployment model, the opportunity of adding wireless links in this scenario is again weighted toward the latter stages of roll out when there is sufficient density of fibre nodes to aggregate wireless link to. As the target site density in this model is 200 m ISD, it is evident that in order to improve the number of sites able to utilise wireless fronthaul an even higher density of sites would be necessary before wireless fronthaul would

become the dominate connectivity solution.

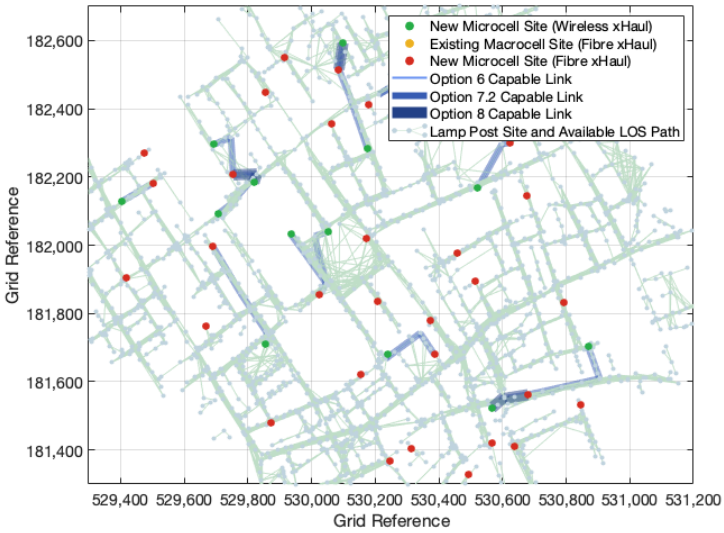

Figure 8.12: Street level only deployment topology using D-band transport.

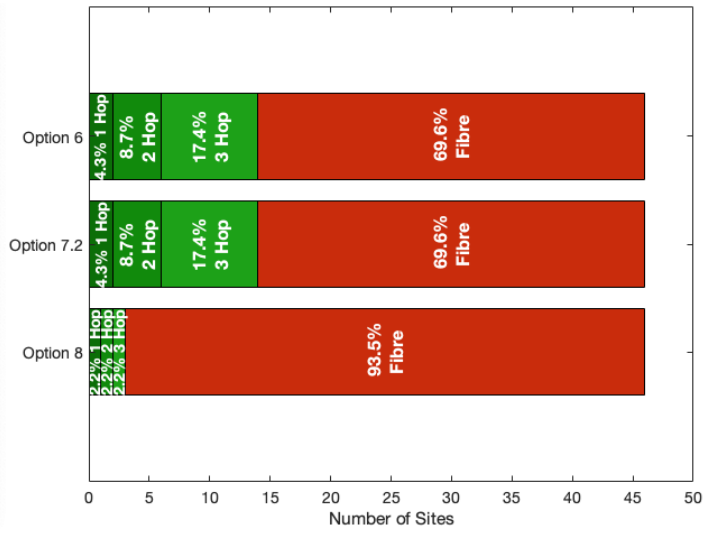

Figure 8.13: Street level only deployment statistics using D-band transport.

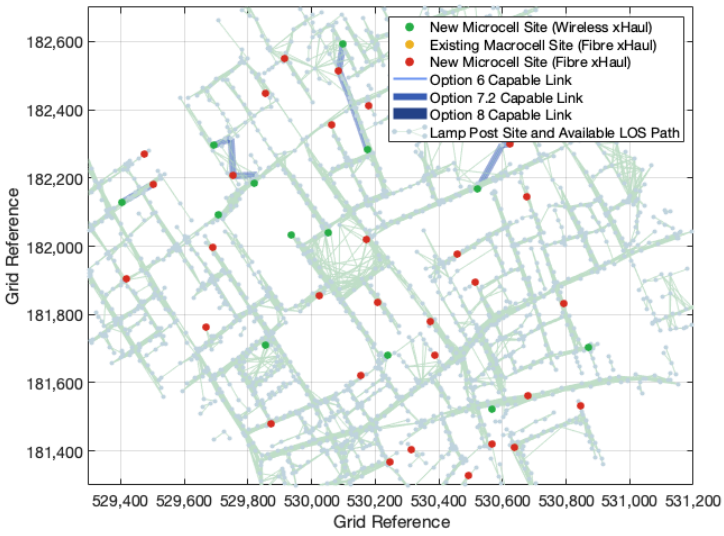

Figure 8.14: Street level only deployment topology using W-band transport.

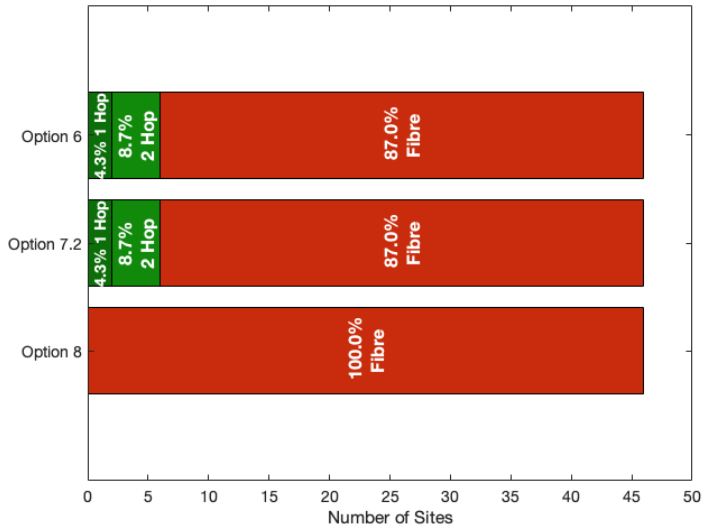

Figure 8.15: Street level only deployment statistics using W-band transport.

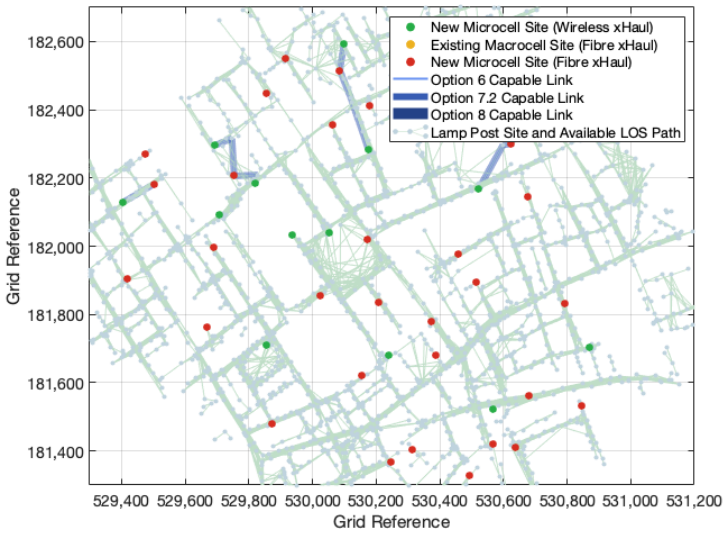

Figure 8.16: Street level only deployment topology using E-band transport.

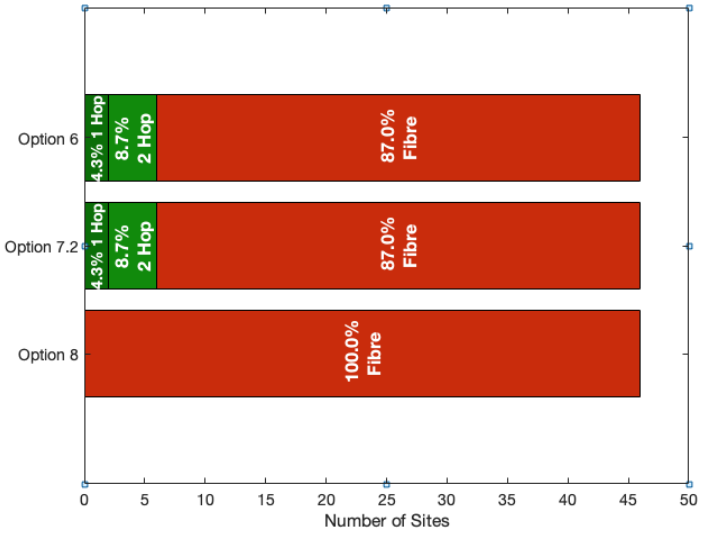

Figure 8.17: Street level only deployment statistics using E-band transport.

8.4.3 Roof or Street Level Wireless Fronthaul Extension

In the final scenario considered, the model is allowed to route fronthaul connectivity to any available fibre location that already exists in the topology - roof top or street level. These results are summarised in Fig. 8.18 - 8.23 and again tabulated in further detail with a break down of failure reasons in Appendix B.

When considering a deployment of new sites using the option 8 fronthaul interface, this scenario is able to connect 11% of newly built sites if D-band is implemented but no sites if W or E-band is chosen - these results mirror the roof

top only scenario. Again, the reason for low wireless fronthaul use is principally capacity constraint. As this deployment scenario offers the most potential for routing new sites to existing fibre node the figure of 11% using D-band transport likely represents the maximum deployment opportunity that could realistically be achieved for an option 8 based wireless fronthaul deployment.

With option 7.2 and 6, results are again aligned where a maximum of 73% of new sites could potentially be connected if a D-band wireless transport solution were to be realised. The equivalent proportion of wireless fronthaul sites if using W or E-band would be 49% where the remaining sites are fibre deployments predominantly due to latency constraints if wireless links were to be used. The analysis suggests that the greater potential of D-band with option 7.2 and 6 can be attributed to the fact that the higher performing individual links provide sufficient performance margin to support additional hops relative to W and E-band. Results show that D-band is able to support 3 hop fronthaul chains in this scenario whereas W and E-band are unable to utilise more than 2 hops before the associated performance budget is exhausted. As a result, the combination of D-band and O-RAN 7.2x fronthaul in this scenario represent the optimal solution for maximising the possibility of wireless transport whilst also maximising the opportunity for centralisation (i.e utilising the lowest fronthaul interface possible).

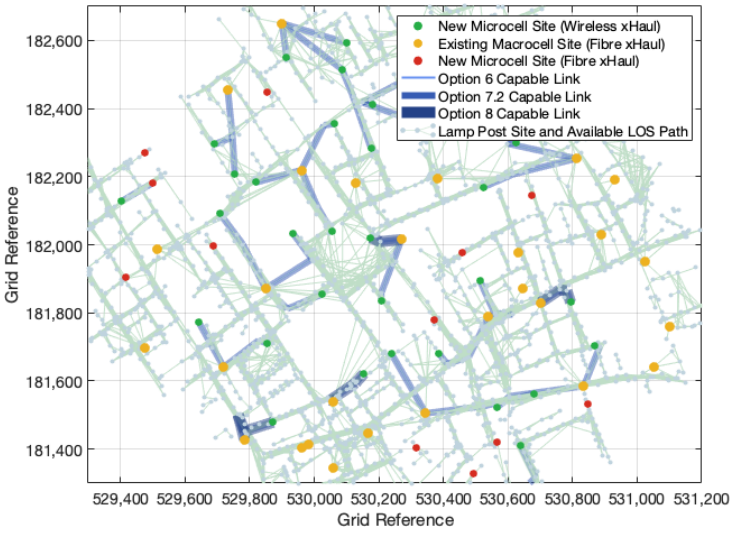

Figure 8.18: Roof or street level deployment topology using D-band transport.

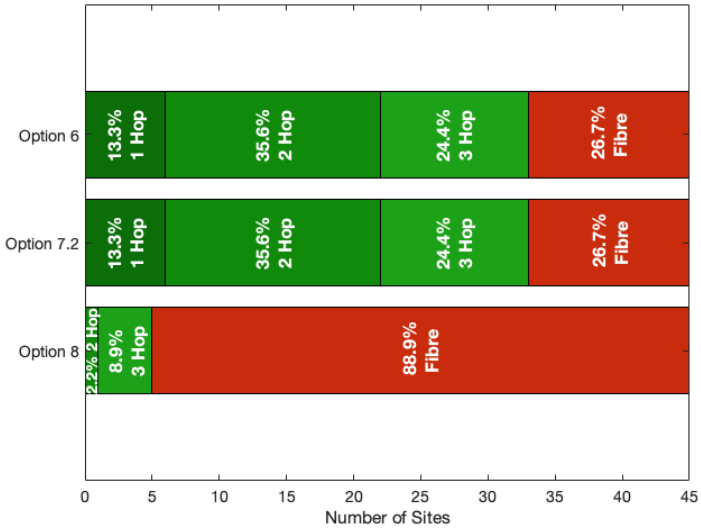

Figure 8.19: Roof or street level deployment statistics using D-band transport.

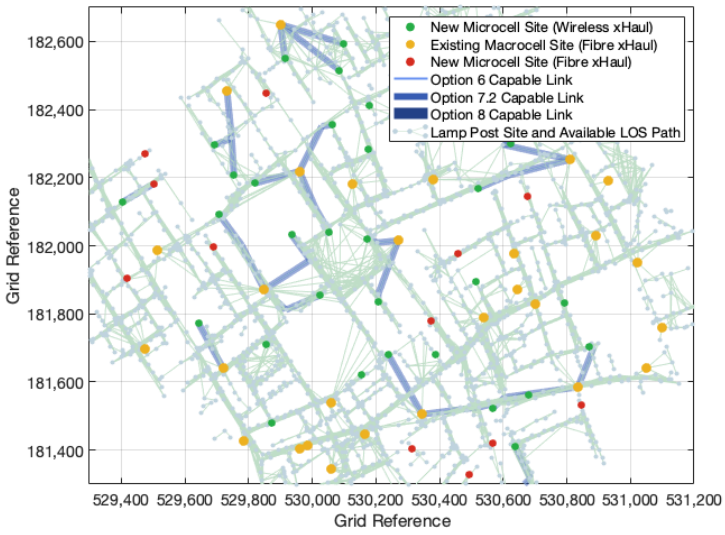

Figure 8.20: Roof or street level deployment topology using W-band transport.

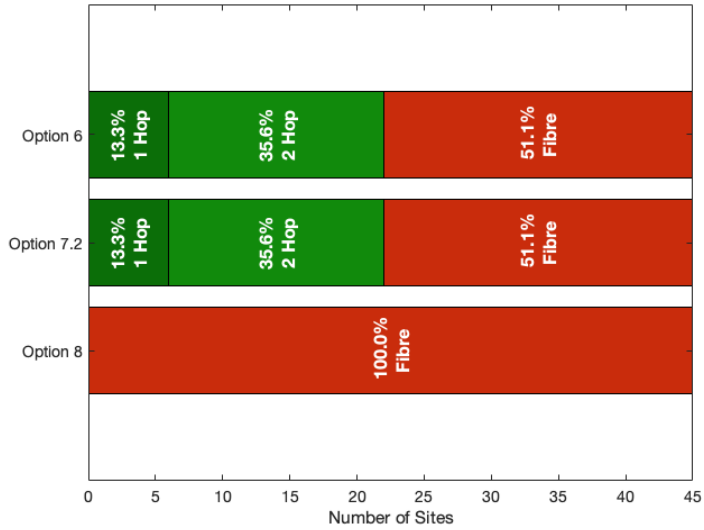

Figure 8.21: Roof or street level deployment statistics using W-band transport.

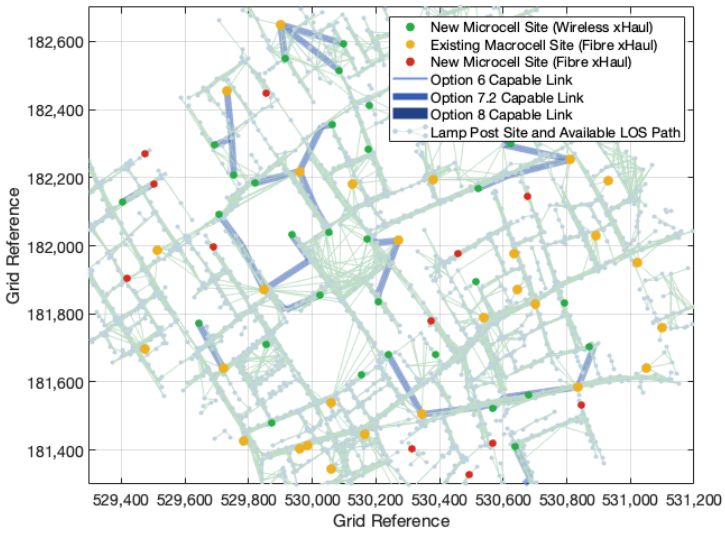

Figure 8.22: Roof or street level deployment topology using E-band transport.

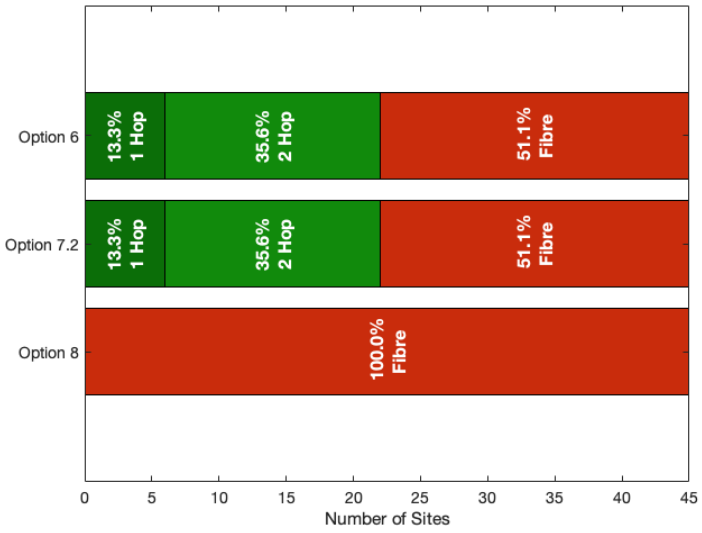

Figure 8.23: Roof or street level deployment statistics using E-band transport.

8.5 Chapter Summary

This chapter aims to arrive at the optimal deployment configuration for a C-RAN based cell site densification strategy supported by a wireless transport capability. In identifying the most appropriate technology selection that would enable wireless transport solutions to complement fibre transport the following criteria is considered; a) use of the lowest functional split possible in order to maximise the centralisation opportunity for multi-cell coordination and centralised processing, b) maximisation of a wireless fronthaul deployment in order to minimised initial capital expenditure and time to market where it is assumed new urban fibre installations would more costly.

With these high-level business case assumptions it has been demonstrated that the most appropriate deployment scenario would be use of a D-band transport solution, running O-RAN option 7.2x cell fronthaul whilst making use of both roof top and new street level fibre locations to aggregate fronthaul (or host local baseband DU / CU components). Finding have shown that in spite of the demanding transport requirements imposed by new fronthaul interfaces, the anticipated performance of emerging wireless transport solutions operating in high mmWave spectrum bands are capable of supporting realistic wireless fronthaul deployments. The capacity requirements for the exemplar 100 MHz 5G RU cell when using an eCPRI option 8 fronthaul split mean this split is only realisable with the large 5 GHz channel bandwidths potentially possible in D-band and even then are only achievable with short link lengths <100 m. This makes the deployment viability of the option 8 configuration in a UK urban environment very low. Alternative splits such as O-RAN option 7.2x and SCF nFAPI option

6 show more promise having been shown to be realisable on the smaller 2 GHz channel bandwidths possible with E and W-band but could be maximised further through the use of D-band. The higher performance anticipated in D-band has demonstrated that up to 3 hops are possible which improve the proportion of wireless transport based sites to as much as 73% of newly built sites.

The findings of this chapter not only demonstrate the feasibility of the wireless fronthaul concept but highlight a real-world opportunity to evolve the distributed-RAN deployments of today, heavily dependent on lower capacity microwave backhaul, towards more centralised fronthaul orientated architectures using high capacity mmWave and sub-THz transport bands.

Chapter 9

Conclusions

The overriding research objectives of this work aim to understand if, and how, wireless transport solutions could be used in future centralised mobile network architectures. Beyond the steady incremental technology advancements in radio access networks the most anticipated and significant advancements in long term scalable capacity growth is a migration towards centralised architectures. The theoretical benefits of centralising the conventional geographically distributed baseband components of the radio network are widely recognised but inherently challenging. As discussed in the opening chapters of this work, to realise these architectural principles, whether they be mid-term network centric deployments ambitions such as distributed-MIMO or multi-TRP access networks, or longer term strategic visions such as user centric cell-free massive-MIMO, each are fundamentally dependent on developing the underlying, but often overlooked, transport network.

9.1 Summary of Findings and Contributions

In the initial background research of this work discussed in Chapter 2, the challenges with the centralisation approach are framed - the majority of existing base station sites worldwide have historically been connected to the network using a wireless transportation solution. Although there has been significant progress made in recent years with wide scale fibre optic deployments, the use of wireless transport solutions in lieu of cost effective (but preferential) fibre, are expected to nevertheless remain. The more demanding transport requirements of fronthaul orientated centralised networks mean traditional microwave wireless solutions are not compatible with such architectural ambition. As a result, the exploration of spectrum bands >100 GHz and potential new fronthaul interfaces are identified in order to progress the direction of this research and understand of whether a wireless solution could be a credible alternative to high capacity fibre and a realistic tool in realising centralised deployments.

The first steps in attempting to answer some of the questions raised by the opening chapters is development of an environmental model in Chapter 3. Here, a LIDAR based digital surface model of large areas of the UK is build where any wireless transport technology choices and deployment scenarios can be simulated and studied in detail. By analysing the base environmental model (prior to developing any further system level models), the physical properties of existing mobile base station sites and the environments in which they operate has been characterised. As it is not practical to build and run system models for the entire national network for this research, the findings of this chapter provide a means of statistically scaling any subsequent analysis to much wider areas with common environmental characteristics. Critically, the results of this chapter have demonstrated that existing system simulation parameters such as those recommended by standards bodies such as ITU and 3GPP and conventionally used for mobile network deployment modelling were found to be not well aligned with the deployment characteristics of modern mobile networks.

In Chapter 4 the statistical properties of the first wireless transport use case are studied. The line-of-sight paths between existing macro cell rooftop sites and street level lamp posts are calculated on a large scale. This approach has two main aims. Firstly, it allows all the line-of-sight paths to be identified in the environmental model and secondly, it allows a line-of-sight probability model to be developed for each cell site classification. This analysis ultimately demonstrates the feasibility of deploying lamp post based cell sites which could be connected back into the network using a high frequency wireless solution via existing macro cell rooftop infrastructure sites. Finding have shown that the resulting probability models do not agree well with existing published models by ITU and 3GPP. The resulting proposed models developed in this chapter address the discrepancy whilst also accounting for the height and distance dependency of the lamp post endpoint relative to the rooftop site.

The second wireless transport use case is studied in Chapter 5. Here, the equivalent line-of-sight propagation paths are identified between neighbouring lamp posts. Again, this output serves not only to identify the valid line-of-sight paths in the model for later deployment modelling but also to generate the statistical probability model of achieving line-of-sight conditions between neighbouring street level lamp posts. Unlike the macro cell line-of-sight probability model, the micro cell probability results did share some correlation with published models however optimisation of fitting parameters were still required and subsequently proposed in a new definition for each urban, suburban and rural environment. The results again provide context for later deployment modelling and demonstrate the impact of achieving line-of-sight conditions suitable for high frequency wireless systems as a function of the endpoint height and distance from the transmitter.

In Chapter 6 the previously discovered line-of-sight paths from both the rooftop to street level use case and inter-street level use cases are combined to

provide a full path topology representative of potential wireless transport links.The environmental model is evolved towards a multi-hop wireless transport deployment where new cells are added sequentially to the model and the ability to connect them back to existing fibre points using a wireless solution analysed. When a representative urban area of the model is built to a cell density of 200 m, results have demonstrated that with an unconstrained hop count, as many as 93% of new sites could be connected with wireless transport. In the scenario where existing rooftop macro cell sites are not used, a wireless multi-hop solution could potentially reduce the dependency on newly deployed street level fibre by as much as 43%. The results in this chapter not only outline the ideal characteristics (in terms of hop counts and link lengths) of a generic wireless transport solution but underline the potential (upper bound) of wireless transport to support cell site densification as an alternative to fibre.

To further advance the deployment model, Chapter 7 aims to derive the fronthaul interface requirements as well as the anticipated wireless transport performance capabilities that can be used as routing metrics in a performance oriented modelling approach. The main contributions of this chapter are to experimentally measure the performance of a state-of-the-art E-band transport solution and use the results to extrapolate performance expectations for future higher bandwidth solutions. Furthermore, an experimental testbed is used to demonstrate a proof-of-concept wireless fronthaul base station proving that the wireless fronthaul concept is not only theoretically possible but experimentally achievable.

The final analytical chapter of this work in Chapter 8 combines all previous topics and chapter contributions to facilitate a deployment model where wireless fronthaul links and candidate spectrum bands are considered in place of the generic line-of-sight link topology. The output of the performance led model has shown that the optimum technology selection to maximise the potential of wireless transport as well as the centralisation opportunity of a dense cell network would be use of O-RAN option 7.2x fronthaul in combination with high capacity D-band transport. In addition, findings outline that a deployment scenario seeking to utilise existing rooftop macro cell infrastructure with select installation of street level fibre points would maximise the potential for wireless transport - as much as 73% of newly deployed street level cell sites when used along side O-RAN option 7.2x and D-band spectrum.

9.2 Thoughts and Perspective

The overall conclusions of this work suggest wireless transport solutions have an essential role in advanced network deployment architectures seeking to achieve high cell site density. Although some assumptions outlined in this work may

mature over time, the wireless fronthaul concept has nevertheless been shown to be achievable in real-world deployments when used with the right technology choices. The challenges in fully realising and combining these technologies still remain but it is hoped that the finding of this work can aid further research in this field.

In terms of fronthaul interface selection, it is perhaps not surprising that the lowest option 8 split has proven fundamentally impractical for wireless transport. It is ultimately the challenging data rate requirements identified that are one of the original drivers for the emergence of alternative functional splits. The option 8 split still presents challenges even for optical transport solutions. The O-RAN option 7.2x interface represents the best compromise between transport requirements and centralisation of baseband functionality. In addition, the ambition of the O-RAN alliance to make this an open and interoperable interface may also prove to be beneficial in a centralised multi-vendor network. In addition, the majority of fibre nodes required in the modelling analysis for this particular interface were a result of latency constraints with a wireless alternative. With appropriate end-to-end network design, the latency aspects of a real world deployment could potential be improved over and above that assumed in modelling which could further improve the deployment potential of option 7.2x. While SCF nFAPI option 6 results also show a promising deployment opportunity, the reduced radio functionality (in terms of support for higher order MIMO and advanced transmission schemes) perhaps limit its long term potential in more advanced coordinated cell schemes.

The choice of spectrum band for supporting wireless fronthaul is clearly weighted towards D-band operating between 130 GHz and 174.8 GHz. The channel bandwidths possible in this spectrum allow for significantly higher performance budget headroom available to meet the fronthaul transport requirements. This has been shown to enable a higher configuration of cell and more hops in a wireless transport chain. The shorter range of potential D-band solutions has not been shown to be a limiting factor in the urban deployment scenarios considered in this study. It is however recognised that this may not be the case for the equivalent suburban and rural environments. The differences between W-band and E-band transport in this work are less evident. As these bands have primarily been modelled using the same maximum channel bandwidth anticipated in these bands, the deployment results are largely equivalent, again demonstrating that such deployment scenarios are generally not link budget limited. While this may suggest these bands could be used interchangeably, the reality is that a mobile network operator's preference is for the certainty of link deployments using coordinated parts of the spectrum. At the time of writing, 2 GHz channels cannot be licensed in the coordinated part of E-band within the UK meaning that only smaller channel bandwidths are realistically attainable without operating links in the less certain uncoordinated part of the band. The larger number of potential channels in W-band mean that 2 GHz (or potentially multiple 2 GHz) channels

are however possible whilst also supporting multiple co-located licensees.

In general, it is also anticipated that future advancements and maturity in wireless transmission systems >100 GHz could further enhance the performance and link lengths achievable in wireless fronthaul transport networks. Advanced radio interface techniques already implemented in lower frequency microwave bands including the simultaneous use of multiple carriers, higher order modulation, a second polarization or line-of-sight MIMO techniques promise to double or even quadruple the aggregate link capacities suggested in this work. As a result, it is conceivable that future wireless transport solutions >100 GHz could realistically achieve performance parity with 40 Gbps or 100 Gbps fibre optic solutions over short distances. Such capability, in addition to expanding the potential of multi-hop single RU C-RAN deployments as outlined in this work could also realise larger multi-sector, multi-carrier macro cell sites as well.

9.3 Future Work

- As already highlighted, a key objective of this work was to establish a framework and capability to model a multitude of different scenarios that could answer the research questions initially set out. The primary focus of this work has centred around the densification of urban areas using street level cell sites as this is where capacity demand is highest and deployment costs greatest. Further insight however, could be achieved with looking at the equivalent deployments but in alternative environments such as suburban and rural settings. In these environments it is anticipated that lower cell density and thus longer wireless links would typically be required and so an assumption that the same technology selection as concluded in the urban environment in this work may no longer be valid.

- Another key assumption of the deployment modelling in this work is that the centralised components of the RAN (namely DU and CU functions) are built at the location of the fibre nodes in the graph topology. This, in essence, provides the maximum fronthaul transport KPI budget to be consumed exclusively over the wireless transport leg(s). This essentially represents centralisation at the edge of the network as a first step. To fully centralise the RAN, it may be desirable to deploy baseband capability deeper in the network, at the exchange building or regional data centre. To assess the feasibility of these different tiers of aggregation, the performance KPIs of the fibre towards such aggregation nodes much also be accounted for in the fronthaul transport budget. While this is a relatively simple expansion of the model, the exact fibre lengths (or reasonable assumptions about where they may terminate) must also be known. Although this dataset does not currently exist in the model, the inclusion of much longer fibre hops will

inevitably be at the detriment of the ability to deploy wireless transport as the final connectivity solution. Consequently, these impacts should be quantified as part of any new research objectives.

- The results of the deployment simulations in this work have naturally tended towards a hub and spoke or star topology due to the emphasis on centralised architecture. There are however alternative transport topologies that could be investigated with the existing model using different routing algorithms. One such case may be the application of ring topologies as a means of creating resilient and redundant paths in the transport network. This is particularly relevant to multi-hop wireless networks as they potentially allow for a highly reconfigurable topology able to adapt to outages or changes in the surrounding network. Although the findings of this research suggest hop counts greater than 3 may be challenging for the technology choices envisioned, the application of highly resilient transport networks may be a critical part of new access network use cases such as ultra-reliable low latency communications (URLLC) and so should nevertheless be considered as another direction of associated research.

Figure 9.1: Final modelling results imported and visualised in Google Earth ©2023 Google. (Central London, D-band 159.125 GHz transport, O-RAN option 7.2x fronthaul, roof top and street level infrastructure, cell density 200 m.)

Appendix A

Appendix to Chapter 7

A.1 Determination of 5G Transport Block Size

The data payload at the 4G / 5G MAC layer is referred to as a transport block TB. The associated datarate at the MAC layer is determined by the transport block size TBS which is governed by the modulation and coding scheme MCS and number of physical resource blocks N_{PRB} allocated to a specific transmission. For 4G LTE, the MAC layer datarate, and associated 3GPP option 6 functional split fronthaul interface user plane flow (i.e. excluding control and management flows) is determined by a lookup table procedure where the transport block index I_{TBS} is identified from the modulation and coding scheme index I_{MCS} in 3GPP TS 36.213 [93] (table 7.1.7.1-1 for physical downlink shared channel (PDSCH) and table 8.6.1.1-1 for physical uplink shared channel (PDSCH)). The I_{TBS} is then used with N_{PRB} to lookup the TBS from Table 7.1.7.2.1-1.

In 5G NR specifications, the wide ranges of numerologies, bandwidths and control signalling configurations mean that a static look-up table approach to determine the TBS is no longer optimal. Instead, for 5G NR a formula base approach is used as defined in 3GPP TS 38.214 [94].

A.1.1 Downlink PDSCH Transport Block Size

1. The first step in deriving the downlink TBS is identification of the number of resource elements N_{RE} per slot. This is determined by first deriving how many resource elements are allocated within a physical resource block N'_{RE} after factoring out the number resource elements allocated to demodulation reference signals N^{PRB}_{DMRS} and higher layer overheads N^{PRB}_{oh}. The number of sub-carriers in a resources block N^{RB}_{sc} for 5G is 12 and the number symbols per slot N^{slot}_{symb} is 14. For maximum datarate / utilisation, the total number of physical resource blocks allocated and scheduled in the transmission n_{PRB} is assumed to be all available physical resource blocks ($n_{PRB} = N_{PRB}$).

$$N'_{RE} = N_{sc}^{RB} \cdot N_{symb}^{slot} - N_{DMRS}^{PRB} - N_{oh}^{PRB} \tag{A.1}$$

$$N_{RE} = min(156, N'_{RE}) \cdot n_{PRB} \tag{A.2}$$

2. The next step is calculation of an unquantized intermediate variable N_{info} which represents the number of information bits using the target coding rate R and modulation order Q_m from tables 5.1.3.1-[1-4] in 3GPP TS 38.214 [94] together with the number of MIMO layers using in the transmission N_{layers}.

$$N_{info} = N'_{RE} \cdot R \cdot Q_m \cdot N_{layers} \tag{A.3}$$

3. Depending on the value of N_{info} the resulting quantized number of information bits N'_{info} is calculated differently. For a low number of bits where $N_{info} \leq 3824$ the resulting N'_{info} can be used with table 5.1.3.2-1 to find the closest TBS:

$$N'_{info} = max(24, 2^n \cdot \left[\frac{N_{info}}{2^n}\right]) \tag{A.4}$$

where

$$n = max(3, [log_2(N_{info})] - 6) \tag{A.5}$$

4. For a high number of bits where $N_{info} \geq 3824$ the TBS can be found using the following equations:

$$N'_{info} = max(3840, 2^n \cdot round\left[\frac{N_{info} - 24}{2^n}\right]) \tag{A.6}$$

where

$$n = [log_2(N_{info} - 24)] - 5 \tag{A.7}$$

4.1 if $R \leq 1/4$:

$$TBS = 8 \cdot C \cdot \left[\frac{N'_{info} + 24}{8 \cdot C}\right] - 24 \tag{A.8}$$

where

$$C = \left[\frac{N'_{info} + 24}{3816}\right] \tag{A.9}$$

4.2 else

4.2.1 if $N'_{info} > 8424$

$$TBS = 8 \cdot C \cdot \left\lceil \frac{N'_{info} + 24}{8 \cdot C} \right\rceil - 24 \tag{A.10}$$

where

$$C = \left\lceil \frac{N'_{info} + 24}{8424} \right\rceil \tag{A.11}$$

4.2.2 else

$$TBS = 8 \cdot \left\lceil \frac{N'_{info} + 24}{8} \right\rceil - 24 \tag{A.12}$$

A.1.2 Uplink PUSCH Transport Block Size

1. The uplink TBS determination procedure follows the downlink procedure where the number of resource elements N_{RE} per slot is determined by first deriving how many resource elements are allocated within an uplink physical resource block N'_{RE} after factoring out resource elements allocated to demodulation reference signals N^{PRB}_{DMRS} and higher layer overheads N^{PRB}_{oh}. In the uplink there is the possibility for transport block processing over multiple slots N which, if configured, may be accounted for in the N_{RE} calculation after which the same steps as in downlink TBS calculation can be followed:

$$N'_{RE} = N^{RB}_{sc} \cdot N^{slot}_{symb} - N^{PRB}_{DMRS} - N^{PRB}_{oh} \tag{A.13}$$

$$N_{RE} = (N \cdot) min(156, N'_{RE}) \cdot n_{PRB} \tag{A.14}$$

Appendix B

Appendix to Chapter 8

B.1 Summary of Deployment Modelling

Table B.1: Summary of Performance Led Deployment Modelling.

Scenario		Option 8				Option 7.2x				Option 6			
		Wireless Sites		Fibre Sites		Wireless Sites		Fibre Sites		Wireless Sites		Fibre Sites	
		Total	Hops	Total	Reason	Total	Hops	Total	Reason	Total	Hops	Total	Reason
Roof Top Only Wireless Fronthaul Extension	D-band	11.1%	0%(1) 20%(2) 80%(3)	88.9%	100%(C)	71.1%	16%(1) 50%(2) 34%(3)	28.9%	15%(C) 85%(L)	71.1%	16%(1) 50%(2) 34%(3)	28.9%	15%(C) 85%(L)
	W-band	0.0%	-	100.0%	100%(C)	46.7%	24%(1) 76%(2)	53.3%	8%(C) 92%(L)	46.7%	24%(1) 76%(2)	53.3%	8%(C) 92%(L)
	E-band	0.0%	-	100.0%	100%(C)	46.7%	24%(1) 76%(2)	53.3%	8%(C) 92%(L)	46.7%	24%(1) 76%(2)	53.3%	8%(C) 92%(L)
Street Level Only Wireless Fronthaul Extension	D-band	6.5%	33.3%(1) 33.3%(2) 33.3%(3)	93.5%	100%(C)	30.4%	12.5%(C) 87.5%(L)	69.6%	14%(1) 29%(2) 57%(3)	30.4%	12.5%(C) 87.5%(L)	69.6%	14%(1) 29%(2) 57%(3)
	W-band	0.0%	-	100.0%	91%(C) 9%(C, J)	13.0%	33%(1) 67%(2)	87.0%	10%(C) 80%(L) 10%(L, J)	13.0%	33%(1) 67%(2)	87.0%	10%(C) 80%(L) 10%(L, J)
	E-band	0.0%	-	100.0%	91%(C) 9%(C, J)	13.0%	33%(1) 67%(2)	87.0%	10%(C) 80%(L) 10%(L, J)	13.0%	33%(1) 67%(2)	87.0%	10%(C) 80%(L) 10%(L, J)
Roof and Street Level Wireless Fronthaul Extension	D-band	11.1%	0%(1) 20%(2) 80%(3)	88.9%	100%(C)	73.3%	18%(1) 49%(2) 33%(3)	26.7%	17%(C) 83%(L)	73.3%	18%(1) 49%(2) 33%(3)	26.7%	17%(C) 83%(L)
	W-band	0.0%	-	100.0%	100%(C)	48.9%	27%(1) 73%(2)	51.1%	9%(C) 91%(L)	48.9%	27%(1) 73%(2)	51.1%	9%(C) 91%(L)
	E-band	0.0%	-	100.0%	100%(C)	48.9%	27%(1) 73%(2)	51.1%	9%(C) 91%(L)	48.9%	27%(1) 73%(2)	51.1%	9%(C) 91%(L)

Reason for fibre connectivity: (C) Capacity constrained (if wireless), (L) Latency constrained (if wireless), (J) Jitter constrained (if wireless)

No new fibre is deployed in this scenario - figures represent 'no solution' possible.

Deployment scenario representing maximum wireless transport utilisation and maximum possibility for centralisation (lowest fronthaul split).

List of Acronyms

3GPP 3rd Generation Partnership Project

ACK Acknowledgement

AR Augmented Reality

BBU Baseband Unit

CAPEX Capital Expenditure

C-RAN Cloud/Centralised Radio Access Network

CBR Constant Bit Rate

CDF Cumulative Distribution Function

CEPT European Conference of Postal and Telecommunications Administrations

CF-mMIMO Cell-Free Massive MIMO

CoMP Coordinated Multipoint

CoS Class of Service

COTS Off The Shelf

CPRI Common Public Radio Interface

CPU Centralised Processing Unit

CU Centralised Unit

D-RAN Distributed Radio Access Network

DSM Digital Surface Model

DU Distributed Unit

ECC Electronic Communications Committee

eCPRI Common Public Radio Interface

eMBB enhanced Mobile Broadband

eNB eNodeB

EPC Evolved Packet Core

eRE eCPRI Radio Equipment

eREC eCPRI Radio Equipment Control

F1-C F1 Control Plane

F1-U F1 User Plane

F2-C F2 Control Plane

F2-U F2 User Plane

FDD Frequency Division Duplex

FFT Fast Fourier Transform

FSO Free Space Optics

FWA Fixed Wireless Access

gNB gNodeB

HARQ Hybrid Automatic Repeat Request

I/Q In-phase / Quadrature

IAB Integrated Access and Backhaul

ICIC Inter-Cell Interference Coordination

IEEE Institute of Electronic and Electrical Engineers

IoT Internet of Things

ISD Inter Site Distance

ITU International Telecommunications Union

KPI Key Performance Indicator

LIDAR Light Detecting and Ranging

LoS Line of Sight

LTE Long Term Evolution

M-TRP Multi-Transmission and Reception Points

MAC Media Access Control

MIMO Multiple-In Multiple-Out

mMIMO Massive Multiple-In Multiple-Out

mmWave millimetre-wave

MNO Mobile Network Operator

MSE Mean Squared Error

MT Mobile Termination

NACK Negative Acknowledgement

nFAPI network Functional API

NG-C Next Generation Control Plane

NG-U Next Generation User Plane

NGC Next Generation Core

nLoS Near Line of Sight

NLoS Non Line of Sight

NR New Radio

NSA Non Stand Alone

O-RAN Open Radio Access Network

OAI Open Air Interface

OFDM Orthogonal Frequency Division Multiplexing

ONT Optical Network Transport

PDCCH Physical Downlink Control Channel

PDCP Packet Data Convergence Protocol

PDF Probability Distribution Function

PHICH Physical HARQ Indicator Channel

PON Passive Optical Network

PPP Poisson Point Process

PRTC Primary Reference Time Clock

PTP Precision Timing Protocol

PUSCH Physical Uplink Shared Channel

QAM Quadrature Amplitude Modulation

QoS Quality of Service

RACH Random Access Channel

RAN Radio Access Network

RAR Random Access Response

RF Radio Frequency

RLC Radio Link Control

RMa Rural Macro

RMi Rural Micro

RoE Radio over Ethernet

RRC Radio Resource Control

RU Radio Unit

SCF Small Cell Forum

SIB Physical Uplink Shared Channel

SISO Single Input Single Output

SMa Suburban Macro

SMi Suburban Micro

SNR Signal to Noise Ratio

T-BC Telecom Boundary Clock

T-GM Telecom Grand Master

T-TSC Telecom Time Slave Clock

TAE Time Alignment Error

TDD Time Division Duplexing

TN Transport Network

TSN Time Sensitive Network

TTI Transmission Time Interval

UE User Equipment

UMa Urban Macro

UMi Urban Micro

URLLC Ultra Reliable Low Latency Communication

V-RAN Virtualised Radio Access Network

VR Virtual Reality

WDM Wavelength Division Multiplexing

WTR Wireless Telegraphy Register

XPIC Cross Polar Interference Cancellation

References

[1] D. Townend and S. D. Walker, "A 3D statistical framework for the UK's mobile network," in *2020 IEEE 31st Annual International Symposium on Personal, Indoor and Mobile Radio Communications*, Aug. 2020.

[2] D. Townend, S. D. Walker, A. Sharples, and A. Sutton, "Urban Line-Of-Sight probability for mmwave mobile access and fronthaul transmission hubs," in *2021 15th European Conference on Antennas and Propagation (EuCAP) (EuCAP 2021)*, Düsseldorf, Germany, Mar. 2021.

[3] ——, "A unified line-of-sight probability model for commercial 5g mobile network deployments," *IEEE Transactions on Antennas and Propagation*, vol. 70, no. 2, pp. 1291–1297, 2022. DOI: 10.1109/TAP.2021.3119099.

[4] ——, "Line-of-sight probability for urban microcell network deployments," in *2022 16th European Conference on Antennas and Propagation (EuCAP)*, 2022, pp. 1–5. DOI: 10.23919/EuCAP53622.2022.9769560.

[5] D. Townend, R. Husbands, S. D. Walker, and A. Sharples, "Toward wireless fronthaul for cloud ran architectures," in *2023 IEEE Wireless Communications and Networking Conference (WCNC)*, 2023, pp. 1–6. DOI: 10.1109/WCNC55385.2023.10119125.

[6] D. Townend, S. D. Walker, A. Sharples, and A. Sutton, "Urban wireless multi-hop x-haul for future mobile network architectures," in *ICC 2022 - IEEE International Conference on Communications*, 2022, pp. 1883–1887. DOI: 10.1109/ICC45855.2022.9838366.

[7] D. Townend, R. Husbands, S. D. Walker, and A. Sutton, "Challenges and opportunities in wireless fronthaul," *IEEE Access*, vol. 11, pp. 106 607–106 619, 2023. DOI: 10.1109/ACCESS.2023.3319073.

[8] BT. (2019). BT Group plc FY 2018/19 results, [Online]. Available: https://www.bt.com/bt-plc/assets/documents/investors/financial-reporting-and-news/quarterly-results/2018-2019/q4-18-19-full-year-slides.pdf.

[9] GSMA. (2021). The Mobile Economy Europe 2021, [Online]. Available: https://www.gsma.com/mobileeconomy/wp-content/uploads/2021/09/GSMA_ME_Europe_2021_R_Web_Singles.pdf.

[10] 3GPP, *TR 38.801 V14.0.0 Study on new radio access technology: Radio access architecture and interfaces*, 2017.

[11] CPRI Cooperation, *eCPRI Specification V2.0*, 2019. [Online]. Available: http://www.cpri.info/spec.html.

[12] ——, (2015). CPRI Specification V7.0, [Online]. Available: http://www.cpri.info/spec.html.

[13] A. Umesh, T. Yajima, T.Uchino, and S.Okuyama, "Overview of O-RAN Fronthaul Specifications," *NTT DOCOMO Technical Journal*, vol. 21, no. 1, pp. 46–59, Jul. 2019.

[14] S. C. Forum, *5G nFAPI Specifications*, 2021.

[15] "IEEE Standard for Radio over Ethernet Encapsulations and Mappings," *IEEE Std 1914.3-2018*, pp. 1–77, 2018. DOI: 10.1109/IEEESTD.2018.8486937.

[16] "IEEE Standard for Packet-based Fronthaul Transport Networks," *IEEE Std 1914.1-2019*, pp. 1–94, 2020. DOI: 10.1109/IEEESTD.2020.9079731.

[17] "IEEE Standard for Local and metropolitan area networks – Time-Sensitive Networking for Fronthaul," *IEEE Std 802.1CM-2018*, pp. 1–62, 2018. DOI: 10.1109/IEEESTD.2018.8376066.

[18] GSMA, *Wireless Backhaul Evolution: Delivering next-generation connectivity*, 2021. [Online]. Available: https://www.gsma.com/spectrum/wp-content/uploads/2022/04/wireless-backhaul-spectrum.pdf.

[19] NGMN, *Guidelines for LTE Backhaul Traffic Estimation*, 2011. [Online]. Available: https://www.ngmn.org/technical-documents.html.

[20] ETSI mWT, *5G Wireless Backhaul/X-Haul*, 2018. [Online]. Available: https://www.etsi.org/committee/1426-mwt.

[21] ITU-R, *F.2323-1 fixed service use and future trends*, 2017.

[22] ——, *F.1497-0 radio-frequency channel arrangements for systems in the fixed service operating in the band 55.78-59 ghz*, 2000.

[23] ——, *F.1497-2 radio-frequency channel arrangements for fixed wireless systems operating in the band 55.78-66 ghz*, 2014.

[24] ——, *F.2006 radio-frequency channel arrangements for fixed wireless systems operating in the 71-76 and 81-86 ghz bands*, 2012.

[25] CEPT, *ECC Recommendation (18)02 - Radio frequency channel/block arrangements for Fixed Service systems operating in the bands 92-94 GHz, 94.1-100 GHz, 102-109.5 GHz and 111.8-114.25 GHz*, 2018.

[26] ——, *ECC Recommendation (18)01 - Radio frequency channel/block arrangements for Fixed Service systems operating in the bands 130-134 GHz, 141-148.5 GHz, 151.5-164 GHz and 167-174.8 GHz*, 2018.

[27] E. mWT, *mmWave Semiconductor Industry Technologies: Status and Evolution*, 2016. [Online]. Available: `https://www.etsi.org/committee/1426-mwt`.

[28] C. Paoloni, F. Magne, F. André, X. Begaud, V. Krozer, M. Marilier, A. Ramirez, J. R. Ruiz Carrasco, R. Vilar, and R. Zimmerman, "Tweether future generation w-band backhaul and access network technology," in *2017 European Conference on Networks and Communications (EuCNC)*, 2017, pp. 1–5. DOI: `10.1109/EuCNC.2017.7980684`.

[29] L. Luini, G. Roveda, M. Zaffaroni, M. Costa, and C. Riva, "Em wave propagation experiment at e band and d band for 5g wireless systems: Preliminary results," in *12th European Conference on Antennas and Propagation (EuCAP 2018)*, 2018, pp. 1–5. DOI: `10.1049/cp.2018.0378`.

[30] ITU-R, *P.838-3 specific attenuation model for rain for use in prediction methods*, 2005.

[31] ——, *P.676-11 attenuation by atmospheric gases*, 2016.

[32] G. Roveda and M. Costa, "Flexible use of d band spectrum for 5g transport: A research field trial as input to standardization," in *2018 IEEE 29th Annual International Symposium on Personal, Indoor and Mobile Radio Communications (PIMRC)*, 2018, pp. 800–804. DOI: `10.1109/PIMRC.2018.8580825`.

[33] A. Pallotta, P. Roux, D. Del Rio, J. F. Sevillano, M. M. Pirbazari, A. Mazzanti, V. Ermolov, A. Lamminen, J. Säily, M. Frecassetti, M. Moretto, and J. De Cos, "Sige:bicmos technology is enabling d-band link with active phased antenna array," in *2021 Joint European Conference on Networks and Communications 6G Summit (EuCNC/6G Summit)*, 2021, pp. 496–501. DOI: `10.1109/EuCNC/6GSummit51104.2021.9482432`.

[34] M. G. L. Frecassetti, A. Mazzanti, J. F. Sevillano, D. del Río, and V. Ermolov, "D-band transport solution to 5g and beyond 5g cellular networks," in *2019 European Conference on Networks and Communications (EuCNC)*, 2019, pp. 214–218. DOI: `10.1109/EuCNC.2019.8802033`.

[35] T. S. Rappaport, S. Sun, R. Mayzus, H. Zhao, Y. Azar, K. Wang, G. N. Wong, J. K. Schulz, M. Samimi, and F. Gutierrez, "Millimeter wave mobile communications for 5G cellular: It will work!" *IEEE Access*, vol. 1, pp. 335–349, 2013.

[36] 3GPP, *TS 38.101-2 v15.8.0 User Equipment (UE) radio transmission and reception; Part 2: Range 2 Standalone*, 2020.

[37] ITU-R, *M.2135-1 guidelines for evaluation of radio interface technologies for IMT-Advanced*, 2009.

[38] 3GPP, *TR 38.900 V14.3.0 Study on channel model for frequency spectrum above 6GHz*, 2017.

[39] J. G. Andrews, F. Baccelli, and R. K. Ganti, "A tractable approach to coverage and rate in cellular networks," *IEEE Transactions on Communications*, vol. 59, no. 11, pp. 3122–3134, Nov. 2011.

[40] W. Lu and M. Di Renzo, "Stochastic geometry modeling of cellular networks: Analysis, simulation and experimental validation," in *Proceedings of the 18th ACM International Conference on Modeling, Analysis and Simulation of Wireless and Mobile Systems*, 2015, pp. 179–188.

[41] A. Guo and M. Haenggi, "Spatial stochastic models and metrics for the structure of base stations in cellular networks," *IEEE Transactions on Wireless Communications*, vol. 12, no. 11, pp. 5800–5812, Nov. 2013.

[42] ITU-R, *P.2108-0 Prediction of clutter loss*, 2017.

[43] F. Letourneux, S. Guivarch, and Y. Lostanlen, "Propagation models for heterogeneous networks," in *2013 7th European Conference on Antennas and Propagation (EuCAP)*, Apr. 2013, pp. 3993–3997.

[44] Department for Environment, Food and Rural Affairs. (2019). Defra Data Services Platform Surveys, [Online]. Available: `https://environment.data.gov.uk`.

[45] Ordnance Survey. (2019). Ordnance Survey Data Hub, [Online]. Available: `https://osdatahub.os.uk`.

[46] M. Tanemura, "Statistical distributions of Poisson Voronoi cells in two and three dimensions," *Forma*, vol. 18, pp. 221–247, Jan. 2003.

[47] ITU-R, *P.1410-5 Propagation data and prediction methods required for the design of terrestrial broadband radio access systems operating in a frequency range from 3 to 60 GHz*, 2012.

[48] J. G. Andrews, R. K. Ganti, M. Haenggi, N. Jindal, and S. Weber, "A primer on spatial modeling and analysis in wireless networks," *IEEE Communications Magazine*, vol. 48, no. 11, pp. 156–163, Nov. 2010.

[49] S. Roy and M. Mehrnoush, "A new Poisson process-based model for LOS/NLOS discrimination in clutter modeling," *IEEE Transactions on Antennas and Propagation*, vol. 67, no. 12, pp. 7538–7549, Dec. 2019.

[50] Ministry of Housing, Communities and Local Government. (2018). Floor space in English homes: main report, [Online]. Available: `https://www.gov.uk/government/publications/floor-space-in-english-homes`.

[51] 3GPP, *TR 21.915 V15.0.0 Technical Specification Group Services and System Aspects; Release 15 Description; Summary of Rel-15 Work Items*, 2019.

[52] T. S. Rappaport, Y. Xing, G. R. MacCartney, A. F. Molisch, E. Mellios, and J. Zhang, "Overview of Millimeter Wave Communications for Fifth-Generation (5G) Wireless Networks—With a Focus on Propagation Models," *IEEE Transactions on Antennas and Propagation*, vol. 65, no. 12, pp. 6213–6230, 2017. DOI: `10.1109/TAP.2017.2734243`.

[53] T. S. Rappaport, S. Sun, R. Mayzus, H. Zhao, Y. Azar, K. Wang, G. N. Wong, J. K. Schulz, M. Samimi, and F. Gutierrez, "Millimeter wave mobile communications for 5G cellular: It will work!" *IEEE Access*, vol. 1, pp. 335–349, 2013.

[54] mmMAGIC. (2017). Measurement Results and Final mmMAGIC Channel Models, H2020-ICT-671650-mmMAGIC/D2.2, [Online]. Available: `https://5g-mmmagic.eu/results/`.

[55] T. S. Rappaport, G. R. MacCartney, S. Sun, H. Yan, and S. Deng, "Small-scale, local area, and transitional millimeter wave propagation for 5g communications," *IEEE Transactions on Antennas and Propagation*, vol. 65, no. 12, pp. 6474–6490, 2017.

[56] S. Rajagopal, S. Abu-Surra, and M. Malmirchegini, "Channel feasibility for outdoor non-line-of-sight mmwave mobile communication," in *2012 IEEE Vehicular Technology Conference (VTC Fall)*, 2012, pp. 1–6.

[57] 3GPP, *TR 38.874 v16.0.0 Study on Integrated Access and Backhaul*, 2019.

[58] ——, *TR 38.900 V14.3.0 Study on channel model for frequency spectrum above 6GHz*, 2017.

[59] B. Mondal, T. A. Thomas, E. Visotsky, F. W. Vook, A. Ghosh, Y. Nam, Y. Li, J. Zhang, M. Zhang, Q. Luo, Y. Kakishima, and K. Kitao, "3D channel model in 3GPP," *IEEE Communications Magazine*, vol. 53, no. 3, pp. 16–23, 2015.

[60] WINNERII, *WINNER II Channel Models, D1.1.2 V1.2, IST-4-027756 WINNER II Deliverable*, 2008.

[61] 3GPP, *TR 36.873 V2.0.0 Study on 3D-Channel Model for LTE*, 2014.

[62] S.-E. Ericsson, *Height Dependent LOS Probability for 3D-Channel Model*, 2013.

[63] 5GCM. (2016). 5G Channel Model for bands up to 100 GHz, [Online]. Available: http://www.5gworkshops.com/5GCM.html.

[64] M. K. Samimi, T. S. Rappaport, and G. R. MacCartney, "Probabilistic omnidirectional path loss models for millimeter-wave outdoor communications," *IEEE Wireless Communications Letters*, vol. 4, no. 4, pp. 357–360, 2015.

[65] O. Teyeb, A. Muhammad, G. Mildh, E. Dahlman, F. Barac, and B. Makki, "Integrated Access Backhauled Networks," in *2019 IEEE 90th Vehicular Technology Conference (VTC2019-Fall)*, 2019, pp. 1–5. DOI: 10.1109/VTCFall.2019.8891507.

[66] A. N. Uwaechia and N. M. Mahyuddin, "A comprehensive survey on millimeter wave communications for fifth-generation wireless networks: Feasibility and challenges," *IEEE Access*, vol. 8, pp. 62 367–62 414, 2020. DOI: 10.1109/ACCESS.2020.2984204.

[67] 3GPP, *TR 36.806 V9.0.0 Technical Specification Group Radio Access Network; Evolved Universal Terrestrial Radio Access (E-UTRA) Relay architectures for E-UTRA (LTE-Advanced)*, 2010.

[68] M. Cudak, A. Ghosh, A. Ghosh, and J. Andrews, "Integrated Access and Backhaul: A Key Enabler for 5G Millimeter-Wave Deployments," *IEEE Communications Magazine*, vol. 59, no. 4, pp. 88–94, 2021. DOI: 10.1109/MCOM.001.2000690.

[69] B. Mondal, T. A. Thomas, E. Visotsky, F. W. Vook, A. Ghosh, Y. Nam, Y. Li, J. Zhang, M. Zhang, Q. Luo, Y. Kakishima, and K. Kitao, "3d channel model in 3gpp," *IEEE Communications Magazine*, vol. 53, no. 3, pp. 16–23, 2015.

[70] NGMN, *Small Cell Cost Sharing - Full Report*, 2020. [Online]. Available: https://www.ngmn.org/technical-documents.html.

[71] A. Checko, H. L. Christiansen, Y. Yan, L. Scolari, G. Kardaras, M. S. Berger, and L. Dittmann, "Cloud ran for mobile networks—a technology overview," *IEEE Communications Surveys Tutorials*, vol. 17, no. 1, pp. 405–426, 2015. DOI: 10.1109/COMST.2014.2355255.

[72] D. Gesbert, S. Hanly, H. Huang, S. Shamai Shitz, O. Simeone, and W. Yu, "Multi-cell mimo cooperative networks: A new look at interference," *IEEE Journal on Selected Areas in Communications*, vol. 28, no. 9, pp. 1380–1408, 2010. DOI: 10.1109/JSAC.2010.101202.

[73] G. Interdonato, E. Björnson, H. Ngo, P. Frenger, and E. Larsson, "Ubiquitous cell-free massive mimo communications," *EURASIP Journal on Wireless Communications and Networking*, Aug. 2019. DOI: 10.1186/s13638-019-1507-0.

[74] GSMA, *Mobile Backhaul: An Overview*, 2019. [Online]. Available: https://www.gsma.com/futurenetworks/wiki/mobile-backhaul-an-overview/.

[75] Y. Yan, Q. Hu, and D. M. Blough, "Optimal path construction with decode and forward relays in mmwave backhaul networks," in *2020 International Conference on Computing, Networking and Communications (ICNC)*, 2020, pp. 579–585. DOI: 10.1109/ICNC47757.2020.9049696.

[76] A. Łukowa, V. Venkatasubramanian, E. Visotsky, and M. Cudak, "On the coverage extension of 5g millimeter wave deployments using integrated access and backhaul," in *2020 IEEE 31st Annual International Symposium on Personal, Indoor and Mobile Radio Communications*, 2020, pp. 1–7. DOI: 10.1109/PIMRC48278.2020.9217260.

[77] O. Teyeb, A. Muhammad, G. Mildh, E. Dahlman, F. Barac, and B. Makki, "Integrated Access Backhauled Networks," in *2019 IEEE 90th Vehicular Technology Conference (VTC2019-Fall)*, 2019.

[78] ETSI, mWT ISG, *Analysis of Spectrum, License Schemes and Network Scenarios in the D-band*, 2018. [Online]. Available: https://www.etsi.org/committee/1426-mwt.

[79] ETSI mWT ISG, *Evolution of Fixed Services for Wireless Backhaul of IMT 2020 / 5G*, 2019. [Online]. Available: https://www.itu.int/en/ITU-R/study-groups/workshops/fsimt2020/Pages/default.aspx.

[80] CEPT, *ECC Report 282 - Point-to-Point Radio Links in the Frequency Ranges 92- 114.25 GHz and 130-174.8 GHz*, 2018.

[81] J. S. Wey and J. Zhang, "Passive optical networks for 5g transport: Technology and standards," *Journal of Lightwave Technology*, vol. 37, no. 12, pp. 2830–2837, 2019. DOI: 10.1109/JLT.2018.2856828.

[82] A. Stancu, A. Vulpe, and S. Halunga, "Evaluation of a wireless transport network emulator used for sdn applications development," *IEEE Access*, vol. 6, pp. 15 870–15 883, 2018. DOI: 10.1109/ACCESS.2018.2815844.

[83] L. M. P. Larsen, A. Checko, and H. L. Christiansen, "A Survey of the Functional Splits Proposed for 5G Mobile Crosshaul Networks," *IEEE Communications Surveys Tutorials*, vol. 21, no. 1, pp. 146–172, 2019. DOI: 10.1109/COMST.2018.2868805.

[84] V. Q. Rodriguez, F. Guillemin, A. Ferrieux, and L. Thomas, "Cloud-ran functional split for an efficient fronthaul network," in *2020 International Wireless Communications and Mobile Computing (IWCMC)*, 2020, pp. 245–250. DOI: 10.1109/IWCMC48107.2020.9148093.

[85] C.-L. I, J. Huang, R. Duan, C. Cui, J. Jiang, and L. Li, "Recent progress on c-ran centralization and cloudification," *IEEE Access*, vol. 2, pp. 1030–1039, 2014. DOI: 10.1109/ACCESS.2014.2351411.

[86] I. A. Alimi, A. L. Teixeira, and P. P. Monteiro, "Toward an efficient c-ran optical fronthaul for the future networks: A tutorial on technologies, requirements, challenges, and solutions," *IEEE Communications Surveys and Tutorials*, vol. 20, no. 1, pp. 708–769, 2018. DOI: 10.1109/COMST.2017.2773462.

[87] N. Ibrahim, A. A. Eltholth, and M. S. El-Soudani, "Hybrid fso/mmwave based fronthaul c-ran optimization for future wireless communications," in *2020 29th Wireless and Optical Communications Conference (WOCC)*, 2020, pp. 1–6. DOI: 10.1109/WOCC48579.2020.9114921.

[88] M. J. Roldan, P. Leithead, and J. Mack, "Experiments and results of a mmw transport platform to enable 5g cloud ran lower layer splits," in *2018 IEEE Long Island Systems, Applications and Technology Conference (LISAT)*, 2018, pp. 1–6. DOI: 10.1109/LISAT.2018.8378032.

[89] C.-Y. Chang, N. Nikaein, R. Knopp, T. Spyropoulos, and S. S. Kumar, "FlexCRAN: A flexible functional split framework over ethernet fronthaul in Cloud-RAN," in *2017 IEEE International Conference on Communications (ICC)*, 2017, pp. 1–7. DOI: 10.1109/ICC.2017.7996632.

[90] J. Bartelt, P. Rost, D. Wubben, J. Lessmann, B. Melis, and G. Fettweis, "Fronthaul and backhaul requirements of flexibly centralized radio access networks," *IEEE Wireless Communications*, vol. 22, no. 5, pp. 105–111, 2015. DOI: 10.1109/MWC.2015.7306544.

[91] D. Chitimalla, K. Kondepu, L. Valcarenghi, M. Tornatore, and B. Mukherjee, "5G fronthaul-latency and jitter studies of CPRI over ethernet," *Journal of Optical Communications and Networking*, vol. 9, no. 2, pp. 172–182, 2017. DOI: 10.1364/JOCN.9.000172.

[92] O-RAN Alliance, *Open Xhaul Transport Working Group 9 - Xhaul Transport Requirements v01.00*, 2021. [Online]. Available: https://o-ran.org/specifications.

[93] 3GPP, *TS 36.213 V17.3.0 Evolved Universal Terrestrial Radio Access (E-UTRA); Physical layer procedures*, 2022.

[94] ——, *TS 38.214 V17.3.0 NR; Physical layer procedures for data*, 2022.

[95] Small Cell Forum, *DARTs - An Analysis Tool for Disaggregated RAN Transport - SCF247.0.1*, 2023. [Online]. Available: https://scf.io.

[96] S. Bjømstad, D. Chen, and R. Veisllari, "Handling Delay in 5G Ethernet Mobile Fronthaul Networks," in *2018 European Conference on Networks and Communications (EuCNC)*, 2018, pp. 1–9. DOI: 10.1109/EuCNC.2018.8442755.

[97] 3GPP, *TSG RAN WG3 R3-161813, Transport requirement for CU and DU functional splits options*, 2016.

[98] ——, *TS 38.331 V17.2.0 NR; Radio Resource Control (RRC) protocol specification*, 2022.

[99] ——, *TS 38.211 V17.3.0 NR; Physical channels and modulation*, 2022.

[100] CPRI Cooperation, *eCPRI Transpot Requirements V1.2*, 2018. [Online]. Available: http://www.cpri.info/spec.html.

[101] ITU-T, *G.8271.1 precision time protocol telecom profile for phase/time synchronization with full timing support from the network*, 2020.

[102] 3GPP, *TS 36.104 V17.7.0 Evolved Universal Terrestrial Radio Access (E-UTRA); Base Station (BS) radio transmission and reception*, 2022.

[103] ——, *TS 38.104 V17.7.0 NR; Base Station (BS) radio transmission and reception*, 2022.

[104] ITU-T, *G.8271 time and phase synchronization aspects of telecommunication networks*, 2020.

[105] Open Air Interface Software Alliance, *Open Air Interface*, 2022. [Online]. Available: https://openairinterface.org.

[106] *Benchmarking Methodology for Network Interconnect Devices*, RFC 2544, Mar. 1999. DOI: 10.17487/RFC2544. [Online]. Available: https://www.rfc-editor.org/info/rfc2544.

[107] ETSI, *TR 101 854 v2.1.1 Fixed Radio Systems; Point-to-point equipment; Derivation of receiver interference parameters useful for planning fixed service point-to-point systems operating different equipment classes and/or capacities*, 2019.

[108] M. Bahnasy, H. Elbiaze, and C. Truchan, "Cpri over ethernet: Towards fronthaul backhaul multiplexing," in *2018 15th IEEE Annual Consumer Communications and Networking Conference (CCNC)*, 2018, pp. 1–7. DOI: 10.1109/CCNC.2018.8319220.

[109] M. Jiang, J. Cezanne, A. Sampath, O. Shental, Q. Wu, O. Koymen, A. Bedewy, and J. Li, "Wireless fronthaul for 5g and future radio access networks: Challenges and enabling technologies," *IEEE Wireless Communications*, vol. 29, no. 2, pp. 108–114, 2022. DOI: 10.1109/MWC.003.2100482.

[110] J. Cezanne, M. Jiang, O. Shental, A. M. Bedewy, A. Sampath, O. Koymen, and J. Li, "Design of wireless fronthaul with mmwave los-mimo and sample-level coding for o-ran and beyond 5g systems," *IEEE Open Journal of the Communications Society*, pp. 1–1, 2023. DOI: 10.1109/OJCOMS.2023.3308713.

[111] P.-H. Kuo and A. Mourad, "Millimeter wave for 5g mobile fronthaul and backhaul," in *2017 European Conference on Networks and Communications (EuCNC)*, 2017, pp. 1–5. DOI: 10.1109/EuCNC.2017.7980750.

[112] M. U. Sheikh, K. Ruttik, E. Mutafungwa, R. Jäntti, J. Hamalainen, and E. Yusta Padilla, "X-haul solutions for different functional split options using thz and sub-thz bands," in *Proceedings of the 20th ACM International Symposium on Mobility Management and Wireless Access*, ser. MobiWac '22, Montreal, Quebec, Canada: Association for Computing Machinery, 2022, pp. 47–53, ISBN: 9781450394802. DOI: 10.1145/3551660.3560921.

[113] I. K. Aksoyak, M. Mock, M. Kaynak, and A. C. Ulusoy, "A d-band power amplifier with 15 dbm psat in 0.13 um sige bicmos technology," in *2022 IEEE 22nd Topical Meeting on Silicon Monolithic Integrated Circuits in RF Systems (SiRF)*, 2022, pp. 5–8. DOI: 10.1109/SiRF53094.2022.9720048.

[114] M. G. L. Frecassetti, J. F. Sevillano, D. del Río, M. I. Saglam, A. Lamminen, and V. Ermolov, "D-band backhaul and fronthaul solutions for 5g radio access network," in *2022 52nd European Microwave Conference (EuMC)*, 2022, pp. 772–775. DOI: 10.23919/EuMC54642.2022.9924325.

[115] M. Babay, M. Moretto, P. Perrault, R. Bara-Maillet, P. Mcillree, E. Froger, P. Di Prisco, and P. Lopez, "Sub-thz radio communication links from research to field trial," in *2022 52nd European Microwave Conference (EuMC)*, 2022, pp. 780–783. DOI: 10.23919/EuMC54642.2022.9924270.

[116] B. Ustundag, E. Turkmen, B. Cetindogan, A. Guner, M. Kaynak, and Y. Gurbuz, "Low-noise amplifiers for w-band and d-band passive imaging systems in sige bicmos technology," in *2018 Asia-Pacific Microwave Conference (APMC)*, 2018, pp. 651–653. DOI: 10.23919/APMC.2018.8617582.